ADDITIVES EFFECTS ON THE CHARGE CARRIER DYNAMICS AND PERFORMANCE METRICS OF FORMAMIDINIUM-RICH MIXED LEAD HALIDE PEROVSKITE SOLAR CELL

BY

RICHARD KIPYEGON KOECH

STUDENT ID: 70187

A dissertation submitted to the faculty at the African University of Science and Technology in partial fulfillment of the requirements for the degree of Doctor of Philosophy in material science and engineering department.

February 23, 2022

CERTIFICATION

This is to certify that the dissertation titled “Additives effects on the charge carrier dynamics and performance metrics of Formamidinium-rich mixed lead halide perovskite solar cell” submitted to the school of postgraduate studies, African University of Science and Technology (AUST), Abuja, Nigeria for the award of the Doctor of Philosophy degree is a record of original research carried out by Richard Kipyegon Koech in the Department of Material Science and Engineering**.**

ADDITIVES EFFECTS ON THE CHARGE CARRIER DYNAMICS AND PERFORMANCE METRICS OF FORMAMIDINIUM-RICH MIXED LEAD HALIDE PEROVSKITE SOLAR CELL

By

Richard Kipyegon Koech

A DISSERTATION APPROVED BY THE MATERIAL SCIENCE AND ENGINEERING DEPARTMENT

RECOMMENDED: ----------

Prof. Esidor Ntsoenzok (Advisor)

Prof. Wole Soboyejo (Co-Advisor)

Dr. Oluwaseun Kehinde Oyewole (Committee)

Dr. Abdulhakeem Bello (Committee)

Dr. Kenfack Anatole (Committee)

Head, Department of Material Science and Engineering

APPROVED BY:

Vice President, Academics

Date----------

COPYRIGHT

ABSTRACT

Perovskite solar cell (PSC) has emerged as a promising photovoltaic technology due to their prospects for high efficiency and low cost. Despite the impressive improvement in their power conversion efficiency (PCE) over the years, it is still limited by non-radiative recombination losses arising from the non-ideal material properties. Further, the rapid degradation in their PCEs when exposed to the ambient conditions is a great impediment to their commercialization. To address these challenges, there is a need to engineer the properties of the charge transport layers (CTLs), the active layer (AL) and the interfaces between them with a view to suppressing the non-radiative recombination and performance degradation pathways. In this work, an in-depth study of the effects of additives incorporated into the electron transport layer (ETL) and the AL on the optoelectronic properties and performance characteristics of Formamidinium (FA)-rich mixed lead halide PSC was carried out. The results of the study revealed that an appropriate proportion of additives in the ETL and/or the AL improve the PCE and stability of FA-rich PSC. In particular, the incorporation of 0.2 volume proportion of tin oxide (SnO_2) into the titanium dioxide (TiO_2)-based ETL improved the PCE by about 7.17%. Furthermore, the addition of Cesium bromide (CsBr) and Polyethylene Oxide (PEO) into the AL improved the morphology of the AL leading to simultaneous improvement in the PCE and stability of FA-rich PSC.

Key words: Electron transport layer, active layer, charge carrier dynamics, interface, tin oxide, titanium dioxide, perovskite solar cell, cesium bromide, polyethylene oxide

This dissertation is dedicated to my loving wife Caren Koech and my children Joy, Ezra and Prudence for their love, patience, understanding and emotional support during my PhD study.

ACKNOWLEDGEMENT

Many thanks go to our omniscient God for giving me good health, protection, and the resilience that enabled me to be focused and productive throughout my PhD Journey.

I would like to appreciate the support I received from my sponsor: the PASET-RSIF; which flattened the mountains and filled the valleys I would have gone through in my PhD studies. They ensured that I got a conducive environment to carry out my research and connected me with the right people who mentored me well and ensured I attained my academic goals.

My sincere gratitude also goes to my academic advisors and committee members namely Prof Esidor, Prof Soboyejo, Dr. Oyewole, Dr. Bello, and Dr. Kenfack for their unrelenting support, guidance, and motivation throughout my PhD journey.

I wish to convey my special appreciation to my colleagues Dr. Deborah, Reisya, and all my lab mates at Worcester Polytechnic Institute for their invaluable help and moral support while I was carrying out my experimental work.

TABLE OF CONTENTS

LIST OF PUBLICATIONS

1. **Richard K. Koech**, M. Kigozi, Yusuf A. Olanrewaju, Reisya Ichwani, Deborah O. Oyewole, Omolara V. Oyelade, Dahiru M Sanni, Sharafadeen A. Adeniji, Erika Colin Ulloa, Lyubov V. Titova, Julia L. Martin, Ronald L. Grimm, Abdulhakeem Bello, Oluwaseun K. Oyewole, Esidor Ntsoenzok and Winston O. Soboyejo (2022): Effects of Polyethylene Oxide Polymer on the photophysical properties and operational stability of FA-Rich perovskite solar cells, *Ready for submission*

2. **Richard K. Koech**; Reisya Ichwani; Deborah O. Oyewole; Moses Kigozi; Daniel Amune; Dahiru Sanni; Sharafadeen A. Adeniji; Oluwaseun K. Oyewole; Abdulhakeem Bello; Esidor Ntsoenzok; Winston Soboyejo (2021): Tin Oxide modified Titanium Dioxide as Electron Transport Layer in Formamidinium-Rich Perovskite Solar Cells, *Energies*, *14*(23), 7870;

3. **Richard K. Koech**, Reisya Ichwani, Julia L. Martin, Deborah O. Oyewole, Omolara V. Oyelade, Yusuf A. Olanrewaju, Dahiru M Sanni, Sharafadeen A. Adeniji, Ronald L. Grimm, Abdulhakeem Bello, Oluwaseun K. Oyewole, Esidor Ntsoenzok and Winston O. Soboyejo (2021): A Study of the Effects of a Thermally Evaporated nanoscale CsBr layer on the Optoelectronic Properties and Stability of Formamidinium-rich Perovskite Solar Cells, *AIP Advances*, 11, 095112

4. **R. K Koech**, M. Kigozi Moses, A. Bello, P. A Onwualu and W.O Soboyejo (2020): Recent advances in solar energy harvesting materials with particular emphasis on photovoltaic materials, *Proc. of 2019 IEEE PES/IAS Power Africa Conference*, pp. 627-632, doi: 10.1109/PowerAfrica.2019.8928859.

5. Jaya Cromwell, Sharafadeen Adeniji, Deborah Oyewole, **Richard Koech**, Reisya Ichwani, Benjamin Agyei-Tuffour, Oluwaseun Oyewole, and Winston Soboyejo (2022). Effects of Blister Formation on the Degradation of Organic Light Emitting Devices, *AIP Advances*, accepted

6. Omolara Oyelade, Oluwaseun Oyewole, Yusuf Olanrewaju, Reisya Ichwani, **Richard Koech**, Deborah Oyewole, Sharafadeen Adeniji, Dahiru Sanni, Jaya Cromwell, Ridwan Ahmed, Kingley Orisekeh, Vitalis Anye, and Winston Soboyejo (2022): Understanding the Effects of Annealing Temperature on the Mechanical Properties of Layers in FAI-Rich Perovskite Solar Cells, *AIP advances*, 12, 025104
7. Yusuf Olanrewaju, Kingsley Orisekeh, Omolara Oyelade, **Richard Koech**, Reisya Ichwani, Abraham Ebunu, Daniel Amune, Abdulhakeem Bello, Vitalis Anye, Oluwaseun Oyewole, and Winston Soboyejo (2022): Effects of Temperature-Dependent Burn-In Decay on the Performance of Triple Cation Mixed Halide Perovskite Solar Cells, *AIP advances,* 12, 015122
8. Reisya Ichwani; **Richard Koech**; Oluwaseun Kehinde Oyewole; Adri Huda; Deborah Olubunmi Oyewole; Jaya Cromwell; Julia L Martin; Ronald L Grimm (2022). Interfacial Fracture of Hybrid Organic-Inorganic Perovskite Solar Cells; *extreme mechanics letters*, 50, 101515
9. D. O. Oyewole, **R. K. Koech**, Reisya Ichwani, Juan Hinostroza Tamayo Sharafadeen Adetunji Adeniji, Jaya Cromwell, Oluwaseun Kehinde Oyewole, Benjamin Agyei-Tuffour, Lyubov Titova, Nancy A. Burnham, Winston O Soboyejo (2021): Annealing Effects on the Interdiffusion in Layered in FA-Rich Perovskite Solar Cells, *AIP Advances,* 11, 065327

10. Dahiru Sanni, Aditya Yerramilli, Esidor Ntsoenzok, Sharafadeen Adeniji, Omolara Oyelade, **Richard Koech**, Adebayo A Fashina, and Terry L. Alford (2021). Impact of precursor concentration on the properties of perovskite solar cells obtained from the dehydrated lead acetate precursors, *Journal of Vacuum Science and Technology, 39, 032801*
11. S. A. Adeniji, J. Cromwell, D. O. Oyewole, O. V. Oyelade, **R. K. Koech**, D. M. Sanni, O. K. Oyewole, B. Babatope, W. O. Soboyejo (2021): Pressure-assisted fabrication of perovskite light emitting devices, *AIP Advances*, 11, 025112
12. Sharafadeen Adeniji, Oluwaseun Oyewole, **Richard Koech**, Deborah Oyewole, Jaya Cromwell, Ridwan Ahmed, Omolara Oyelade, Dahiru Sanni, Kingsley Orisekeh, Abdulhakeem Bello, Winston Soboyejo (2021). Failure Mechanisms of Stretchable Perovskite Light-Emitting Devices under Monotonic and Cyclic Deformations, *Journal Macromolecular Materials and Engineering*, 305 (30).
13. Dahiru Sanni, Esidor Ntsoenzok, Eddy Saintaimé, Sharafadeen Adeniji, Omolara Oyelade, **Richard Koech**, Daniel Amune, and Abdulhakeem Bello (2020): The role of hafnium acetylacetonate buffer layer on the performance of lead halide perovskite solar cells derived from dehydrated lead acetate as Pb source, *AIP Advances*, 10, 075006
14. O. K. Oyewole, D. O. Oyewole, O. V. Oyelade, S. A. Adeniji, **R. K. Koech**, J. Asare, B. Agyei-Tuffour and W. O. Soboyejo (2020): Failure of Stretchable Organic Solar Cells Under Monotonic and Cyclic Loading, *Journal Macromolecular Materials and Engineering*, 305 (30).

LIST OF TABLES

LIST OF FIGURES

LIST OF ABBREVIATIONS

AEO	Africa energy outlook
AL	Active layer
BIPV	Building integrated photovoltaics
CBM	Conduction band minimum
CBO	Conduction band offset
CTL	Charge transport layer
DMF	N,N Dimethylformamide
DMSO	Dimethylsulfoxide
DSSC	Dye sensitized solar cell
EDS	Energy dispersive x-ray spectroscopy
EI	Electrochemical impedance
EIS	Electrochemical impedance spectroscopy
EQE	External quantum efficiency
ETL	Electron transport layer
FF	Fill factor
FTIR	Fourier transform infrared
FTO	Fluorine doped tin oxide
HOMO	Highest occupied molecular orbital
HTL	Hole transport layer
IEA	International energy outlook

IPA	Isopropyl alcohol
IPCC	Intergovernmental panel on climate change
ITO	Indium doped tin oxide
LUMO	Lowest unoccupied molecular orbital
NREL	National renewable energy laboratory
PCE	Power conversion efficiency
PDMS	Polydimethylsiloxane
PEN	Polyethylene naphthalate
PEO	Polyethylene oxide
PET	Polyethylene terephthalate
PL	Photoluminescence
PSC	Perovskite solar cell
PV	Photovoltaics
REN21	Renewable energy policy network for the 21st century
SCLC	Space charge limited conduction
SEM	Scanning electron microscope
TAS	Transient absorption spectroscopy
TRPL	Time resolved photoluminescence
UNDP	United nations development programme
UPS	Ultraviolet photoelectron spectroscopy
VBM	Valence band maximum
VBO	Valence band offset
WEC	World economic council

XPS	X-ray photoelectron spectroscopy
XRD	X-ray diffraction

CHAPTER ONE

INTRODUCTION

1.1 Introduction

In this chapter, brief background information on the global energy scenario, the need to transit to renewable energy resources, and the evolution of photovoltaic technology is explored. The problem statement, the research objectives, the justification, and the scope of the study are also highlighted.

1.2 Background information

Energy is the fundamental underpinning for socio-economic and technological advancement in any nation (Stern, 2011). It is a primary factor of production in every sector of the economy and is required to power various machines and electronic devices at homes and other institutions. The rapid expansion in the major economic sectors; in conjunction with the increasing human population and rising standards of living; has led to a corresponding increase in the global energy demand (Administration, 2018; Energy Information Administration, 2019; McKinsey Global Institute, 2019). The demand is projected to increase further as the world economies continue to grow with higher growth rates coming from developing nations; most of which being in Asia and Africa (Administration, 2019). As a continent with the highest population growth rate, Africa's energy demand is projected to increase significantly in the coming years (AEO, 2019). This increase will put pressure on the existing energy infrastructure and may pose significant challenges particularly to the energy poverty-stricken and the mostly fossil fuel-reliant nations in sub-Saharan Africa. Figure 1.1 shows the growth in energy demand globally and in Africa from the year 2000 to date with

projections to 2040.

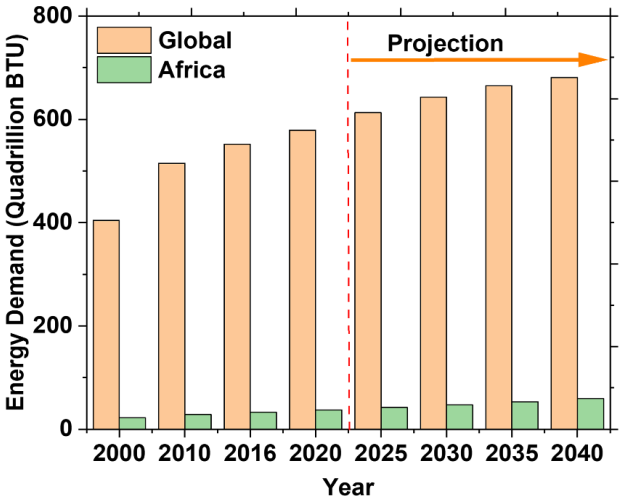

Figure 1.1: Global and Africa energy demand growth and projections (Data source: BP Energy Economics, 2018)

With the increased awareness of the strong correlation between energy use, economic growth, and climate change; the policymakers in the energy sector have now considered access to affordable, reliable, and sustainable forms of energy as an integral part of sustainable development (UNDP, 2015). Furthermore, as the world wades through the wave of technological transformations brought about by the fourth (4^{th}) industrial revolution, the provision of steady, cost-effective, and sustainable forms of energy is very crucial. The conventional energy resources based on fossil fuels such as petroleum, coal, and natural gas; which are currently dominant in the global energy sectors; are not sustainable. The continued dependence on these energy resources will cause an increase in greenhouse gas emissions which will accelerate the climate change situation globally thus bringing adverse impacts on the environment and human health (IPCC, 2014; Perera, 2018). In addition, the increased pressure on conventional energy resources implies that their finite reserves will gradually be

depleted; leading to an escalation in their prices and increased competition for the few available reserves; which can impact negatively on global security and sustainable development. The global energy sector is thus faced with a serious trilemma of ensuring energy access, energy supply security, and environmental sustainability (WEC, 2016).

For the energy sectors to respond well to these challenges, concerted efforts are being made by all the stakeholders to make a transition from conventional fossil fuel-based energy resources to renewable energy resources. This move is the best option since the renewable energy resources are inexhaustible, can be installed anywhere, and are sustainable. They, therefore, offer several additional benefits such as increased reliability and resilience, improved health, energy equity, and job creation (REN21, 2018). Among the renewable energy resources, solar energy has been considered the best alternative due to its potential to supply the world with sufficient, inexhaustible, and sustainable forms of energy (Kabir et al., 2018; Onyeji-Nwogu, 2017).

Though small-scale utilization of solar energy has been in existence since time immemorial, the advent of new solar harnessing technologies has diversified the scope of its application and the contribution of solar energy to the global energy mix has been increasing (REN21, 2017). Large-scale utilization of solar energy has also been accelerated by the various research efforts and government policies which have been instituted to overcome barriers to its widespread adoption such as intermittency and high costs of solar energy harnessing technologies (Aquila et al., 2017; Barton & Infield, 2004). The energy from the sun can be captured and converted to usable forms of energy using several technologies which are summarized in Figure 1.2 (Liu et al., 2013).

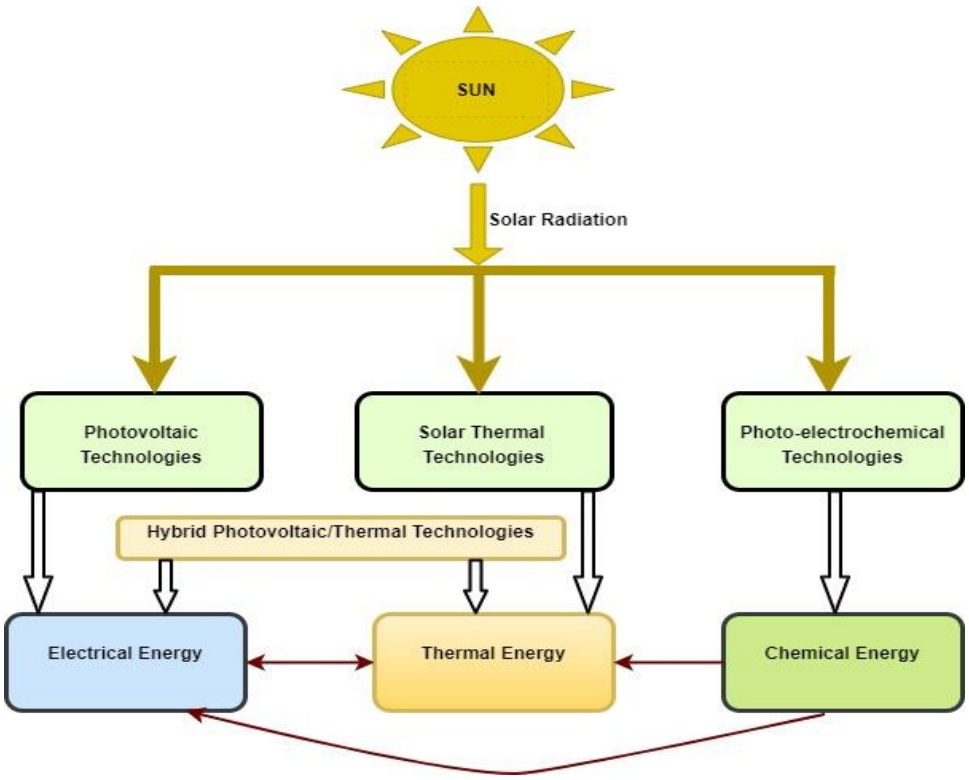

Figure 1.2: Solar energy harnessing technologies

Photovoltaic (PV) technology is a solar energy harnessing technology that uses a solar cell to absorb and convert solar radiation into direct electricity through the photovoltaic effect (Parida et al., 2011). In a typical PV system, many solar cells are usually connected either in series or in parallel or both to form a PV module with the desired power output. The solar cell is therefore a basic functional unit in a PV system that determines its overall power conversion efficiency (PCE), cost, and its lifetime. The quest for an efficient and low-cost PV system with a longer operational lifetime has provided the impetus for continuous research in this field which has seen various solar cell generations being developed (Green & Bremner, 2017). The first (1^{st}) generation solar cells are those that are based on crystalline silicon technology. This solar cell technology has achieved a record power conversion efficiency (PCE) of 26.7% and is presently the most dominant in the PV market (Green et al., 2018;

Polman et al., 2016). The second (2nd) generation solar cells; which are based on thin-film technology; are cheaper than their crystalline silicon-based counterpart but they exhibit relatively low efficiencies and poor outdoor reliability (Sharma et al., 2015). The third (3rd) generation solar cells are the emerging solar cell technologies that aim to achieve the highest PCEs at the least possible unit cost (Green, 2002; Li et al., 2012). They have high light absorption coefficients and are therefore able to use thin layers of semiconducting materials to absorb sunlight. They include nanocrystal-based solar cells, organic solar cells, dye-sensitized solar cells (DSSCs), and Perovskite solar cells (PSCs) (Sharma et al., 2015). A summary of the existing solar cell technologies is given in Figure 1.3.

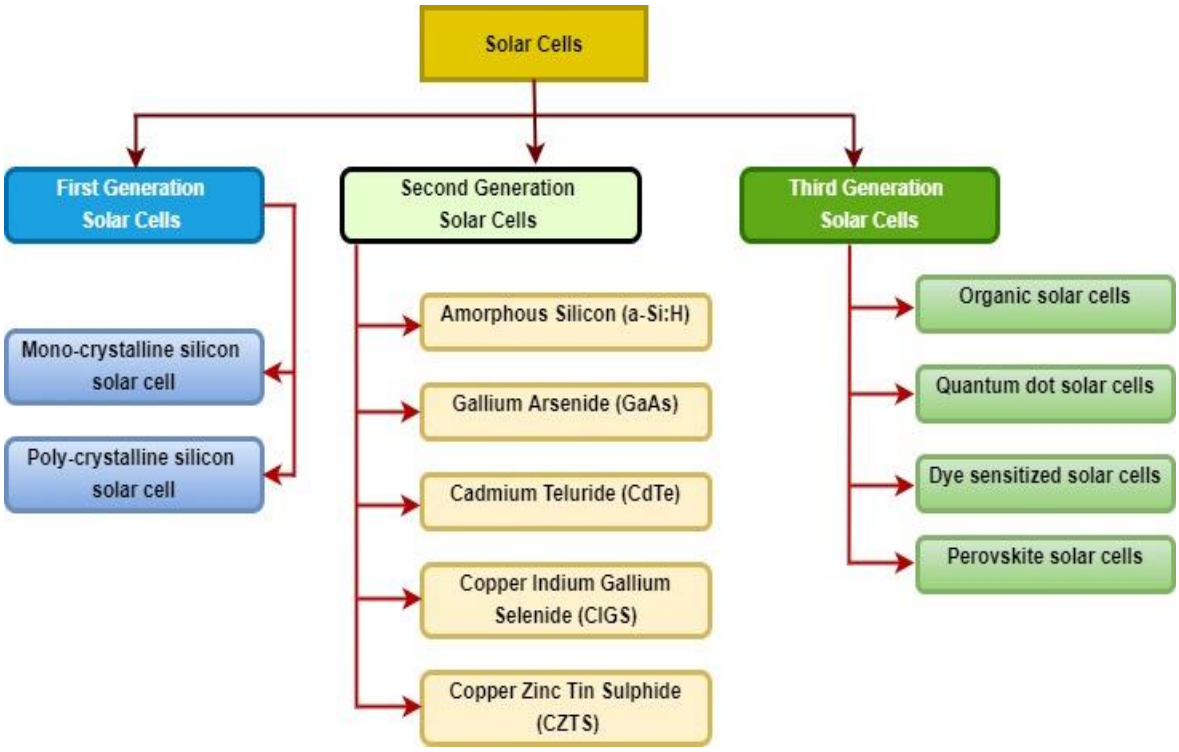

Figure 1.3: Solar cell technologies (Adapted from Green & Bremner, 2017)

Among the 3rd generation solar cell concepts, PSCs have received intense research attention due to their excellent optoelectronic properties, their versatility, and low costs (Green et al., 2014; Kim et al., 2015). They derive their names from their active layers (ALs)

which assume the perovskite structure, ABX_3, resulting from a unique structural combination of different cations and halides. The part A represents a monovalent cation such as methyl-ammonium ($CH_3NH_3^+$), ethyl-ammonium ($CH_3CH_2NH_3^+$), formamidinium ($NH_2CH{=}NH_2^+$) or Cesium (Cs^+) while part B and X represent a divalent cation (typically Pb^{2+} or Sn^{2+}) and an halide (such as iodide (I^-), bromide (Br^-) or chloride (Cl^-)) respectively (Da et al., 2018; Shen et al., 2018). Cation A occupies a cubo-octahedral site shared with twelve X anions, while cation B occupies an octahedral site shared with six X anions. The general structure of a perovskite material is depicted in Figure 1.4 (Supreeth & Shreya, 2016). The size of the A-site cation and the BX_6 octahedra controls the dimensionality of the perovskite structure. This structure makes PSCs have more advantages compared to other PV technologies as far as their electronic and optical properties are concerned (Green et al., 2014; Shen et al., 2018). It allows tuning of their optoelectronic properties through cation/anion substitution or mixing thus providing scientists with a wide parameter space for different material choices and combinations.

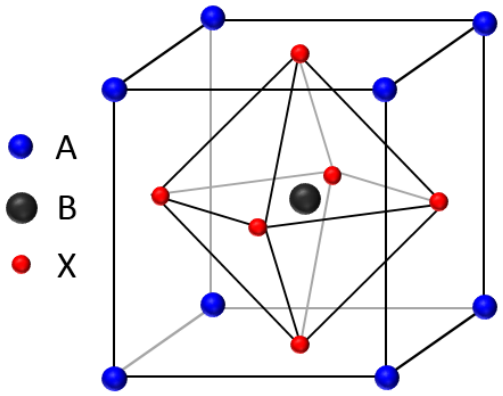

Figure 1.4: Structure of perovskite

The discovery of PSC stemmed from an attempt to address the problem of poor light absorption in dye-sensitized solar cells (DSSCs) in 2009 by replacing the liquid electrolyte

with a solid-state material (Kojima, Teshima, Shirai, 2009). Upon their inception, several theoretical and experimental research works that focused on understanding the device physics, structure, and their mode of operations were carried out (Krishna et al., 2021; Roy et al., 2020a; Xiao & Yan, 2017). Through these studies, a better understanding of the structure and the working principles of PSC was achieved. This motivated scientists; drawn from different disciplines; to work together on developing structural designs and techniques geared towards improving their PV performance and lifetime. These efforts have led to a cheerful increase in the PCE of PSCs from a value less than 4% to 25.8% and lifetime from a few hours to several months within a short period from their discovery (Filip et al., 2018; Min et al., 2021; NREL, 2019; Shi & Jayatissa, 2018; Wali et al., 2020). Figure 1.5 shows the progress in PCE of PSCs from 2009 to 2021 (Dai et al., 2021; Min et al., 2021).

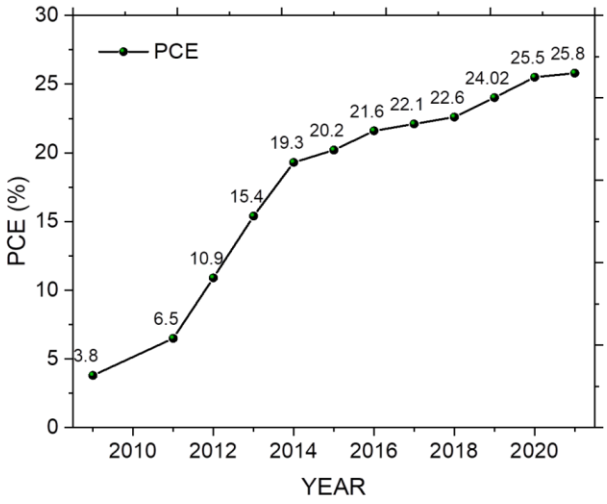

Figure 1.5: Recorded improvement in the PCE of PSCs (adapted from Dai et al., 2021)

PSCs based on organo-lead halide perovskite ALs have achieved the best PCEs due to their excellent optoelectronic properties (Jeon et al., 2015; Shi & Jayatissa, 2018). The perovskite structure of the AL allows engineering of their morphology and optoelectronic

properties through cation/anion mixing and incorporation of some additives (Kim et al., 2019; Zhang & Zhu, 2019; Zhou et al., 2018). These systems have demonstrated high optical absorption in the visible region of the solar spectrum, low exciton binding energies, long charge carrier diffusion lengths, and defect tolerance that enable them to have better utilization of the incident sunlight and good charge carrier collection efficiencies (Bush et al., 2018; Zhang et al., 2017; Zuo et al., 2016). They can also be fabricated from solutions via various low-temperature and low-cost processing techniques such as roll to roll, spin-coating, dip coating, magnetron sputtering, and atomic layer deposition (Ávila et al., 2017; Li et al., 2018). This makes them attractive for applications in flexible, portable, and wearable electronics, electric vehicles, and in building-integrated photovoltaics (BIPV) (Cannavale et al., 2017; Gaspera et al., 2015; Hanusch et al., 2014). Their recent application in photo-detectors and light-emitting devices have also opened new frontiers for perovskite-based light-emitting diodes and field-effect transistors (Tian et al., 2018).

The PCE of PSCs depends upon the effectiveness of charge carrier generation and separation in the AL; charge carrier extraction and transportation through the charge transport layers (CTLs) and their eventual collection at electrodes. These processes are governed by light absorption in the AL and the accompanying charge carrier dynamics within the solar cell structure which are controlled by the properties of the individual components of the PSC device and the nature of the interfaces formed between them (Shen et al., 2015; Bing Wang et al., 2019). In addition to other factors such as deposition method and out-door exposure conditions, the low stability and current density-voltage (J-V) hysteresis problems in PSCs have also been attributed to many factors which include perovskite phase instability, bulk and surface defects in the AL, device architecture and ferroelectric effects due to electrode

polarization (Asghar et al., 2017; Chen et al., 2016; Lan, 2019; Rolston et al., 2016; Wang et al., 2016; Yuan & Huang, 2016). These factors are also dependent on the properties of the CTLs and the interfaces between them.

Research efforts involving elemental adjusting, morphological control, engineering of CTLs, interface engineering, device encapsulation, and introduction of buffer layers have been tried in order to address these issues; but a breakthrough has not been attained (Boyd et al., 2019; Kang & Park, 2019; Ze Wang et al., 2017). Tuning the morphological properties of the AL through compositional engineering, use of additives and other post-treatment approaches such as annealing have been shown to be critical in enhancing its crystal quality and optoelectronic properties which consequently improves the PCE and stability of PSCs (Li et al., 2018; Matsui et al., 2019; Salim et al., 2021). This results mainly from an increase in the formation energies of defects and tuning of the Goldschmidt tolerance factor which leads to a reduction in defect densities, enhancement in charge carrier lifetimes, and reduction of phase segregation in the AL (Li et al., 2016a; Muscarella et al., 2019; Park, 2016; Pham et al., 2019; Saidaminov et al., 2018; Wang et al., 2018; Zhao et al., 2018).

Among the single cation lead halide perovskite ALs, those based on Formamidinium lead iodide ($FAPbI_3$) are known to exhibit the best properties such as good light absorption abilities, better film morphology, and good thermal stability (Koh et al., 2014; Liu et al., 2018). However, phase stability is a great challenge in $FAPbI_3$-based perovskite films as they readily transform from the desired black trigonal perovskite (α-) phase to the yellow hexagonal non-perovskite (δ-) phase. In order to stabilize the α-phase of $FAPbI_3$ without inducing much change in its spectral absorption, small proportions of A-site and X-site dopants such as methyl-ammonium chloride (MACl) and bromide-based salts such as methyl-

ammonium bromide (MABr), methyl-ammonium lead bromide (MAPbBr), and Cesium lead bromide (CsPbBr) are usually added (Joo & Choi, 2021; Shen et al., 2021). The resulting perovskite films based on the mixed cations and halides exhibit improved structural and thermal stabilities (Ono et al., 2017). They also have better optoelectronic properties relative to their single cation/anion counterparts which enable them to have good PV performance. They are termed FA-rich mixed lead halide PSCs since FA forms the largest proportion in the precursor solution.

The performance of FA-rich mixed lead halide PSCs may further be improved through morphological optimization of the AL, modification of the properties of CTLs, and the interface between them (Azam et al., 2020; Courtier et al., 2019; Yin et al., 2016). For example, proper morphological control in the AL has been cited as one of the best techniques to enhance the perovskite film quality through a reduction in the bulk and surface defects; an important route towards the fabrication of highly efficient, stable, and reproducible PSCs (Bi et al., 2017; Yang et al., 2019). The CTLs also play a key role in the charge carrier extraction and injection dynamics that control the non-radiative recombination power losses and performance degradation in PSCs (Courtier et al., 2019; Le Corre, Stolterfoht, Perdigón Toro, et al., 2019; Stolterfoht et al., 2019a; Wolff et al., 2019). The non-radiative recombination losses that occur due to the non-optimized properties of the CTLs can be reduced if their bulk and surface properties are further improved. This will cause an improvement in their electrical conductivities, charge carrier mobilities and reduction in interfacial potential barriers at CTL/AL interface through the formation of favorable band edges with the AL. As a result, the fill factor (*FF*) and the open circuit (V_{oc}) will be enhanced leading to improvement in the PCE in PSCs (Ono & Qi, 2016; Wolff et al., 2019).

Despite the various optimization studies that have been done on FA-rich mixed PSCs, a breakthrough in performance has not yet been achieved due to the challenges associated with proper control of their fabrication conditions. A systematic study on the effects of additive incorporation on the optoelectronic properties of the CTLs and the ALs and how they influence the PCE and stability of FA-rich PSCs needs to be explored further. This research work is aimed at investigating the influence of additives incorporated into the electron transport layer (ETL) and the AL on their optoelectronic properties and performance metrics of the resulting planar FA-rich mixed lead-halide PSCs. The additive considered for the ETL was tin oxide (SnO_2) owing to its high optical transparency and high electron mobility which was expected to improve the electron transport and the PCE of PSCs. For the AL, Cesium Bromide (CsBr) and Polyethylene Oxide (PEO) additives were used because of their good defect passivation abilities and low costs. The study involved the processing of the thin films of ETL and perovskite AL and studying the evolution of their optoelectronic properties with the incorporation of different proportions of additives. The full PSC devices incorporating the modified ETLs/ALs were then fabricated and the effects of the different modification strategies on their PV performance parameters were studied.

1.3 Problem statement

Despite the commendable progress that has been achieved as far as the PCE and stability of PSCs is concerned, some issues need to be addressed to allow for their commercialization. First, the efficiency of PSC is still limited by non-radiative recombination losses that arise due to non-optimized properties of the CTLs, AL, and the interfaces between them. The presence of defects in the bulk and surfaces of the AL and CTLs in PSCs hinder proper extraction and transportation of charge carriers (electrons and holes) leading to photovoltage and fill factor

losses which consequently reduce their PCEs. Secondly, the PCE of PSCs undergoes rapid degradation due to intrinsic processes that take place in the device and exposure to the conditions in the real outdoor environment which include moisture, oxygen, UV radiation, high temperature, and mechanical stresses. The rapid degradation in performance coupled with the anomalous current density voltage (J-V) hysteresis makes reproducibility in PCE calculations to be a difficult task. These issues have also been attributed to the non-ideal properties of the AL and the CTLs. Addressing these challenges requires further optimization of the properties of the AL and CTLs with a systematic investigation of how the optimization techniques influence the optoelectronic properties and the overall behavior of the ensuing PSC device.

1.4 Objectives of the study

The primary objective of this work is to study the effects of additives on the charge transport kinetics and the performance metrics of planar FA-rich mixed lead halide PSC.

The specific objectives of this research were to:

(i) Investigate the evolution of the optoelectronic properties and PV performance characteristics of TiO_2-based FA-rich mixed lead halide PSC with the incorporation of tin oxide in the ETL.

(ii) Assess the impacts of nanoscale CsBr layer on the PV parameters and long-term stability of FA-rich PSC.

(iii) Analyze the effects of PEO additive on the photophysical properties and performance characteristics of FA-rich PSC.

1.5 Justification of the study

Though the performance of PSCs has improved tremendously over the last few years, a breakthrough in the quest for cheap and efficient solar cells that can withstand ambient conditions for a longer period has not been achieved. It is therefore imperative to carry out more studies that are geared towards improving the charge extraction and transportation phenomena in PSCs in order to suppress the non-radiative recombination and performance degradation pathways. Modification of the bulk and surface properties of CTLs and AL through the incorporation of additives is the best method to engineer their charge transport properties and to reduce photovoltage and fill losses in PSCs.

The incorporation of additives is therefore important in the efforts to improve the PCE in PSCs. However, the influence of the additives on the charge carrier dynamics and performance of FA-rich PSC need to be fully understood. An in-depth investigation of the evolution of the properties of TiO_2-based ETL and the charge carrier dynamics in perovskite films with the proportion of SnO_2 additive in the ETL can provide leeway for further performance optimization in FA-rich PSCs. Furthermore, the role of CsBr and PEO additives in the AL on the optoelectronic properties and performance characteristics of these solar cells need further investigation.

1.6 Scope of this work

The main aim of this research was to investigate the influence of additives; incorporated in the ETL and the AL; on the performance characteristics of planar FA-rich PSCs. The study involved the fabrication of the thin films of ETL and/or AL on FTO-coated glass substrates and examining the variation of their optoelectronic properties with the proportions of the

additives. The evolution of the PV performance parameters of FA-rich PSC with the proportion of the additives in the ETL/AL was studied with the main aim of establishing the proportion of the additives that will give better performance.

First, the TiO_2-based ETL was modified with different proportions of SnO_2 so as to improve its charge extraction and transport properties for improved performance in FA-rich PSC. After obtaining the proportion of SnO_2 in the ETL that gave better PV performance characteristics, further performance optimization strategies involving the incorporation of CsBr and PEO additives in the AL were explored. The evolution of the structural, morphological, and optoelectronic properties of the AL thin films and their charge carrier dynamics with the proportion of the additives was then investigated. Finally, planar FA-rich PSCs; with the right proportion of SnO_2 in the ETL; were fabricated with CsBr and PEO additives in their ALs so that the overall effect of these additives on the PV performance characteristics could be understood. Furthermore, a comparison was made between the PSCs with the modified and pristine ALs in terms of their operational stabilities.

1.7 Dissertation outline

This dissertation consists of seven sections structured in the form of chapters with each chapter discussing different aspects of PSCs. Chapter one is the introductory chapter that gives a brief background on the global energy scenario, the need for renewable energy resources, the evolution of photovoltaic technology, the problem statement, and the justification of this study. Chapter two is mainly about the literature review where the structure, the working principles, the research progress, and the unresolved issues on perovskite solar cells are discussed. The chapter begins with a review of fundamental semiconductor physics so as to help the reader understand the basic operating principles of a

solar cell. The chapter then proceeds to highlight the fundamental aspects of PSCs, the various research works on PSCs that have been carried out to date, and the issues that remain unresolved. In chapter three, a brief discussion of the methodology and materials characterization techniques is given with emphasis being laid on the working principles of the characterization equipment used.

Chapter four, chapter five, and chapter six are based on the published research articles that are derived from the objectives of this research. In Chapter four, the modification of TiO_2-based ETL as a strategy to enhance its charge extraction and transport abilities in FA-rich PSC is discussed. Emphasis was given to the influence of SnO_2 incorporation on the micro-structural and optoelectronic properties of TiO_2-based ETL and PV performance characteristics of FA-rich PSC. Chapter five and chapter six respectively present the results on the effects of thermally evaporated CsBr layer and PEO additive on the PV performance characteristics and stability of FA-rich PSCs while the last chapter (Chapter seven) gives a summary of the concluding remarks and recommendations for future work based on the results of the studies that were carried out.

1.8 References

Administration, U. S. E. I. (2018). Annual Energy Outlook 2018. *Journal of Physics A: Mathematical and Theoretical*. https://doi.org/DOE/EIA-0383(2017)

Administration, U. S. E. I. (2019). International Energy Outlook 2019 with projections to 2050. *Choice Reviews Online*. https://doi.org/10.5860/CHOICE.44-3624

Africa Energy Outlook 2019 – Analysis - IEA. (n.d.). Retrieved November 9, 2021, from https://www.iea.org/reports/africa-energy-outlook-2019

Akihiro Kojima, Kenjiro Teshima, Yasuo Shirai, and T. M. (2009). Organometal Halide Perovskites as Visible-Light Sensitizers for Photovoltaic Cells. *J Am Chem Soc*. https://doi.org/10.1021/ja809598r

Aquila, G., Pamplona, E. de O., Queiroz, A. R. de, Rotela Junior, P., & Fonseca, M. N. (2017). An overview of incentive policies for the expansion of renewable energy generation in electricity power systems and the Brazilian experience. In *Renewable and Sustainable Energy Reviews*. https://doi.org/10.1016/j.rser.2016.12.013

Asghar, M. I., Zhang, J., Wang, H., & Lund, P. D. (2017). Device stability of perovskite solar cells – A review. In *Renewable and Sustainable Energy Reviews*. https://doi.org/10.1016/j.rser.2017.04.003

Ávila, J., Momblona, C., Boix, P. P., Sessolo, M., & Bolink, H. J. (2017). Vapor-Deposited Perovskites: The Route to High-Performance Solar Cell Production? In *Joule*. https://doi.org/10.1016/j.joule.2017.07.014

Azam, M., Liu, K., Sun, Y., Wang, Z., Liang, G., Qu, S., Fan, P., & Wang, Z. (2020). Recent advances in defect passivation of perovskite active layer via additive engineering: A review. In *Journal of Physics D: Applied Physics*. https://doi.org/10.1088/1361-6463/ab6f8d

Barton, J. P., & Infield, D. G. (2004). Energy storage and its use with intermittent renewable energy. *IEEE Transactions on Energy Conversion*, *19*(2), 441–448. https://doi.org/10.1109/TEC.2003.822305

Bi, D., Luo, J., Zhang, F., Magrez, A., Athanasopoulou, E. N., Hagfeldt, A., & Grätzel, M. (2017). Morphology Engineering: A Route to Highly Reproducible and High Efficiency Perovskite Solar Cells. *ChemSusChem*, *10*(7). https://doi.org/10.1002/cssc.201601387

Boyd, C. C., Cheacharoen, R., Leijtens, T., & McGehee, M. D. (2019). Understanding Degradation Mechanisms and Improving Stability of Perovskite Photovoltaics. In *Chemical Reviews*. https://doi.org/10.1021/acs.chemrev.8b00336

BP Energy Economics. (2018). 2018 BP Energy Outlook. *BP*. https://doi.org/10.1088/1757-899X/342/1/012091

Bush, K. A., Frohna, K., Prasanna, R., Beal, R. E., Leijtens, T., Swifter, S. A., & McGehee, M. D. (2018). Compositional Engineering for Efficient Wide Band Gap Perovskites with Improved Stability to Photoinduced Phase Segregation. *ACS Energy Letters*. https://doi.org/10.1021/acsenergylett.7b01255

Cannavale, A., Hórantner, M., Eperon, G. E., Snaith, H. J., Fiorito, F., Ayr, U., & Martellotta, F. (2017). Building integration of semitransparent perovskite-based solar cells: Energy performance and visual comfort assessment. *Applied Energy*. https://doi.org/10.1016/j.apenergy.2017.03.011

Chen, B., Yang, M., Priya, S., & Zhu, K. (2016). Origin of J-V Hysteresis in Perovskite Solar Cells. In *Journal of Physical Chemistry Letters*. https://doi.org/10.1021/acs.jpclett.6b00215

Courtier, N. E., Cave, J. M., Foster, J. M., Walker, A. B., & Richardson, G. (2019). How transport layer properties affect perovskite solar cell performance: Insights from a coupled charge transport/ion migration model. *Energy and Environmental Science*. https://doi.org/10.1039/c8ee01576g

Da, Y., Xuan, Y., & Li, Q. (2018). Quantifying energy losses in planar perovskite solar cells. *Solar Energy Materials and Solar Cells*. https://doi.org/10.1016/j.solmat.2017.09.002

Dai, T., Cao, Q., Yang, L., Aldamasy, M. H., Li, M., Liang, Q., Lu, H., Dong, Y., & Yang, Y. (2021). Strategies for high-performance large-area perovskite solar cells toward commercialization. *Crystals*, *11*(3). https://doi.org/10.3390/CRYST11030295

Della Gaspera, E., Peng, Y., Hou, Q., Spiccia, L., Bach, U., Jasieniak, J. J., & Cheng, Y. B. (2015). Ultra-thin high efficiency semitransparent perovskite solar cells. *Nano Energy*. https://doi.org/10.1016/j.nanoen.2015.02.028

Energy Information Administration. (2019). International Energy Outlook. *Outlook*. https://doi.org/https://www.eia.gov/outlooks/ieo/pdf/ieo2019.pdf

Filip, M. R., Liu, X., Miglio, A., Hautier, G., & Giustino, F. (2018). Phase Diagrams and Stability of Lead-Free Halide Double Perovskites $Cs_2BB'X_6$: B = Sb and Bi, B′ = Cu, Ag, and Au, and X = Cl, Br, and i. *Journal of Physical Chemistry C*. https://doi.org/10.1021/acs.jpcc.7b10370

Gopal Krishna, B., Rathore, G. S., Shukla, N., & Tiwari, S. (2021). Perovskite solar cells: A review of architecture, processing methods, and future prospects. *Hybrid Perovskite Composite Materials*, 375–412. https://doi.org/10.1016/B978-0-12-819977-0.00018-4

Green, M. A. (2002). Third generation photovoltaics: Solar cells for 2020 and beyond. *Physica E: Low-Dimensional Systems and Nanostructures*. https://doi.org/10.1016/S1386-9477(02)00361-2

Green, M. A., & Bremner, S. P. (2017). Energy Conversion Approaches and Materials for High Efficiency Photovoltaics. *Nature Materials*. https://doi.org/10.1038/nmat4676

Green, M. A., Hishikawa, Y., Dunlop, E. D., Levi, D. H., Hohl-Ebinger, J., & Ho-Baillie, A.

W. Y. (2018). Solar cell efficiency tables (version 51). *Prog. Photovolt: Res. Appl.* https://doi.org/10.1002/pip.2978

Green, M. A., Ho-Baillie, A., & Snaith, H. J. (2014). The emergence of perovskite solar cells. *Nat Photon*. https://doi.org/10.1038/nphoton.2014.134

Hanusch, F. C., Wiesenmayer, E., Mankel, E., Binek, A., Angloher, P., Fraunhofer, C., Giesbrecht, N., Feckl, J. M., Jaegermann, W., Johrendt, D., Bein, T., & Docampo, P. (2014). Efficient planar heterojunction perovskite solar cells based on formamidinium lead bromide. *Journal of Physical Chemistry Letters*. https://doi.org/10.1021/jz501237m

IPCC. (2014). Climate Change 2014: Mitigation of Climate Change. In *Working Group III Contribution to the Fifth Assessment Report of the Intergovernmental Panel on Climate Change*. https://doi.org/10.1017/CBO9781107415416

Jeon, N. J., Noh, J. H., Yang, W. S., Kim, Y. C., Ryu, S., Seo, J., & Seok, S. Il. (2015). Compositional engineering of perovskite materials for high-performance solar cells. *Nature*. https://doi.org/10.1038/nature14133

Joo, S. H., & Choi, H. W. (2021). Compositional Engineering of $FAPbI_3$ Perovskite Added MACl with $MAPbBr_3$ or $FAPbBr_3$. *Coatings 2021, Vol. 11, Page 1184*, *11*(10), 1184. https://doi.org/10.3390/COATINGS11101184

Kabir, E., Kumar, P., Kumar, S., Adelodun, A. A., & Kim, K. H. (2018). Solar energy: Potential and future prospects. In *Renewable and Sustainable Energy Reviews*. https://doi.org/10.1016/j.rser.2017.09.094

Kang, D. H., & Park, N. G. (2019). On the Current–Voltage Hysteresis in Perovskite Solar Cells: Dependence on Perovskite Composition and Methods to Remove Hysteresis. In *Advanced Materials*. https://doi.org/10.1002/adma.201805214

Kim, H. S., Hagfeldt, A., & Park, N. G. (2019). Morphological and compositional progress in halide perovskite solar cells. *Chemical Communications*. https://doi.org/10.1039/c8cc08653b

Kim, J. H., Liang, P. W., Williams, S. T., Cho, N., Chueh, C. C., Glaz, M. S., Ginger, D. S., & Jen, A. K. Y. (2015). High-performance and environmentally stable planar heterojunction perovskite solar cells based on a solution-processed copper-doped nickel oxide hole-transporting layer. *Advanced Materials*. https://doi.org/10.1002/adma.201404189

Koh, T. M., Fu, K., Fang, Y., Chen, S., Sum, T. C., Mathews, N., Mhaisalkar, S. G., Boix, P. P., & Baikie, T. (2014). Formamidinium-containing metal-halide: An alternative material for near-IR absorption perovskite solar cells. *Journal of Physical Chemistry C*, *118*(30), 16458–16462. https://doi.org/10.1021/JP411112K

Lan, D. (2019). The physics of ion migration in perovskite solar cells: Insights into hysteresis, device performance, and characterization. *Progress in Photovoltaics: Research and Applications*. https://doi.org/10.1002/pip.3203

Le Corre, V. M., Stolterfoht, M., Perdigón Toro, L., Feuerstein, M., Wolff, C., Gil-Escrig, L., Bolink, H. J., Neher, D., & Koster, L. J. A. (2019). Charge Transport Layers Limiting the Efficiency of Perovskite Solar Cells: How to Optimize Conductivity, Doping, and Thickness. *ACS Applied Energy Materials*. https://doi.org/10.1021/acsaem.9b00856

Li, G., Zhu, R., & Yang, Y. (2012). Polymer solar cells. *Nat. Photon.* https://doi.org/10.1038/nphoton.2012.11

Li, Y., Ji, L., Liu, R., Zhang, C., Mak, C. H., Zou, X., Shen, H. H., Leu, S. Y., & Hsu, H. Y. (2018). A review on morphology engineering for highly efficient and stable hybrid perovskite solar cells. In *Journal of Materials Chemistry A*. https://doi.org/10.1039/c8ta04120b

Li, Z., Klein, T. R., Kim, D. H., Yang, M., Berry, J. J., Van Hest, M. F. A. M., & Zhu, K. (2018). Scalable fabrication of perovskite solar cells. In *Nature Reviews Materials*. https://doi.org/10.1038/natrevmats.2018.17

Li, Z., Yang, M., Park, J. S., Wei, S. H., Berry, J. J., & Zhu, K. (2016). Stabilizing Perovskite Structures by Tuning Tolerance Factor: Formation of Formamidinium and Cesium Lead Iodide Solid-State Alloys. *Chemistry of Materials*. https://doi.org/10.1021/acs.chemmater.5b04107

Liu, F., Wang, W., Wang, L., & Yang, G. (2013). Working principles of solar and other energy conversion cells. *Nanomaterials and Energy*. https://doi.org/10.1680/nme.12.00024

Liu, G., Zheng, H., Xu, X., Zhu, L., Alsaedi, A., Hayat, T., Pan, X., & Dai, S. (2018). Efficient solar cells with enhanced humidity and heat stability based on benzylammonium–caesium–formamidinium mixed-dimensional perovskites. *Journal of Materials Chemistry A*, *6*(37), 18067–18074. https://doi.org/10.1039/C8TA04936J

Matsui, T., Yamamoto, T., Nishihara, T., Morisawa, R., Yokoyama, T., Sekiguchi, T., & Negami, T. (2019). Compositional Engineering for Thermally Stable, Highly Efficient Perovskite Solar Cells Exceeding 20% Power Conversion Efficiency with 85 °C/85% 1000 h Stability. *Advanced Materials*. https://doi.org/10.1002/adma.201806823

McKinsey Global Institute. (2019). Global Energy Perspective 2019 : Reference Case. *Energy Insights*.

Min, H., Lee, D. Y., Kim, J., Kim, G., Lee, K. S., Kim, J., Paik, M. J., Kim, Y. K., Kim, K. S., Kim, M. G., Shin, T. J., & Il Seok, S. (2021). Perovskite solar cells with atomically coherent interlayers on SnO_2 electrodes. *Nature 2021 598:7881*, *598*(7881), 444–450. https://doi.org/10.1038/s41586-021-03964-8

Muscarella, L. A., Petrova, D., Jorge Cervasio, R., Farawar, A., Lugier, O., McLure, C., Slaman, M. J., Wang, J., Ehrler, B., Von Hauff, E., & Williams, R. M. (2019). Air-Stable and Oriented Mixed Lead Halide Perovskite (FA/MA) by the One-Step Deposition Method Using Zinc Iodide and an Alkylammonium Additive. *ACS Applied Materials and Interfaces*. https://doi.org/10.1021/acsami.9b03810

NREL. (2019). *Best Research-Cell Efficiency Chart*. National Renewable Enery Laboratory.

Ono, L. K., Juarez-Perez, E. J., & Qi, Y. (2017). Progress on Perovskite Materials and Solar Cells with Mixed Cations and Halide Anions. In *ACS Applied Materials and Interfaces*. https://doi.org/10.1021/acsami.7b06001

Ono, L. K., & Qi, Y. (2016). Surface and Interface Aspects of Organometal Halide Perovskite Materials and Solar Cells. *J. Phys. Chem. Lett*. https://doi.org/10.1021/acs.jpclett.6b01951

Onyeji-Nwogu, I. (2017). Harnessing and Integrating Africa's Renewable Energy Resources. In *Renewable Energy Integration: Practical Management of Variability, Uncertainty, and Flexibility in Power Grids: Second Edition*. https://doi.org/10.1016/B978-0-12-809592-8.00003-2

Parida, B., Iniyan, S., & Goic, R. (2011). A review of solar photovoltaic technologies. In *Renewable and Sustainable Energy Reviews*. https://doi.org/10.1016/j.rser.2010.11.032

Park, N. G. (2016). Crystal growth engineering for high efficiency perovskite solar cells. *CrystEngComm*. https://doi.org/10.1039/c6ce00813e

Perera, F. (2018). Pollution from fossil-fuel combustion is the leading environmental threat to global pediatric health and equity: Solutions exist. In *International Journal of Environmental Research and Public Health*. https://doi.org/10.3390/ijerph15010016

Pham, N. D., Zhang, C., Tiong, V. T., Zhang, S., Will, G., Bou, A., Bisquert, J., Shaw, P. E., Du, A., Wilson, G. J., & Wang, H. (2019). Tailoring Crystal Structure of FA 0.83 Cs 0.17 PbI 3 Perovskite Through Guanidinium Doping for Enhanced Performance and Tunable Hysteresis of Planar Perovskite Solar Cells. *Advanced Functional Materials*. https://doi.org/10.1002/adfm.201806479

Polman, A., Knight, M., Garnett, E. C., Ehrler, B., & Sinke, W. C. (2016). Photovoltaic materials: Present efficiencies and future challenges. In *Science*. https://doi.org/10.1126/science.aad4424

REN21. (2017). RENEWABLES 2017 GLOBAL STATUS REPORT. In *Renewable and Sustainable Energy Reviews*. https://doi.org/10.1016/j.rser.2016.09.082

REN21. (2018). Renewables 2018 Global Status Report (Paris: REN21 Secretariat). In *Paris: Renewable energy policy network for the 21st Century*. https://doi.org/978-3-9818911-3-3

Rolston, N., Watson, B. L., Bailie, C. D., McGehee, M. D., Bastos, J. P., Gehlhaar, R., Kim, J. E., Vak, D., Mallajosyula, A. T., Gupta, G., Mohite, A. D., & Dauskardt, R. H. (2016). Mechanical integrity of solution-processed perovskite solar cells. *Extreme Mechanics Letters*. https://doi.org/10.1016/j.eml.2016.06.006

Roy, P., Kumar Sinha, N., Tiwari, S., & Khare, A. (2020). A review on perovskite solar cells: Evolution of architecture, fabrication techniques, commercialization issues and status. *Solar Energy*, *198*, 665–688. https://doi.org/10.1016/J.SOLENER.2020.01.080

Saidaminov, M. I., Kim, J., Jain, A., Quintero-Bermudez, R., Tan, H., Long, G., Tan, F., Johnston, A., Zhao, Y., Voznyy, O., & Sargent, E. H. (2018). Suppression of atomic vacancies via incorporation of isovalent small ions to increase the stability of halide perovskite solar cells in ambient air. *Nature Energy*. https://doi.org/10.1038/s41560-018-0192-2

Salim, K. M. M., Masi, S., Gualdrón-Reyes, A. F., Sánchez, R. S., Barea, E. M., Krecmarová, M., Sánchez-Royo, J. F., & Mora-Seró, I. (2021). Boosting Long-Term Stability of Pure Formamidinium Perovskite Solar Cells by Ambient Air Additive Assisted Fabrication. *ACS Energy Letters*, *6*(10), 3511–3521. https://doi.org/10.1021/ACSENERGYLETT.1C01311/SUPPL_FILE/NZ1C01311_SI_001.PDF

Sharma, S., Jain, K. K., & Sharma, A. (2015). Solar Cells: In Research and Applications—A Review. *Materials Sciences and Applications*. https://doi.org/10.4236/msa.2015.612113

Shen, H., Duong, T., Wu, Y., Peng, J., Jacobs, D., Wu, N., Weber, K., White, T., & Catchpole, K. (2018). Metal halide perovskite: a game-changer for photovoltaics and solar devices via a tandem design. In *Science and Technology of Advanced Materials*. https://doi.org/10.1080/14686996.2017.1422365

Shen, L., Song, P., Zheng, L., Liu, K., Lin, K., Tian, W., Luo, Y., Tian, C., Xie, L., & Wei, Z. (2021). Perovskite-type stabilizers for efficient and stable formamidinium-based lead iodide perovskite solar cells. *Journal of Materials Chemistry A*, *9*(36), 20807–20815. https://doi.org/10.1039/D1TA05537B

Shen, Q., Ogomi, Y., Chang, J., Toyoda, T., Fujiwara, K., Yoshino, K., Sato, K., Yamazaki, K., Akimoto, M., Kuga, Y., Katayama, K., & Hayase, S. (2015). Optical absorption, charge separation and recombination dynamics in Sn/Pb cocktail perovskite solar cells and their relationships to photovoltaic performances. *Journal of Materials Chemistry A*. https://doi.org/10.1039/c5ta01246e

Shi, Z., & Jayatissa, A. H. (2018). Perovskites-based solar cells: A review of recent progress, materials and processing methods. *Materials*. https://doi.org/10.3390/ma11050729

Shi, Zhengqi, & Jayatissa, A. H. (2018). Perovskites-based solar cells: A review of recent progress, materials and processing methods. In *Materials*. https://doi.org/10.3390/ma11050729

Stern, D. I. (2011). The role of energy in economic growth. *Annals of the New York Academy of Sciences*. https://doi.org/10.1111/j.1749-6632.2010.05921.x

Stolterfoht, M., Caprioglio, P., Wolff, C. M., Márquez, J. A., Nordmann, J., Zhang, S., Rothhardt, D., Hörmann, U., Amir, Y., Redinger, A., Kegelmann, L., Zu, F., Albrecht, S., Koch, N., Kirchartz, T., Saliba, M., Unold, T., & Neher, D. (2019). The impact of energy alignment and interfacial recombination on the internal and external open-circuit voltage of perovskite solar cells. *Energy and Environmental Science*. https://doi.org/10.1039/c9ee02020a

Supreeth, A., & Shreya, Y. S. (2016). Perovskite solar cells : a review. *International Journal of Engineering Development and Research*.

Tian, Y., Zhou, C., Worku, M., Wang, X., Ling, Y., Gao, H., Zhou, Y., Miao, Y., Guan, J., & Ma, B. (2018). Highly Efficient Spectrally Stable Red Perovskite Light-Emitting Diodes. *Advanced Materials*. https://doi.org/10.1002/adma.201707093

UNDP. (2015). Sustainable Development Goals (SDGs) | UNDP. In *2015*.

Wali, Q., Iftikhar, F. J., Khan, M. E., Ullah, A., Iqbal, Y., & Jose, R. (2020). Advances in stability of perovskite solar cells. In *Organic Electronics*. https://doi.org/10.1016/j.orgel.2019.105590

Wang, B., Iocozzia, J., Zhang, M., Ye, M., Yan, S., Jin, H., Wang, S., Zou, Z., & Lin, Z. (2019). The charge carrier dynamics, efficiency and stability of two-dimensional material-based perovskite solar cells. *Chemical Society Reviews*, *48*(18), 4854–4891. https://doi.org/10.1039/C9CS00254E

Wang, D., Wright, M., Elumalai, N. K., & Uddin, A. (2016). Stability of perovskite solar cells. In *Solar Energy Materials and Solar Cells*. https://doi.org/10.1016/j.solmat.2015.12.025

Wang, H., Zhang, H., Chueh, C. C., Zhao, T., Mao, C., Chen, W., & Jen, A. K. Y. (2018). Enhanced crystallization and performance of formamidinium lead triiodide perovskite solar cells through PbI_2-$SrCl_2$ modulation. *Materials Today Energy*. https://doi.org/10.1016/j.mtener.2017.10.002

Wang, Z., Shi, Z., Li, T., Chen, Y., & Huang, W. (2017). Stability of Perovskite Solar Cells: A Prospective on the Substitution of the A Cation and X Anion. In *Angewandte Chemie - International Edition*. https://doi.org/10.1002/anie.201603694

Wolff, C. M., Caprioglio, P., Stolterfoht, M., & Neher, D. (2019). Nonradiative Recombination in Perovskite Solar Cells: The Role of Interfaces. *Advanced Materials*. https://doi.org/10.1002/adma.201902762

World Energy Council. (2016). World Energy Trilemma 2016 Defining Measures To Accelarate the Energy Transition. *World Energy Council Report*.

Xiao, Z., & Yan, Y. (2017). Progress in Theoretical Study of Metal Halide Perovskite Solar Cell Materials. *Advanced Energy Materials*, *7*(22), 1701136. https://doi.org/10.1002/AENM.201701136

Yang, J., Chen, S., Xu, J., Zhang, Q., Liu, H., Liu, Z., & Yuan, M. (2019). A Review on Improving the Quality of Perovskite Films in Perovskite Solar Cells via the Weak Forces Induced by Additives. *Applied Sciences 2019, Vol. 9, Page 4393*, *9*(20), 4393. https://doi.org/10.3390/APP9204393

Yin, W., Pan, L., Yang, T., & Liang, Y. (2016). Recent advances in interface engineering for planar heterojunction perovskite solar cells. In *Molecules*. https://doi.org/10.3390/molecules21070837

Yuan, Y., & Huang, J. (2016). Ion Migration in Organometal Trihalide Perovskite and Its Impact on Photovoltaic Efficiency and Stability. *Accounts of Chemical Research*. https://doi.org/10.1021/acs.accounts.5b00420

Zhang, Fei, & Zhu, K. (2019). Additive Engineering for Efficient and Stable Perovskite Solar Cells. In *Advanced Energy Materials*. https://doi.org/10.1002/aenm.201902579

Zhang, Fengying, Yang, B., Li, Y., Deng, W., & He, R. (2017). Extra long electron-hole diffusion lengths in $CH_3NH_3PbI_{3-x}Cl_x$ perovskite single crystals. *Journal of Materials Chemistry C*. https://doi.org/10.1039/c7tc02802d

Zhao, Y., Tan, H., Yuan, H., Yang, Z., Fan, J. Z., Kim, J., Voznyy, O., Gong, X., Quan, L. N., Tan, C. S., Hofkens, J., Yu, D., Zhao, Q., & Sargent, E. H. (2018). Perovskite seeding growth of formamidinium-lead-iodide-based perovskites for efficient and stable solar cells. *Nature Communications*. https://doi.org/10.1038/s41467-018-04029-7

Zhou, X., Zhang, Y., Kong, W., Hu, M., Zhang, L., Liu, C., Li, X., Pan, C., Yu, G., Cheng, C., & Xu, B. (2018). Crystallization manipulation and morphology evolution for highly efficient perovskite solar cell fabrication: Via hydration water induced intermediate phase formation under heat assisted spin-coating. *Journal of Materials Chemistry A*. https://doi.org/10.1039/c7ta08947c

Zuo, C., Bolink, H. J., Han, H., Huang, J., Cahen, D., & Ding, L. (2016). Advances in perovskite solar cells. In *Advanced Science*. https://doi.org/10.1002/advs.201500324

CHAPTER TWO

LITERATURE REVIEW

2.1 Introduction

In this section, a brief background on semiconductors, general working principles of a p-n junction solar cell, the structure and working principles of PSC, the recent progress on efficiency and stability improvement strategies in PSCs is surveyed. The latest theoretical and experimental research works on PSCs are also reviewed with a view to identifying the existing research gaps and areas for further improvement.

2.2 Semiconductor physics

A semiconductor is a material whose electrical properties are intermediate between those of a conductor and an insulator. A pure (intrinsic) semiconductor has an equal concentration of electrons and holes and the charge carriers are only created through optical or thermal excitation of electrons from the valence band to the conduction band. The electrical properties of a semiconductor can be enhanced by changing the electron and hole concentration at thermal equilibrium through the process of doping, giving rise to two classes of semiconductors namely the n-type semiconductor (having excess electrons) and p-type semiconductor (having excess holes) (Martín-Palma & Martínez-Duart, 2017). Due to the difference in the concentration of the charge carriers, the position of the Fermi level (E_f) shifts towards the band edges i.e near the conduction band for an n-type semiconductor and close to the valence band for a p-type semiconductor.

A semiconductor can also be classified as a direct or indirect bandgap semiconductor

depending on the excitation dynamics of electrons from the valence band to the conduction band. Unlike the indirect bandgap semiconductor, a direct bandgap semiconductor has the minimum energy level of its conduction band aligning with the maximum energy level of the valence band thus the possibility of radiative recombination occurring is higher. However, direct bandgap semiconductors possess high light absorption coefficients, which allow very thin layers of semiconducting materials to absorb light thereby reducing their production costs.

2.2.1 The p-n junction

When a p-type semiconductor is joined to an n-type semiconductor, a p-n junction is formed. The different concentrations of charge carriers generate a diffusion gradient that will see the electrons from the n-type semiconductor region diffuse to the p-type semiconductor region. Similarly, the holes will diffuse to the p-type region until a built-in potential is created between the two regions that prevent further diffusion of the charge carriers. A depletion (space charge) region is therefore created between the two regions as shown in Figure 2.1 (a). This makes the p-n junction behave differently under different bias conditions. The width of the depletion region is controlled by the doping concentrations in the p and n regions. When an intrinsic semiconductor is sandwiched between two oppositely doped semiconductors, a p-i-n or n-i-p junction is formed as shown in Figure 2.1 (b). This configuration is important in solar cells as it enhances light absorption which is important in its performance. When the three semiconductors are in contact, the Fermi levels of the n and p regions are aligned, and a potential difference is developed across the intrinsic region.

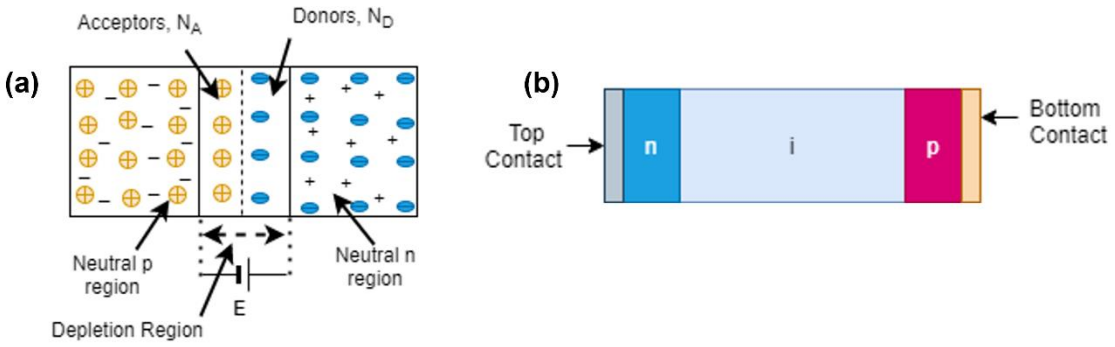

Figure 2.1: Sketch of a (a) p-n junction (b) n-i-p junction

2.2.2 Theory of solar cells

A solar cell; also known as a photovoltaic (PV) cell; is a device that absorbs the incident light and converts it into direct electrical energy through the photovoltaic effect. It is basically a p-n junction diode formed by combining oppositely doped thin films of semiconductor materials (Nelson, 2003). There are three basic principles of operation of a solar cell namely: light absorption, charge carrier generation, charge carrier separation, transportation, and collection at electrodes.

In a solar cell, the charge carriers are generated in the AL upon absorption of light photons whose energy is enough to excite electrons from the valence band to the conduction band. The generation process is mainly dependent on the intensity of the incident light, the optical properties of the AL, and those of the window layers which are all functions of wavelength (λ). The generation rate (G) is usually calculated by integrating the product of the incident photon flux (ϕ) and the absorption coefficient (α) of the AL as in equation (2.1):

$$G(\lambda, x) = \int \alpha(\lambda)\phi(\lambda)e^{-(\alpha(\lambda)x)}d\lambda \qquad (2.1)$$

where x is the thickness of the AL.

Recombination is the reverse process of charge carrier generation where the charge carriers come together and annihilate each other. It is an undesirable process in a solar cell that leads to loss of charge carriers thus reducing its PCE. To suppress recombination in solar cells, efficient charge carrier separation is required. The mechanisms of charge carrier separation may vary for different types of solar cells depending on the nature of its AL (Kirchartz et al., 2015). Once the charge carriers are separated, the built-in asymmetry in the solar cell ensures that they are selectively transported to their respective electrodes. However, due to the non-ideal material properties of the different components of a solar cell, recombination usually occurs either through radiative or non-radiative means. The total recombination rate (R) is the sum of the Shockley Read Hall recombination (R_{-SRH}), radiative recombination (R_{-Rad}), and Auger recombination (R_{-Aug}) (Schroder, 2005). R_{-SRH} is caused by the presence of defects that form trap states with energies near the band edges of a semiconductor. It is controlled majorly by the defect density (N_t) and their position within the bandgap (E_t) and is usually calculated using equation (2.2) (Shockley & Read, 1952).

$$R_{-SRH} = \frac{np - ni^2}{\tau_n (p + p_t) + \tau_p (n + n_t)} \tag{2.2}$$

The effective recombination lifetime ($\tau_{n,p}$) can be expressed as a function of N_t, the electron and hole capture cross-sections ($\sigma_{n,p}$) and the electron and hole thermal velocities ($v_{n,p}$) as in equation (2.3).

$$\tau_{n,p} = \frac{1}{\sigma_{n,p} N_t v_{n,p}} \tag{2.3}$$

The electron and hole carrier densities can be expressed as a function of the intrinsic carrier density (n_i) as per equations (2.4) and (2.5).

$$n_t = n_i \exp\left(\frac{E_t - E_i}{k_B T}\right) \tag{2.4}$$

$$p_t = n_i \exp\left(\frac{E_i - E_t}{k_B T}\right) \tag{2.5}$$

where E_i, E_t, k_B, and T denote the intrinsic Fermi level, defect Fermi level, the Boltzmann's constant, and temperature respectively.

The radiative (band-to-band) recombination (R_{-Rad}) occurs when an electron in the conduction band directly recombines with a hole in the valence band with the emission of a light photon. It is the dominant recombination mechanism in the direct bandgap semiconductors and is calculated using the expression given in equation (2.6).

$$R_{-RAD} = B(np - ni^2) \tag{2.6}$$

where B is bimolecular recombination constant.

On the other hand, Auger recombination (R_{-Aug}) is a recombination mechanism where an electron recombines with a hole in the valence band and the excess energy is given to a third carrier (i.e an electron in the conduction band) which eventually thermalizes to the conduction band edge. It mainly occurs at high doping levels and is usually calculated as in equation (2.7) (Richter et al., 2012).

$$R_{-AUG} = C_p(p^2 n - {p_o}^2 n_o) + C_n(n^2 p - {n_o}^2 p_o) \tag{2.7}$$

Where $C_{p,n}$ is the Auger capture probabilities for holes and electrons whereas p_o and n_o are the hole and electron carrier densities at equilibrium. A simplified diagram showing the charge carrier generation and recombination processes in a semiconductor is given in Figure 2.2 (Staub et al., 2018).

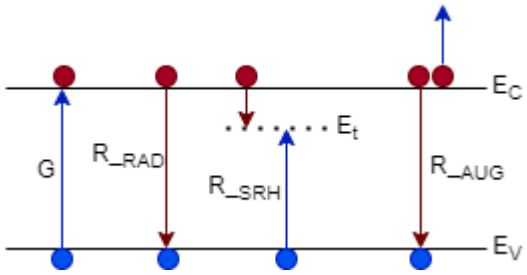

Figure 2.2: Generation and recombination processes

When the AL absorbs the incident sunlight, charge carriers are generated, separated by an in-built field, and transported to their respective electrodes via drift and diffusion mechanisms. The charge transport process can therefore be expressed mathematically using a combination of Poisson's equation, Fick's law of diffusion, and continuity equation as in equations (2.8) - (2.12).

$$\frac{\partial}{\partial x}\left(\varepsilon\frac{\partial V}{\partial x}\right)=-q\left(p-n+N_D{}^{+}-N_A{}^{-}\right) \tag{2.8}$$

Where ε, n, p, $N_D{}^{+}$ and $N_A{}^{-}$ are the dielectric constant, electron concentration, hole concentration, donor and acceptor concentration respectively. The current densities of electrons and holes are expressed as:

$$J_n=-qn\mu_n\frac{\partial V}{\partial x}+qD_n\frac{\partial n}{\partial x} \tag{2.9}$$

$$J_p=-qp\mu_p\frac{\partial V}{\partial x}-qD_p\frac{\partial p}{\partial x} \tag{2.10}$$

Where μ and D denote the charge carrier mobilities and diffusion coefficients respectively. The continuity equations for electrons and holes are expressed as:

$$\frac{1}{q}\frac{dJ_n}{dx}+G-R=0 \tag{2.11}$$

$$-\frac{1}{q}\frac{dJ_p}{dx}+G-R=0 \qquad (2.12)$$

The charge generation rate (G) and the recombination rate (R) are two competing mechanisms in a solar cell that determines its PV performance. It is desired that R should be greatly reduced so that more of the photo-generated charge carriers can be harnessed to generate electric current in a solar cell.

A solar cell is usually modeled as a diode using the equivalent circuit shown in Figure 2.3.

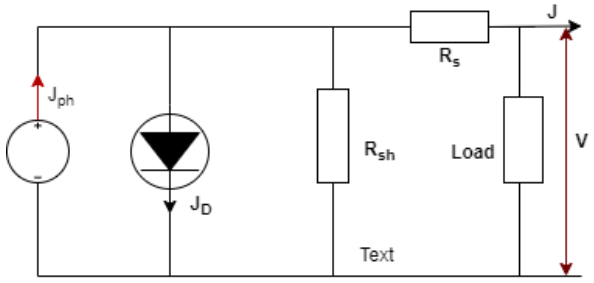

Figure 2.3: Equivalent Circuit of a solar cell

Under illumination, the J-V characteristics of a solar cell can be described using the Shockley diode equation given in equation (2.13).

$$J=J_{ph}-J_o\left(e^{\frac{q(V+JR_s)}{nK_BT}}-1\right)-\frac{V+JR_s}{R_{sh}} \qquad (2.13)$$

where J_{ph}, J_0, q, V, n and T are the photocurrent current, saturation current density, elementary charge, applied voltage, ideality factor, and temperature respectively. The current flowing through the diode in the dark is obtained by setting $J_{ph}=0$ in equation (2.13). Therefore, the current through the diode in the dark is given by:

$$J = -J_o\left(e^{\frac{q(V+JR_s)}{nK_BT}} - 1\right) - \frac{V+JR_s}{R_{sh}} \qquad (2.14)$$

Under illumination, the J-V characteristic of a solar cell is represented as shown in Figure 2.4

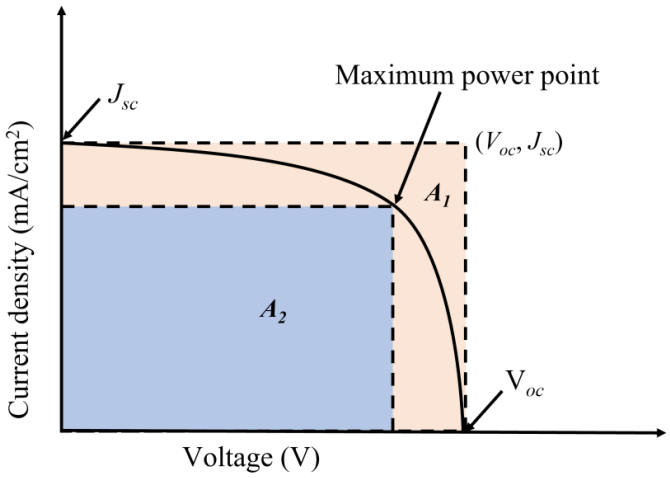

Figure 2.4: Typical J-V Curve of an illuminated solar cell

From the J-V curve, the PV parameters of the solar cell are extracted and the PCE (η) is calculated using equation (2.15) (Angmo et al., 2014).

$$\eta = \frac{V_{oc} \times J_{sc} \times FF}{P_{in}} \qquad (2.15)$$

Where J_{sc} is the short-circuit current density, V_{oc} is the open-circuit voltage, and FF is the fill factor. J_{sc} is the value of current density when V is zero and it is dependent upon the amount of light absorbed by the solar cell. FF is the ratio of the shaded area A_2 to A_1 (Figure 2.4) and denotes the degree of internal losses in a solar cell caused by recombination at material interfaces and also due to the series and shunt resistance resulting from processing defects in a solar cell (Angmo et al., 2014). P_{in} is the power of the incident solar radiation given by the product of the area of the solar cell (A) and the incident irradiance (I).

2.3 Structure and the working principles of PSC

A typical PSC is a multilayered device consisting of an optically active perovskite layer sandwiched between an n-type electron transport layer (ETL) and a p-type hole transport layer (HTL) with electrodes on either side (Jung & Park, 2015; Thakur et al., 2017). The AL is a very important component of PSC that absorbs the incident solar radiation and generates the charge carriers through the photovoltaic effect. The ETL and HTL; collectively termed as charge transport layers (CTLs); collect the charge carriers generated in the AL and transport them to their respective electrodes. Specifically, the ETL collects the photo-generated electrons and transports them to the anode which is a transparent conductive oxide (TCO); mostly Fluorine-doped Tin Oxide (FTO) or Indium-doped Tin Oxide (ITO); that is usually patterned on a rigid or flexible substrate material (Liu et al., 2017). On the other hand, the HTL collects the photo-generated holes and transports them to the cathode (mostly gold or silver).

PSCs are classified into regular (n-i-p) or inverted (p-i-n) device architectures depending on the position of the CTLs relative to the incident light. In PSC with n-i-p configuration, the ETL is deposited on the substrate first and forms the top layer that faces the incident light but in p-i-n device configuration, the HTL faces the incident light (T. Liu et al., 2016). The two categories can also be classified into mesoscopic or planar configurations depending on where the AL is deposited. In the mesoscopic configuration, the AL is deposited on top of a mesoporous scaffold usually meant to improve the interfacial contact and hence charge injection at the ETL/perovskite interface. The planar PSC configuration, however, uses a flat layer-by-layer stacking of components and exhibits higher charge carrier mobilities and slower trap-mediated recombination due to its larger perovskite grains (Pascoe et al., 2016). A

typical structure of a planar PSC with n-i-p configuration is as shown in Figure 2.5 (Hussain et al., 2018).

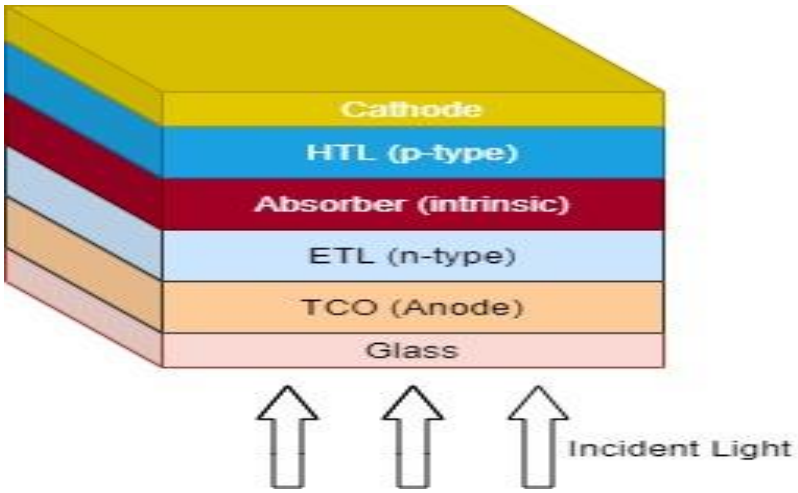

Figure 2.5: Structure of a PSC

When light is incident on PSC, charge carriers are generated in the AL, separated by a built-in electric potential, and transported in opposite directions to their respective electrodes through the ETL and HTL as shown in Figure 2.6 (Hussain et al., 2018; Lattante, 2014). To ensure proper charge selectivity at the interface between the CTLs and the AL, the conduction band offset (CBO) and the valence band offset (VBO) formed should be favorable for charge carrier extraction. This means that the conduction band edge of the ETL should be below that of the AL while the valence band edge of the HTL should be above that of the AL. The band offset between the band edges of the CTLs and that of the AL is a critical parameter in the charge injection in PSC (Ding et al., 2018).

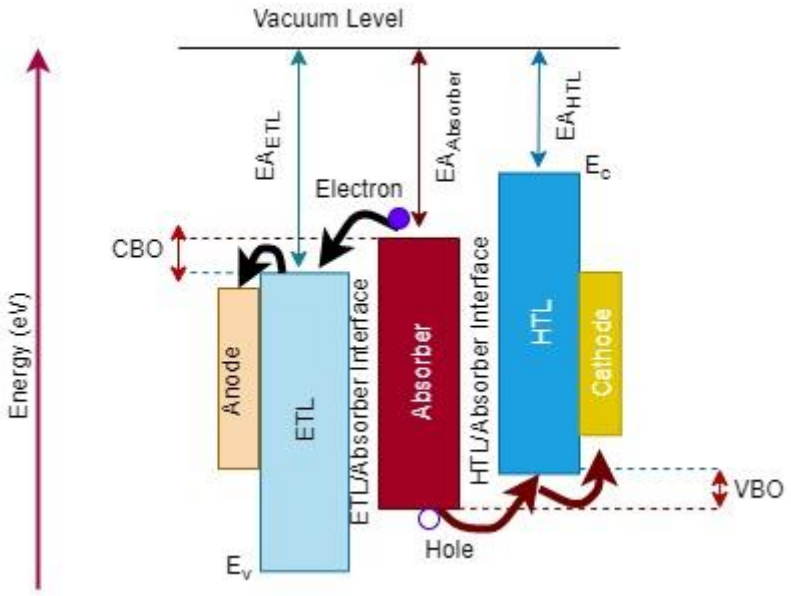

Figure 2.6: operating principles of PSC

Organo-metal halide PSCs have attracted research attention in photovoltaics since their inception; nearly a decade ago; due to their excellent optoelectronic properties, ease of processing, low cost, and their potential for a wide range of applications (Ponseca et al., 2014; Tian et al., 2018; Y. Zhao & Zhu, 2013). Research in these systems has mainly been focusing on three areas namely PCE improvement, stability improvement, and lead replacement in the AL.

2.4 Power conversion efficiency improvement

The PCE of a solar cell is defined as the ratio of its electrical power output (P_{out}) to the incident power from the sun (P_{in}). It is determined by biasing an illuminated solar cell and plotting its current density-voltage (J-V) characteristic curve from which the values of J_{sc}, V_{oc} and FF are obtained. The PCE is then calculated as per equation (2.15) (Angmo et al., 2014). The V_{oc}, FF, J_{sc} and η are the major indicators of the photovoltaic (PV)

performance of the solar cell and are termed as PV parameters. The values of these parameters are mainly controlled by the effectiveness of charge carrier generation and their collection probability which depend on the light absorption properties and ensuing charge carrier dynamics within the solar cell structure (Mori et al., 2014; Wurfel et al., 2015). Several strategies have been used to optimize the PV parameters of PSCs in order to achieve high PCE. These include bandgap and morphological engineering of AL through solvent engineering, compositional engineering and use of additives; engineering the CTLs and the interface they form with the AL as well as engineering the electrode materials (Azam et al., 2020; Bush et al., 2018; Seo et al., 2016; Xiao et al., 2017; Yin et al., 2016; Zhou et al., 2018).

2.4.1 Bandgap engineering

The bandgap of the AL material determines the amount of the incident light that can be absorbed by the solar cell and therefore dictates the maximum available output voltage and current density (Shockley & Queisser, 1961). A material with a smaller bandgap can absorb a larger portion of the solar spectrum and exhibit a larger photocurrent. However, its output voltage is lower leading to low energy conversion efficiency. On the other hand, a wide bandgap semiconductor material absorbs limited high-energy photons thereby generating a lower photocurrent, higher output voltage, and higher energy conversion efficiency. This means therefore that there is an optimum bandgap in a single junction solar cell for high efficiency which is usually around 1.3 eV (Zdanowicz et al., 2005).

Perovskite semiconductors can be fabricated with a wide range of bandgaps and can therefore be tuned to absorb a wide spectrum of light photons from ultraviolet to near-infrared regions. This bandgap tunability is a unique property that gives perovskite semiconductors a greater advantage over the other semiconductor materials as they can be fabricated with

bandgaps that match a particular spectrum of light (Ju et al., 2018). Their tunable optoelectronic properties make them ideal for fabricating multifunctional optoelectronic devices. Bandgap engineering has been used to tune the electronic and optical properties of the perovskite AL in PSCs mainly through compositional substitution (Bush et al., 2018; Eperon et al., 2016). The substitutions of the A and B site cations as well as the X site anion the AL can be used to directly alter their conduction band and valence band energies. For example, substituting a methylammonium (MA) cation with formamidinium (FA) cation in methylammonium lead tri-iodide ($MAPbI_3$) causes a reduction in bandgap from about 1.59 eV to about 1.45-1.52 eV and hence improves light absorption (Amat et al., 2014). It has also been shown that substituting bromide (Br) by iodide (I) in formamidinium lead bromide ($FAPbBr_3$) leads to a decrease in the optical bandgap from 2.23 eV to 1.48 eV (Walsh, 2015). Therefore cation/anion substitution in the AL can alter the bandgap and hence the light absorption property in PSCs. This arises due to their ability to modify the electronic band structure of the AL by altering the position of the band edges (Kulkarni et al., 2014; Ono et al., 2017). Cation substitution/mixing usually affects the position of the conduction band minimum (CBM) while anion substitution/mixing alters the position of valence band maximum (VBM). Bandgap tuning through cation/anion substitution/mixing requires adequate control of the amount of the extrinsic elements during device fabrication to avoid the possible degradation in material quality and performance that can be caused by phase segregation, phase transition, and local lattice strains caused by ionic size mismatch, chemical mismatch, and local crystal misorientation (Bush et al., 2018; Hoke et al., 2015; Wu et al., 2021).

Dimensionality tailoring is another good strategy that can be used to tune the band structure and hence the bandgap of perovskite films. Reducing the dimension of perovskite semiconductors increases their optical bandgaps. Therefore, low dimensional perovskite structures such as quantum dots, nanorods, and nanosheets have higher bandgaps when compared to bulk perovskite semiconductors due to quantum confinement effects (Wen & Luo, 2021). Dimensionality tailoring is very important in the development of tandem solar cells as a way to push the efficiency of solar cells beyond the Shockley-Queisser limit. Bandgap engineering in perovskite materials may also be caused by external factors such as moisture, light, temperature, and pressure. A review of the bandgap engineering strategies in perovskite films has been done by Hu and co-workers (Hu et al., 2019) and also by Ou and his research team (Ou et al., 2019).

2.4.2 Control of morphology and crystallization of the active layer

The crystallization kinetics of the AL in PSC is important in determining its crystal structure and morphology which are critical parameters in its performance (Mastroianni et al., 2015). Good quality perovskite films with large grains are known to exhibit high absorption coefficients and long carrier diffusion lengths due to reduced charge carrier trapping resulting from their low defect densities (Eperon et al., 2014; Song et al., 2016). They are also homogeneous and have fewer grain boundaries, fewer pinholes, and good surface coverage thus exhibiting reduced parasitic resistance and large charge carrier lifetimes that lead to improved PCEs in PSCs (Luo et al., 2016; Zhou et al., 2018). The grain boundaries in the AL are sources of defects that not only act as centers for recombination but also provide the paths for the migration of ionic species under the influence of an applied electric field (Phung et al., 2020). Therefore, the presence of many grain boundaries in the AL increases the density of

defects that are detrimental to the performance of PSCs and are also responsible for undesirable effects such as ion migration and J-V hysteresis (Jin et al., 2020). PSCs with good quality AL films will therefore have improved PCEs, good stability, and suppressed or no hysteresis (Shao et al., 2016). It is therefore important to fabricate perovskite ALs with good crystal qualities in order to realize high PCEs and improved stability in PSCs. Several approaches which include compositional engineering, solvent engineering, use of additives, pre-cursor aging, and other post-treatment techniques such as annealing have been shown to be very important in enhancing the crystal quality of the AL and hence the stability and performance of PSCs (Bush et al., 2018; Li et al., 2017; Yang Li et al., 2018; Matsui et al., 2019).

2.4.2.1 Compositional engineering

The perovskite structure (ABX_3) of the AL in PSC provides scientists with a wide parameter space to engineer their composition and structure through the substitution or mixing of cations and anions. This enables them to tune the optoelectronic properties of the perovskite layer which will consequently alter the photophysical properties of the entire solar cell. Compositional engineering is also important in improving the morphology and film quality of the AL by suppressing defect formation which in turn leads to improvement in both the PCE and stability (Rehman et al., 2017). Some cations and anions can be blended in the AL as long as they can form the perovskite structure. The ability of any combination of cations and anions to form a perovskite structure can be predicted using the Goldschmidt tolerance factor (t) or Octahedral factor (u) defined as in equation (2.15) and (2.16) respectively (Hussain et al., 2018; Kieslich et al., 2015).

$$t = \frac{(r_A + r_X)}{\sqrt{2}(r_B + r_X)} \tag{2.15}$$

$$u = \frac{r_B}{r_X} \tag{2.16}$$

where r_A, r_B and r_X are the ionic radii of A, B, and X site ions in the perovskite respectively. A stable perovskite structure is only formed when t and u satisfy the conditions $0.813 \leq t \leq 1.107$ and $0.442 \leq u \leq 0.895$ (Li et al., 2008). In general, tolerance factors between 0.89 and 1 give cubic perovskite structure while values outside this range result in less symmetric tetragonal or hexagonal perovskite structures.

Lead halide PSCs based on single A cation ALs such as $MAPbI_3$, formamidinium lead tri-iodide ($FAPbI_3$), or cesium lead tri-iodide ($CsPbI_3$) are generally unstable since they easily undergo a transformation from the preferred cubic (α) phase to the tetragonal (β) phase or hexagonal (δ) phase when they are exposed to harsh environmental conditions such as high temperatures or moisture (Weber et al., 2018; Whitfield et al., 2016). Compositional engineering has been used by several authors to achieve phase stabilization through suppression of phase segregation, inhibiting the formation of unstable perovskite phases and improving resistance to moisture, high temperature, and light in PSC thus improving their operational stability (Boyd et al., 2019; Poorkazem & Kelly, 2018; Xie et al., 2020). For example, the incorporation of MA^+ cations into $FAPbI_3$ perovskite film has been shown experimentally to cause phase stabilization as a result of the enhancement of iodide and hydrogen (I-H) bonds and increase in Madelung energy of $FAPbI_3$ structure (Binek et al., 2015). It has also been shown that incorporation of certain proportions of FA^+, Cs^+, Br^- and Cl^- into $MAPbI_3$-based perovskites results in phase stabilization in addition to the

improvement in light absorption and charge carrier lifetimes (Alcocer et al., 2014; Maqsood et al., 2020; Stranks et al., 2013; Zarick et al., 2018; Zhang et al., 2017).

Recent studies have also revealed that size-mismatch induced localized lattice distortions in the perovskite structure; that occur when cations are mixed; creates steric effects that increase the formation and activation energies of mobile ions (Tan et al., 2020). This leads to perovskites with suppressed ion migration, a property that is important in developing hysteresis-free PSCs with improved reproducibility. With all these benefits, PSCs based on hybrid mixed cation-mixed halide perovskite layers are causing a paradigm shift in this field with most current research attention being directed on them. Optimizing the composition of the A- and X- sites, therefore, leads to perovskite films with good crystal quality and PSCs with improved PCEs and long-term stabilities.

2.4.2.2 Additive engineering

Additives are compounds that are usually incorporated into the perovskite precursor solution during the perovskite film fabrication process with the main aim of manipulating its crystallization kinetics without necessarily being involved in the formation of perovskite structure (Liu et al., 2020). They influence the perovskite film formation process through interaction with solutes and solvents in the precursor solution, changing the substrate surface wettability, changing the activation energies for defect formation, modulating the perovskite crystallization rate, and coordinating with surface terminating atomic species (Liu et al., 2020; Wu, Cui, et al., 2021; Yang et al., 2019). Additives may also contain various functional groups such as amine, carboxyl, and phenyl; among others; which are known to be useful in passivating the charged defect states in perovskite films. In this way, they enhance the

perovskite film morphology leading to the formation of uniform and compact perovskite films with reduced defect densities (Zheng et al., 2017).

Additive engineering has become a useful technique to improve both the PCE and stability in PSCs (Apurba Mahapatra et al., 2020). The incorporation of additives into the perovskite precursor solution has been shown to play an important role in retarding the perovskite film crystallization rate which leads to enhancement in the film quality, increase in crystal grain size, and suppression of defects and pin-holes during perovskite film formation (Azam et al., 2020; Apurba Mahapatra et al., 2019). They thus reduce ion migration caused by halide segregation and reduce recombination which leads to an improvement in stability, PCE, and reproducibility in PSCs (Li et al., 2017; Zhang & Zhu, 2019). Additives are also capable of modulating the interfacial charge transfer in PSCs depending on the way they are incorporated into the device (Zou et al., 2021).

There are two main ways in which additives can be incorporated into the perovskite layer in PSCs. First, they can be incorporated directly into the perovskite precursor solutions or antisolvent during the single-step deposition of the perovskite layer or into the perovskite seed crystal and/or the organic components during the two-step deposition process. Secondly, they can be introduced indirectly as ETL/HTL modifiers so as to reach the perovskite layer via interdiffusion during thermal annealing (Zhang & Zhu, 2019). Additives in perovskite films can be grouped into several categories namely: lewis bases and lewis acids, ionic liquids, alkali metal halides, ammonium salts, and low-dimensional perovskites (Boopathi et al., 2016). The various classes of additives and how they can be introduced into AL in PSCs are summarized in Figure 2.7. Additives incorporated into the perovskite films in the right proportions are important in reducing the trap states, passivating grain boundaries, and

stabilizing the perovskite phase in perovskite films, modulating the interfacial band alignment as well as suppressing the non-radiative recombination and J-V hysteresis in PSCs (Liu et al., 2020).

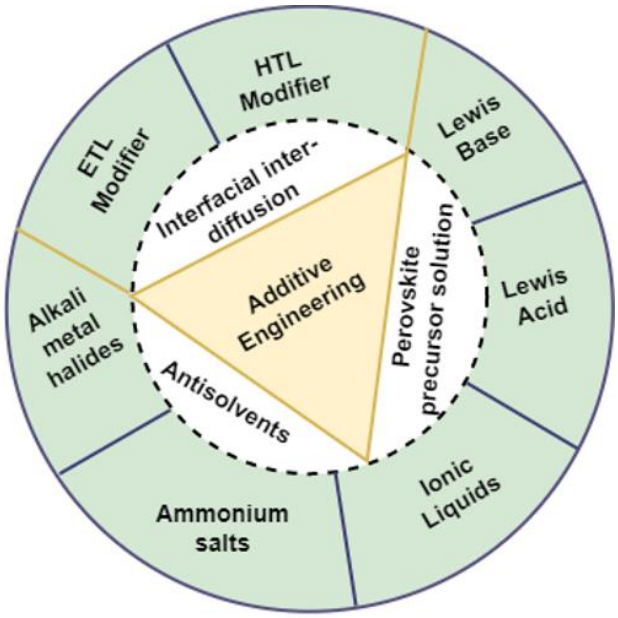

Figure 2.7: Common additive engineering strategies in PSCs (Adapted from Zhang & Zhu, 2019)

2.4.2.3 Annealing

Thermal annealing is a post-treatment technique where the perovskite film is heated to high temperatures and then allowed to cool slowly to room temperature. It is an important process that allows for solvent extraction, proper perovskite film crystallization, and growth of large perovskite grains which leads to suppression of bulk and surface defects in the film (Cui et al., 2015; Yang et al., 2017). The annealing parameters such as temperature, time, and the prevailing ambient conditions affect the morphological evolution and crystal quality of the resulting perovskite film (Chen et al., 2017; Huang et al., 2021; You et al., 2014). The annealing conditions for optimum performance in PSCs depend on several factors which

include the perovskite precursor solution, annealing procedure, fabrication technique, ambient conditions and the components of the PSC (Chen et al., 2017; Kim et al., 2017; Ling et al., 2021; Raga et al., 2015). For example, Yang *et al*. (2017); in their study of the effects of annealing temperature and time on the performance of PSC based on $MA_{0.7}FA_{0.3}Pb(I_{0.9}Br_{0.1})_3$); found that the best performance was obtained at an annealing temperature of 100 ^{0}C and annealing time of 30 minutes (Yang et al., 2017). In another study, Kim et al. (2017) showed that annealing the perovskite film at high temperature of 400 ^{o}C for a short time (4 seconds) leads to the formation of uniform, smooth and large grained films which gives better performance in formamidinium acetate-based PSC (Kim et al., 2017). For ambient air-processed FA-rich PSCs, our research group recently found that an annealing temperature of 130 ^{o}C for 20 minutes yields optimum PV performance characteristics (Oyewole et al., 2021).

2.4.3 Engineering of charge transport layers

The CTLs are very important components of PSCs due to their crucial role in ensuring efficient transportation and collection of photo-generated charge carriers (Han et al., 2018). The presence of CTLs in PSCs helps to reduce recombination by suppressing electrical shunting between the AL and the electrodes whilst promoting charge carrier extraction by increasing the built-in potential within the space charge region. The development of CTLs with compact morphologies and good optoelectronic properties is important in reducing series resistance, interfacial energy barriers, and increasing shunt resistance which is one of the best ways to achieve high V_{oc}, *FF*, and PCE (Yan et al., 2018).

An ideal CTL for PSC should have a suitable work function and should form a favorable interfacial band alignment with the AL so as to ensure proper extraction of the

photo-generated charge carriers. They should also have good electrical conductivity, high charge carrier mobility, low surface recombination rate, good chemical stability, high hydrophobicity, and a simple preparation process (Ameen et al., 2016; Sadia Ameen et al., 2018). The ETL serves to extract the electrons from the AL and transports them to the anode while the HTL extracts the holes and transports them to the cathode. For this process to be effective, an adequate match of the Lowest Unoccupied Molecular Orbital (LUMO) level of the ETL and the conduction band of the AL, as well as, the Highest Occupied Molecular Orbital (HOMO) level of the HTL and the valence band of the AL is important (Dong et al., 2017). As shown in Figure 2.6, the LUMO of the ETL should be lower than that of the absorber (active) layer whereas the HOMO of the HTL should be higher than that of the AL.

The presence of the ETL in PSCs ensures proper electron collection efficiency which is important in the overall performance of the device. In PSC, the electron diffusion length is usually smaller than the hole diffusion length, meaning that the electron transfer rate at the ETL/AL interface is poor compared to the hole transfer rate at the HTL/AL interface (Elbaz et al., 2017). This is responsible for most undesirable properties such as charge accumulation, capacitive currents, J-V hysteresis, and performance degradation in PSCs (Manspeaker et al., 2017; Yu et al., 2020). The electron extraction and transportation ability of ETL is dependent upon its material properties (Zhang et al., 2015; Juarez-Perez et al., 2014a). In search of the ETL material that can boost the PCE and address the aforementioned challenges in PSCs, several organic and inorganic materials which include metal oxides, metal oxide composites, and metal oxide hetero-structured nanoparticles have been developed (Mahmood et al., 2017). Among them, Titanium dioxide (TiO_2) has remained the most preferred ETL material due to its low toxicity, good chemical and thermal stability, suitable band alignment with the AL,

and its ability to be processed from solution (Bai et al., 2014; Chen & Mao, 2007). However, its characteristic high defect density state, poor electrical conductivity, low electron mobility, and its photocatalytic nature under UV light exposure hinders its widespread adoption as the best ETL material (Chen & Mao, 2007). Research efforts are however ongoing to improve the material properties of TiO_2 so as to offer better PCE and operational stability in PSCs (Zhen et al., 2019).

The HTL is also a very important component in PSCs as it helps in enhancing the extraction efficiency of holes, suppressing recombination by acting as an electron blocking layer, and reducing perovskite degradation by avoiding direct contact with the cathode (Urieta-Mora et al., 2018). The material properties of HTL such as the position of the valence band edge relative to that of the AL, its electrical conductivity, hole mobility as well as its thickness and crystal quality have been shown to have an important effect on the current density-voltage (J-V) characteristics, PCE and stability of PSC (Galatopoulos et al., 2017). The development of HTLs with good optoelectronic properties is therefore an important step in the push for higher efficiency and stability in PSCs. On account of this, several organic or inorganic materials have been studied as HTLs in PSCs yielding different PCEs and stability depending on their individual properties (Pitchaiya et al., 2020; Singh et al., 2019; Zhao & Wang, 2018). The inorganic material-based HTLs which have been used in PSCs include metal oxides such as copper oxides (CuO_x), Nickel oxides (NiO_x), Molybdenum trioxide (MoO_3), copper (I) thiocyanate (CuSCN), copper iodide (CuI) among others (Elseman et al., 2019; Kung et al., 2018; Singh et al., 2019; Yin et al., 2019; Zhao & Wang, 2018). The organic materials that have been employed as HTLs in PSCs are mostly the conducting small molecular and polymeric compounds such as thiophene, porphyrin, poly(3-hexylthiopene-2,5-

diyl) (P3HT), polytriarylamine (PTAA) and 2,2′,7,7′-tetrakis(N,N-di-p-ethoxyphenylamine)-9,9’-spirobifluorene (Spiro-OMeTAD) (Pitchaiya et al., 2020; Ulfa et al., 2018).

Among the several organic and inorganic materials, Spiro-OMeTAD is mostly used as HTL in the best performing PSC devices due to its favorable energy level alignment, excellent solubility and ease of functionalization, good film-forming properties, chemical stability, and simple processing conditions that are compatible with most perovskite films (Hawash et al., 2018; Zhao & Wang, 2018). The major challenge with Spiro-OMeTAD arises due to its low electrical conductivity which necessitates the need to incorporate dopants such as lithium bis(trifluoromethyl sulfony)imide (Li-TFSI) salt and 4-tert-butylpyridine (tBP) (Urieta-Mora et al., 2018). These dopants have been shown to accelerate performance degradation in PSCs due to their deliquescent, hygroscopic, and corrosive nature that not only degrades the perovskite layer but also weakens its adhesion to the perovskite layer (Lee et al., 2017; Wang et al., 2018). However, these issues can be circumvented in Spiro-OMeTAD-based PSCs through the use of appropriate interlayer materials at the Spiro-OMeTAD/AL interface, proper device encapsulation, and use of additives in the AL that can increase its degradation resistance.

The CTLs, therefore, play a very important role in the performance of PSCs and it is necessary to improve the electrical properties of the commonly used CTLs so that the performance can further be improved. Doping is the most widely used method for improving the properties of CTL materials, particularly the charge carrier mobilities and electrical conductivity. Depending on the type and the amount of dopant used, doping can lead to enhancement in material crystallinity, the shift of band edges, and reduction in carrier recombination rate which culminate into an improved PCE. It is mainly achieved through the

addition of some elements such as lithium salts, functionalized carbon nanotubes, niobium, yttrium, lanthanum, europium e.t.c into the host matrix (Kim et al., 2015; Schloemer et al., 2019; Teresa et al., 2016; Zhou et al., 2014; Zhou et al., 2016). Gao et al. (Gao et al., 2016) fabricated and compared the performance of two PSCs, one with Lanthanum doped mesoporous TiO_2 as ETL and another one with un-doped mesoporous TiO_2. Their results showed that the PCE of PSC with doped ETL was 27.3% higher than that of PSC with un-doped ETL. They attributed their findings to the fact that doping induces oxygen vacancies that raises the Fermi level of the ETL leading to higher PCE. Xu and co-workers also demonstrated that doping mesoporous TiO_2 ETL with Europium leads to an improvement in its work function and reduction in series resistance that causes an increase in the PCE of PSC (Xu et al., 2017).

Though doping is an important performance improvement technique in PSCs, over-doping can have detrimental impacts (Kim et al., 2015). Some dopants are also hygroscopic and may contain mobile ions that can affect the stability of the PSC. This implies that doping should be done with the right dopants in the right proportions to avoid negative impacts on device performance and lifetime.

2.4.4 Electrodes

The electrodes provide the point where the charge carriers generated in the solar cell are collected to the external circuit. The electrode that forms the front surface in PSC should be made of a material that is highly transparent and conductive and the commonly used materials have been FTO and ITO. Graphene has also been used as a front electrode due to its excellent conductivity (You et al., 2015). The back contact material does not need to be transparent but should have a high work function, low cost, and good chemical and

photochemical stability. The metallic materials such as Silver (Ag), gold (Au), platinum (Pt), chromium (Cr), Nickel (Ni), Copper (Cu), and carbon-based materials such as graphene have been used as back contact electrodes in PSCs and have demonstrated different performance depending on the CTL in use (Behrouznejad et al., 2016; Fagiolari & Bella, 2019). Au has proved to be the best back electrode material in PSCs since it enables them to have good performance (Behrouznejad et al., 2016).

2.4.5 Interface engineering

An interface is a point of contact between any two adjacent layers in PSC which greatly influences its PCE. The interface has been cited as the primary non-radiative recombination pathway that can be responsible for low V_{oc} values especially if it is not well designed (Stolterfoht et al., 2018). In PSC, the interfaces between the CTLs and electrodes are usually considered Ohmic such that their contribution to power losses is negligible. However, the interface between the AL and the CTLs determines the barrier potential that influences the charge extraction and recombination phenomena (Shao & Loi, 2020). The difference between the band edges of the AL and the CTLs dictates the interface band offsets and hence the interfacial charge recombination (Ding et al., 2018). For example, the CBO between the ETL and the AL can form a cliff or spike structure depending on the difference between the conduction band minimum of the ETL and that of the AL (Minemoto & Murata, n.d.). When the CBM of the ETL is lower than that of the AL (i.e negative CBO), a cliff structure is formed and there is no potential barrier for electrons that increases interfacial recombination. On the other hand, a spike structure (i.e positive CBO) is formed when the CBM of the ETL is higher than that of the AL and it usually results in less recombination.

The presence of trap states at the interface between the CTLs and the AL not only causes charge carrier recombination but is also responsible for charge accumulation that causes the J-V hysteresis effect in PSCs (Aygüler et al., 2018). In an attempt to suppress recombination losses at the interface between the CTL and the AL, researchers have applied various techniques which include proper design of CTLs, surface passivation, appropriate doping of the CTLs or the AL, and inserting an ultrathin inter-layer material at the interface (Agresti et al., 2017; Stolterfoht et al., 2018; Tavakoli et al., 2016; Zhu et al., 2014). All these techniques; if done with the right materials in the right proportions; will modify the interface defects state and hence the interfacial energetics for enhanced charge extraction and transportion which will lead to improved PV performance, suppressed hysteresis, and improved stability in PSCs.

2.5 Stability improvement

The performance of PSCs is never stable but undergoes rapid degradation when exposed to the real conditions in the environment thus affecting their operational lifetimes. This problem has been a great hindrance to the commercialization of this new solar concept. The degradation occurs due to structural, morphological, and compositional changes resulting from phase segregation, ion migration, and chemical decomposition that are induced by the presence of defects in the AL and at AL/CTLs interface in addition to exposure to harsh environmental conditions (Boyd et al., 2019; Kundu & Kelly, 2020).

The factors that are responsible for the degradation problem in PSCs may be categorized into intrinsic and extrinsic factors (Christians et al., 2018). The intrinsic factors are those that are related to the fabrication of PSC such as perovskite stoichiometry, nature of materials used, ion migration, and strength of bonds between cations and anions. The extrinsic

factors are related to external conditions such as air, moisture, temperature, and exposure to UV radiation. The hygroscopic nature of organic cations and the hydrophilic properties of perovskite make the materials to readily absorb water from the surroundings leading to degradation through hydrolysis reaction (Berhe et al., 2016). Furthermore, high temperatures lead to phase transformation that causes structural, chemical, morphological, and even optical degradation. The use of chemically active, hydrophilic, and thermally unstable materials as CTLs or metal electrodes may also enhance degradation in PCE of the PSC device upon exposure to the conditions in the surrounding (Rong et al., 2018).

The main approaches that have been explored to develop stable PSCs focus on developing remedies to common degradation mechanisms which involve improving the resilience and stability of the AL itself as well as shielding the AL from the effects of external factors (Assadi et al., 2018; Mazumdar et al., 2021; Qin et al., 2017). This has been achieved mainly through altering the elemental composition of the AL, modifying the AL with some additives, substituting organic cations with inorganic cations, and use of interfacial structures such as chromium (Cr) or reduced graphene (Almosni et al., 2018; Liang et al., 2018; Zhang et al., 2018). Liang and co-authors fabricated an all-inorganic PSC with PCE of 6.7% that was able to retain 90-95% of its efficiency under humid air for over 3 months and could also endure high temperatures (Liang et al., 2016). This approach was however noted to introduce a phase transition at ambient temperature which produces poor photoluminescence property thus compromising the PCE. Li *et al*. (Li et al., 2018) fabricated a $CsPbI_3$-based PSC with improved stability by applying a poly-vinylpyrrolidone (PVP) passivation layer on the surface of the AL so as to improve its moisture resistance. The device exhibited an extra-long carrier diffusion length (over 1.5 μm) and PCE of 10.74% with excellent thermal/moisture stability.

The latest studies aimed at improving the stability of PSC have focused on inhibiting defect formation resulting from the migration of ionic species through the immobilization of ions in the perovskite films. For example, a study done by Li *et al*. (Li et al., 2019); in which sodium Fluoride was incorporated into the perovskite film; resulted in a stable PSC which was able to retain about 90% of its initial PCE after 1000 hrs while operating at maximum power point. The improvement in the stability was caused by the ability of the Fluoride ions to increase ionic bonding within the perovskite crystal that immobilized the organic cation and halide anions. Furthermore, Li and co-workers (Li et al., 2020) developed a reaction-and-assembly approach using a neutral monoamine zinc porphyrin (ZnP) polymer to immobilize ions in the perovskite structure. The polymer reacted with MA^+ and I^- in the perovskite to form a compound that brought about surface and grain boundary binding effects in the perovskite film which greatly reduced defect formation and ion migration. The resulting PSC with 0.05% ZnP polymer was able to retain 90% of its PCE for up to 6000 hours in a humid environment and up to 2000 hrs when thermally stressed at 85 ^{0}C in a nitrogen environment.

The engineering of the CTLs layers and the metal electrodes has also been used to improve the operational stability of PSCs. Christians *et al*. (Christians et al., 2018) fabricated a PSC device with SnO_2, 9-(2-ethylhexyl)-N,N,N,N-tetrakis(4-methoxyphenyl)-9H-carbazole-2,7-diamine (EH44) and aluminum as ETL, HTL and electrode respectively. The device could retain 94% of its PCE for over 1000 hours of continuous exposure to ambient conditions in an un-encapsulated state and the PCE only degraded by 2% under continuous operation in an inert atmosphere after 1500 hours. Other approaches that have been applied to improve the stability of PSCs include the use of additives, development of mixed cation/anion perovskite structures, employing 2D/3D perovskite stacking structures, adding perovskite protective

layers, and device encapsulation (Ava et al., 2019; Mahapatra et al., 2022; Wang, Lin, et al., 2017; Zhou et al., 2016).

With all these approaches, the stability of PSCs under exposure to harsh environmental conditions has greatly improved and the technology has edged closer to the commercialization stage (Ava et al., 2019; Han et al., 2017; Li et al., 2020; Wang et al., 2021; Wang et al., 2019; McMeekin, et al., 2017). It is important to note that some of the strategies for improving the stability in PSCs may have a counter effect on its PCE. This, therefore, means that the efforts to develop stable PSCs should go hand in hand with strategies that are meant to improve its PCE so that this promising solar cell technology can become more competitive relative to the other PV technologies.

2.6 Lead replacement

The presence of lead (Pb) in the AL of lead halide PSCs has generated a lot of debate due to its toxicity. Pb occupies the B- site in the perovskite structure which is associated with numerous advantages such as high electrical mobility, a tunable bandgap, mechanical and thermal stability, magnetic and dielectric transition, and mechanical plasticity, as well as structural and functional diversity (Zhang et al., 2018). Attempts to replace Pb with alternative classes of eco-friendly divalent cations such as Germanium (Ge^{2+}), Bismuth (Bi^{3+}), or Tin (Sn^{2+}) to obtain lead-free PSCs has been made by some researchers but the resulting devices exhibit very low PCEs and are easily oxidized when exposed to air and moisture limiting their practical applications (Fu, 2019). Furthermore, finding a suitable Pb substitute has been a bit challenging due to the possible impact on the perovskite structure and the other requirements of availability, low cost, ability to be processed from solutions, flexibility, and recyclability

that the new cations have to meet in addition to the requirement for high efficiency in the resulting PSC device (Zhang et al., 2018).

2.7 Flexible systems

Flexible PV systems are currently regarded as the 4th generation PV technology that aims to have low-cost and lightweight systems that are resistant to mechanical stress (Heo et al., 2019). In addition to their low cost, flexibility is another important feature that will make PSC technology so unique relative to the other well-established PV technologies. Flexible PV systems are gaining popularity as their demand in building-integrated photovoltaics (BIPV), wearable and portable electronic devices, electric vehicles, and aerospace applications increases (Kim et al., 2015). Designing flexible and lightweight PSCs that are compatible with cheap processing techniques such as the roll-to-roll method will offer a pathway for the mass production of these systems. Some researchers have explored flexible PSC (fPSC) systems by depositing them on flexible polymeric substrates such as polyethylene terephthalate (PET), polyethylene naphthalate (PEN), poly-di-methyl-syloxane (PDMS), and ultra-thin glass and have proved that the systems are technically feasible (Das et al., 2015; Yaowen Li et al., 2016; Tavakoli et al., 2015; Wang et al., 2016). The major challenge in designing fPSC lies in the development of the perovskite layers that can withstand mechanical stresses owing to their rigid and fragile nature.

Research in PSCs has therefore taken a multi-faceted approach as researchers try to establish a strategy that will address most of the challenges bedeviling the practical use of this solar cell technology. From the literature review, it is notable that the development of good quality AL and CTL films with low bulk and surface defect densities is a prerequisite for achieving high PCEs and stability in PSCs. The presence of bulk and surface defects in the

AL and the CTLs contribute greatly to non-radiative power losses, performance degradation, and J-V hysteresis in PSCs. Surface defects in the AL and CTLs also influence the surface properties of the films which control the interface energetics and affect charge carrier extraction. It is therefore necessary to come up with strategies geared towards suppressing defects and optimizing the band offsets at the CTL/AL interface so as to develop efficient and stable PSC devices. Compositional and additive engineering has been shown to work well in the fabrication of perovskite films with good quality crystals, suppressed bulk and surface trap states, and long carrier diffusion lengths. However, more research works are needed to explore more additives and innovative techniques of incorporating them into the perovskite precursors in order to develop efficient and stable PSC systems. It is also necessary to further explore more options to improve the electron transport ability of TiO_2 ETL so as to further improve the PCE of TiO_2-based PSCs. This dissertation reports the results of a study carried out on a regular, planar FA-rich PSC that used FTO, Spiro-OMeTAD, and Au as the anode, HTL, and cathode respectively. The focus of the research was to explore the effects of additives in the ETL and the AL on the optoelectronic properties of these layers and the overall performance of the ensuing PSC.

2.8 References

Agresti, A., Pescetelli, S., Palma, A. L., Del Rio Castillo, A. E., Konios, D., Kakavelakis, G., Razza, S., Cinà, L., Kymakis, E., Bonaccorso, F., & Di Carlo, A. (2017). Graphene Interface Engineering for Perovskite Solar Modules: 12.6% Power Conversion Efficiency over 50 cm 2 Active Area. *ACS Energy Letters*. https://doi.org/10.1021/acsenergylett.6b00672

Alcocer, M. J. P., Leijtens, T., Herz, L. M., Petrozza, A., & Snaith, H. J. (2014). Electron-Hole Diffusion Lengths Exceeding Trihalide Perovskite Absorber. *Science (New York, N.Y.)*. https://doi.org/10.1126/science.1243982

Almosni, S., Delamarre, A., Jehl, Z., Suchet, D., Cojocaru, L., Giteau, M., Behaghel, B., Julian, A., Ibrahim, C., Tatry, L., Wang, H., Kubo, T., Uchida, S., Segawa, H., Miyashita, N., Tamaki, R., Shoji, Y., Yoshida, K., Ahsan, N., … Guillemoles, J. F. (2018). Material challenges for solar cells in the twenty-first century: directions in emerging technologies. In *Science and Technology of Advanced Materials*. https://doi.org/10.1080/14686996.2018.1433439

Amat, A., Mosconi, E., Ronca, E., Quarti, C., Umari, P., Nazeeruddin, M. K., Grätzel, M., & De Angelis, F. (2014). Cation-induced band-gap tuning in organohalide perovskites: Interplay of spin-orbit coupling and octahedra tilting. *Nano Letters*. https://doi.org/10.1021/nl5012992

Ameen, S., Rub, M. A., Kosa, S. A., Alamry, K. A., Akhtar, M. S., Shin, H. S., Seo, H. K., Asiri, A. M., & Nazeeruddin, M. K. (2016). Perovskite Solar Cells: Influence of Hole Transporting Materials on Power Conversion Efficiency. *ChemSusChem*. https://doi.org/10.1002/cssc.201501228

Ameen, Sadia, Akhtar, M. S., Shin, H. S., & Nazeeruddin, M. K. (2018). Charge-Transporting Materials for Perovskite Solar Cells. *Advances in Inorganic Chemistry*. https://doi.org/10.1016/bs.adioch.2018.05.009

Angmo, D., Espinosa, N., & Krebs, F. (2014). Indium tin oxide-free polymer solar cells: Toward commercial reality. In *Green Energy and Technology*. https://doi.org/10.1007/978-1-4471-6473-9_8

Assadi, M. K., Bakhoda, S., Saidur, R., & Hanaei, H. (2018). Recent progress in perovskite solar cells. In *Renewable and Sustainable Energy Reviews*. https://doi.org/10.1016/j.rser.2017.06.088

Ava, T., Al Mamun, A., Marsillac, S., & Namkoong, G. (2019). A Review: Thermal Stability of Methylammonium Lead Halide Based Perovskite Solar Cells. *Applied Sciences*. https://doi.org/10.3390/app9010188

Aygüler, M. F., Hufnagel, A. G., Rieder, P., Wussler, M., Jaegermann, W., Bein, T.,

Dyakonov, V., Petrus, M. L., Baumann, A., & Docampo, P. (2018). Influence of Fermi Level Alignment with Tin Oxide on the Hysteresis of Perovskite Solar Cells. *ACS Applied Materials and Interfaces*. https://doi.org/10.1021/acsami.8b00990

Azam, M., Liu, K., Sun, Y., Wang, Z., Liang, G., Qu, S., Fan, P., & Wang, Z. (2020). Recent advances in defect passivation of perovskite active layer via additive engineering: A review. In *Journal of Physics D: Applied Physics*. https://doi.org/10.1088/1361-6463/ab6f8d

Bai, Y., Mora-Seró, I., Angelis, F. De, Bisquert, J., & Wang, P. (2014). Titanium Dioxide Nanomaterials for Photovoltaic Applications. *Chemical Reviews*, *114*(19), 10095–10130. https://doi.org/10.1021/CR400606N

Behrouznejad, F., Shahbazi, S., Taghavinia, N., Wu, H. P., & Wei-Guang Diau, E. (2016). A study on utilizing different metals as the back contact of $CH_3NH_3PbI_3$ perovskite solar cells. *Journal of Materials Chemistry A*. https://doi.org/10.1039/C6TA05938D

Berhe, T. A., Su, W. N., Chen, C. H., Pan, C. J., Cheng, J. H., Chen, H. M., Tsai, M. C., Chen, L. Y., Dubale, A. A., & Hwang, B. J. (2016). Organometal halide perovskite solar cells: Degradation and stability. In *Energy and Environmental Science* (Vol. 9, Issue 2). https://doi.org/10.1039/c5ee02733k

Binek, A., Hanusch, F. C., Docampo, P., & Bein, T. (2015). Stabilization of the trigonal high-temperature phase of formamidinium lead iodide. *Journal of Physical Chemistry Letters*. https://doi.org/10.1021/acs.jpclett.5b00380

Boopathi, K. M., Mohan, R., Huang, T. Y., Budiawan, W., Lin, M. Y., Lee, C. H., Ho, K. C., & Chu, C. W. (2016). Synergistic improvements in stability and performance of lead iodide perovskite solar cells incorporating salt additives. *Journal of Materials Chemistry A*, *4*(5). https://doi.org/10.1039/c5ta10288j

Boyd, C. C., Cheacharoen, R., Leijtens, T., & McGehee, M. D. (2019). Understanding Degradation Mechanisms and Improving Stability of Perovskite Photovoltaics. In *Chemical Reviews*. https://doi.org/10.1021/acs.chemrev.8b00336

Bush, K. A., Frohna, K., Prasanna, R., Beal, R. E., Leijtens, T., Swifter, S. A., & McGehee, M. D. (2018). Compositional Engineering for Efficient Wide Band Gap Perovskites with Improved Stability to Photoinduced Phase Segregation. *ACS Energy Letters*. https://doi.org/10.1021/acsenergylett.7b01255

Chen, D., Zou, X., Yang, H., Zhang, N., Jin, W., Bai, X., & Yang, Y. (2017). Effect of Annealing Process on $CH_3NH_3PbI_{3-X}$ Cl_X Film Morphology of Planar Heterojunction Perovskite Solar Cells with Optimal Compact TiO_2 Layer. *International Journal of Photoenergy*. https://doi.org/10.1155/2017/7190801

Chen, X., & Mao, S. S. (2007). Titanium dioxide nanomaterials: Synthesis, properties, modifications and applications. In *Chemical Reviews*. https://doi.org/10.1021/cr0500535

Christians, J. A., Schulz, P., Tinkham, J. S., Schloemer, T. H., Harvey, S. P., Tremolet de

Villers, B. J., Sellinger, A., Berry, J. J., & Luther, J. M. (2018). Tailored interfaces of unencapsulated perovskite solar cells for >1,000 hour operational stability. *Nature Energy*. https://doi.org/10.1038/s41560-017-0067-y

Cui, P., Fu, P., Wei, D., Li, M., Song, D., Yue, X., Li, Y., Zhang, Z., Li, Y., & Mbengue, J. M. (2015). Reduced surface defects of organometallic perovskite by thermal annealing for highly efficient perovskite solar cells. *RSC Advances*. https://doi.org/10.1039/c5ra16669a

Das, S., Yang, B., Gu, G., Joshi, P. C., Ivanov, I. N., Rouleau, C. M., Aytug, T., Geohegan, D. B., & Xiao, K. (2015). High-Performance Flexible Perovskite Solar Cells by Using a Combination of Ultrasonic Spray-Coating and Low Thermal Budget Photonic Curing. *ACS Photonics*. https://doi.org/10.1021/acsphotonics.5b00119

Ding, C., Zhang, Y., Liu, F., Kitabatake, Y., Hayase, S., Toyoda, T., Yoshino, K., Minemoto, T., Katayama, K., & Shen, Q. (2018). Effect of the conduction band offset on interfacial recombination behavior of the planar perovskite solar cells. *Nano Energy*. https://doi.org/10.1016/j.nanoen.2018.08.031

Dong, W., Zhang, T., Chen, X., Wang, B., & Zhu, B. (2017). Charge transport study of perovskite solar cells through constructing electron transport channels. *Physica Status Solidi (A) Applications and Materials Science*. https://doi.org/10.1002/pssa.201700089

Elbaz, G. A., Straus, D. B., Semonin, O. E., Hull, T. D., Paley, D. W., Kim, P., Owen, J. S., Kagan, C. R., & Roy, X. (2017). Unbalanced Hole and Electron Diffusion in Lead Bromide Perovskites. *Nano Letters*. https://doi.org/10.1021/acs.nanolett.6b05022

Elseman, A. M., Sajid, S., Shalan, A. E., Mohamed, S. A., & Rashad, M. M. (2019). Recent progress concerning inorganic hole transport layers for efficient perovskite solar cells. In *Applied Physics A: Materials Science and Processing*. https://doi.org/10.1007/s00339-019-2766-7

Eperon, G. E., Beck, C. E., & Snaith, H. J. (2016). Cation exchange for thin film lead iodide perovskite interconversion. *Materials Horizons*. https://doi.org/10.1039/c5mh00170f

Eperon, G. E., Burlakov, V. M., Docampo, P., Goriely, A., & Snaith, H. J. (2014). Morphological control for high performance, solution-processed planar heterojunction perovskite solar cells. *Advanced Functional Materials*. https://doi.org/10.1002/adfm.201302090

Fagiolari, L., & Bella, F. (2019). Carbon-based materials for stable, cheaper and large-scale processable perovskite solar cells. *Energy & Environmental Science*, *12*(12), 3437–3472. https://doi.org/10.1039/C9EE02115A

Fu, H. (2019). Review of lead-free halide perovskites as light-absorbers for photovoltaic applications: From materials to solar cells. *Solar Energy Materials and Solar Cells*. https://doi.org/10.1016/j.solmat.2018.12.038

Galatopoulos, F., Savva, A., Papadas, I. T., & Choulis, S. A. (2017). The effect of hole

transporting layer in charge accumulation properties of p-i-n perovskite solar cells. *APL Materials*. https://doi.org/10.1063/1.4991030

Gao, X. X., Ge, Q. Q., Xue, D. J., Ding, J., Ma, J. Y., Chen, Y. X., Zhang, B., Feng, Y., Wan, L. J., & Hu, J. S. (2016). Tuning the Fermi-level of TiO_2 mesoporous layer by lanthanum doping towards efficient perovskite solar cells. *Nanoscale*. https://doi.org/10.1039/c6nr05917a

Han, G. S., Yoo, J. S., Yu, F., Duff, M. L., Kang, B. K., & Lee, J. K. (2017). Highly stable perovskite solar cells in humid and hot environment. *Journal of Materials Chemistry A*, *5*(28), 14733–14740. https://doi.org/10.1039/C7TA03881J

Han, Q., Ding, J., Bai, Y., Li, T., Ma, J. Y., Chen, Y. X., Zhou, Y., Liu, J., Ge, Q. Q., Chen, J., Glass, J. T., Therien, M. J., Liu, J., Mitzi, D. B., & Hu, J. S. (2018). Carrier Dynamics Engineering for High-Performance Electron-Transport-Layer-free Perovskite Photovoltaics. *Chem*. https://doi.org/10.1016/j.chempr.2018.08.004

Hawash, Z., Ono, L. K., & Qi, Y. (2018). Recent Advances in Spiro-MeOTAD Hole Transport Material and Its Applications in Organic–Inorganic Halide Perovskite Solar Cells. In *Advanced Materials Interfaces*. https://doi.org/10.1002/admi.201700623

Heo, J. H., Lee, D. S., Shin, D. H., & Im, S. H. (2019). Recent advancements in and perspectives on flexible hybrid perovskite solar cells. In *Journal of Materials Chemistry A*. https://doi.org/10.1039/c8ta09452g

Hoke, E. T., Slotcavage, D. J., Dohner, E. R., Bowring, A. R., Karunadasa, H. I., & McGehee, M. D. (2015). Reversible photo-induced trap formation in mixed-halide hybrid perovskites for photovoltaics. *Chemical Science*. https://doi.org/10.1039/c4sc03141e

Hu, Z., Lin, Z., Su, J., Zhang, J., Chang, J., & Hao, Y. (2019). A Review on Energy Band-Gap Engineering for Perovskite Photovoltaics. *Solar RRL*, *3*(12), 1900304. https://doi.org/10.1002/SOLR.201900304

Huang, P. H., Chen, Y. H., Lien, S. Y., Lee, K. W., Wang, N. F., & Huang, C. J. (2021). Effect of annealing on innovative $CsPbI_3$-QDs doped perovskite thin films. *Crystals*, *11*(2). https://doi.org/10.3390/cryst11020101

Hussain, I., Tran, H. P., Jaksik, J., Moore, J., Islam, N., & Uddin, M. J. (2018). Functional materials, device architecture, and flexibility of perovskite solar cell. *Emergent Materials*. https://doi.org/10.1007/s42247-018-0013-1

Jin, H., Debroye, E., Keshavarz, M., Scheblykin, I. G., Roeffaers, M. B. J., Hofkens, J., & Steele, J. A. (2020). It's a trap! on the nature of localised states and charge trapping in lead halide perovskites. In *Materials Horizons*. https://doi.org/10.1039/c9mh00500e

Ju, D., Dang, Y., Zhu, Z., Liu, H., Chueh, C. C., Li, X., Wang, L., Hu, X., Jen, A. K. Y., & Tao, X. (2018). Tunable Band Gap and Long Carrier Recombination Lifetime of Stable Mixed $CH_3NH_3Pb_xSn_{1-x}Br_3$ Single Crystals. *Chemistry of Materials*, *30*(5), 1556–1565. https://doi.org/10.1021/ACS.CHEMMATER.7B04565/SUPPL_FILE/CM7B04565_SI_0

07.PDF

Juarez-Perez, E. J., Wußler, M., Fabregat-Santiago, F., Lakus-Wollny, K., Mankel, E., Mayer, T., Jaegermann, W., & Mora-Sero, I. (2014). Role of the selective contacts in the performance of lead halide perovskite solar cells. *Journal of Physical Chemistry Letters*. https://doi.org/10.1021/jz500059v

Jung, H. S., & Park, N. G. (2015). Perovskite solar cells: From materials to devices. In *Small*. https://doi.org/10.1002/smll.201402767

Kieslich, G., Sun, S., & Cheetham, A. K. (2015). An extended Tolerance Factor approach for organic-inorganic perovskites. *Chemical Science*. https://doi.org/10.1039/c5sc00961h

Kim, B. J., Kim, D. H., Lee, Y. Y., Shin, H. W., Han, G. S., Hong, J. S., Mahmood, K., Ahn, T. K., Joo, Y. C., Hong, K. S., Park, N. G., Lee, S., & Jung, H. S. (2015). Highly efficient and bending durable perovskite solar cells: Toward a wearable power source. *Energy and Environmental Science*. https://doi.org/10.1039/c4ee02441a

Kim, D. H., Han, G. S., Seong, W. M., Lee, J. W., Kim, B. J., Park, N. G., Hong, K. S., Lee, S., & Jung, H. S. (2015). Niobium Doping Effects on TiO_2 Mesoscopic Electron Transport Layer-Based Perovskite Solar Cells. *ChemSusChem*. https://doi.org/10.1002/cssc.201403478

Kim, M., Kim, G. H., Oh, K. S., Jo, Y., Yoon, H., Kim, K. H., Lee, H., Kim, J. Y., & Kim, D. S. (2017). High-Temperature-Short-Time Annealing Process for High-Performance Large-Area Perovskite Solar Cells. *ACS Nano*. https://doi.org/10.1021/acsnano.7b02015

Kirchartz, T., Bisquert, J., Mora-Sero, I., & Garcia-Belmonte, G. (2015). Classification of solar cells according to mechanisms of charge separation and charge collection. *Physical Chemistry Chemical Physics*, *17*(6). https://doi.org/10.1039/c4cp05174b

Kulkarni, S. A., Baikie, T., Boix, P. P., Yantara, N., Mathews, N., & Mhaisalkar, S. (2014). Band-gap tuning of lead halide perovskites using a sequential deposition process. *Journal of Materials Chemistry A*. https://doi.org/10.1039/c4ta00435c

Kundu, S., & Kelly, T. L. (2020). In situ studies of the degradation mechanisms of perovskite solar cells. *EcoMat*. https://doi.org/10.1002/eom2.12025

Kung, P. K., Li, M. H., Lin, P. Y., Chiang, Y. H., Chan, C. R., Guo, T. F., & Chen, P. (2018). A Review of Inorganic Hole Transport Materials for Perovskite Solar Cells. In *Advanced Materials Interfaces*. https://doi.org/10.1002/admi.201800882

Lattante, S. (2014). Electron and Hole Transport Layers: Their Use in Inverted Bulk Heterojunction Polymer Solar Cells. *Electronics*, *3*(1), 132–164. https://doi.org/10.3390/electronics3010132

Lee, I., Yun, J. H., Son, H. J., & Kim, T. S. (2017). Accelerated Degradation Due to Weakened Adhesion from Li-TFSI Additives in Perovskite Solar Cells. *ACS Applied Materials and Interfaces*. https://doi.org/10.1021/acsami.6b14089

Li, B., Zhang, Y., Fu, L., Yu, T., Zhou, S., Zhang, L., & Yin, L. (2018). Surface passivation engineering strategy to fully-inorganic cubic $CsPbI_3$ perovskites for high-performance solar cells. *Nature Communications*. https://doi.org/10.1038/s41467-018-03169-0

Li, C., Lu, X., Ding, W., Feng, L., Gao, Y., & Guo, Z. (2008). Formability of ABX_3 (X = F, Cl, Br, I) halide perovskites. *Acta Crystallographica Section B: Structural Science*. https://doi.org/10.1107/S0108768108032734

Li, M., Li, H., Fu, J., Liang, T., & Ma, W. (2020). Recent Progress on the Stability of Perovskite Solar Cells in a Humid Environment. *The Journal of Physical Chemistry C*, *124*(50), 27251–27266. https://doi.org/10.1021/ACS.JPCC.0C08019

Li, N., Tao, S., Chen, Y., Niu, X., Onwudinanti, C. K., Hu, C., Qiu, Z., Xu, Z., Zheng, G., Wang, L., Zhang, Y., Li, L., Liu, H., Lun, Y., Hong, J., Wang, X., Liu, Y., Xie, H., Gao, Y., … Zhou, H. (2019). Cation and anion immobilization through chemical bonding enhancement with fluorides for stable halide perovskite solar cells. *Nature Energy*. https://doi.org/10.1038/s41560-019-0382-6

Li, T., Pan, Y., Wang, Z., Xia, Y., Chen, Y., & Huang, W. (2017). Additive engineering for highly efficient organic-inorganic halide perovskite solar cells: Recent advances and perspectives. In *Journal of Materials Chemistry A*. https://doi.org/10.1039/c7ta01798g

Li, X., Li, C., Wu, Y., Cao, J., & Tang, Y. (2020). A reaction-and-assembly approach using monoamine zinc porphyrin for highly stable large-area perovskite solar cells. *Science China Chemistry*. https://doi.org/10.1007/s11426-020-9710-7

Li, Yang, Ji, L., Liu, R., Zhang, C., Mak, C. H., Zou, X., Shen, H. H., Leu, S. Y., & Hsu, H. Y. (2018). A review on morphology engineering for highly efficient and stable hybrid perovskite solar cells. In *Journal of Materials Chemistry A*. https://doi.org/10.1039/c8ta04120b

Li, Yaowen, Meng, L., Yang, Y., Xu, G., Hong, Z., Chen, Q., You, J., Li, G., Yang, Y., & Li, Y. (2016). High-efficiency robust perovskite solar cells on ultrathin flexible substrates. *Nature Communications*. https://doi.org/10.1038/ncomms10214

Liang, J., Liu, Z., Qiu, L., Hawash, Z., Meng, L., Wu, Z., Jiang, Y., Ono, L. K., & Qi, Y. (2018). Enhancing Optical, Electronic, Crystalline, and Morphological Properties of Cesium Lead Halide by Mn Substitution for High-Stability All-Inorganic Perovskite Solar Cells with Carbon Electrodes. *Advanced Energy Materials*. https://doi.org/10.1002/aenm.201800504

Liang, J., Wang, C., Wang, Y., Xu, Z., Lu, Z., Ma, Y., Zhu, H., Hu, Y., Xiao, C., Yi, X., Zhu, G., Lv, H., Ma, L., Chen, T., Tie, Z., Jin, Z., & Liu, J. (2016). All-Inorganic Perovskite Solar Cells. *Journal of the American Chemical Society*. https://doi.org/10.1021/jacs.6b10227

Ling, P. S. V., Hagfeldt, A., & Sanchez, S. (2021). Flash infrared annealing for perovskite solar cell processing. *Journal of Visualized Experiments*, *2021*(168). https://doi.org/10.3791/61730

Liu, J., Wang, G., Luo, K., He, X., Ye, Q., Liao, C., & Mei, J. (2017). Understanding the Role of the Electron-Transport Layer in Highly Efficient Planar Perovskite Solar Cells. *ChemPhysChem*, *18*(6), 617–625. https://doi.org/10.1002/CPHC.201601245

Liu, S., Guan, Y., Sheng, Y., Hu, Y., Rong, Y., Mei, A., & Han, H. (2020). A Review on Additives for Halide Perovskite Solar Cells. In *Advanced Energy Materials* (Vol. 10, Issue 13). https://doi.org/10.1002/aenm.201902492

Liu, T., Chen, K., Hu, Q., Zhu, R., & Gong, Q. (2016). Inverted Perovskite Solar Cells: Progresses and Perspectives. *Advanced Energy Materials*. https://doi.org/10.1002/aenm.201600457

Liu, Z., Ono, L. K., & Qi, Y. (2020). Additives in metal halide perovskite films and their applications in solar cells. In *Journal of Energy Chemistry* (Vol. 46). https://doi.org/10.1016/j.jechem.2019.11.008

Luo, Y., Meng, F., Zhao, E., Zheng, Y. Z., Zhou, Y., & Tao, X. (2016). Fine control of perovskite-layered morphology and composition via sequential deposition crystallization process towards improved perovskite solar cells. *Journal of Power Sources*. https://doi.org/10.1016/j.jpowsour.2016.01.102

Mahapatra, A., Kumar, S., Kumar, P., & Pradhan, B. (2022). Recent progress in perovskite solar cells: challenges from efficiency to stability. *Materials Today Chemistry*, *23*, 100686. https://doi.org/10.1016/J.MTCHEM.2021.100686

Mahapatra, Apurba, Prochowicz, D., Tavakoli, M. M., Trivedi, S., Kumar, P., & Yadav, P. (2019). A review of aspects of additive engineering in perovskite solar cells. In *Journal of Materials Chemistry A*. https://doi.org/10.1039/c9ta07657c

Mahapatra, Apurba, Prochowicz, D., Tavakoli, M. M., Trivedi, S., Kumar, P., & Yadav, P. (2020). A review of aspects of additive engineering in perovskite solar cells. In *Journal of Materials Chemistry A* (Vol. 8, Issue 1, pp. 27–54). Royal Society of Chemistry. https://doi.org/10.1039/c9ta07657c

Mahmood, K., Sarwar, S., & Mehran, M. T. (2017). Current status of electron transport layers in perovskite solar cells: materials and properties. In *RSC Advances*. https://doi.org/10.1039/c7ra00002b

Manspeaker, C., Venkatesan, S., Zakhidov, A., & Martirosyan, K. S. (2017). Role of interface in stability of perovskite solar cells. In *Current Opinion in Chemical Engineering*. https://doi.org/10.1016/j.coche.2016.08.013

Maqsood, A., Li, Y., Meng, J., Song, D., Qiao, B., Zhao, S., & Xu, Z. (2020). Perovskite Solar Cells Based on Compact, Smooth $FA_{0.1}MA_{0.9}PbI_3$ Film with Efficiency Exceeding 22%. *Nanoscale Research Letters*. https://doi.org/10.1186/s11671-020-03313-0

Martín-Palma, R. J., & Martínez-Duart, J. M. (2017). Review of Semiconductor Physics. *Nanotechnology for Microelectronics and Photonics*, 51–80. https://doi.org/10.1016/B978-0-323-46176-4.00003-1

Mastroianni, S., Heinz, F. D., Im, J. H., Veurman, W., Padilla, M., Schubert, M. C., Würfel, U., Grätzel, M., Park, N. G., & Hinsch, A. (2015). Analysing the effect of crystal size and structure in highly efficient $CH_3NH_3PbI_3$ perovskite solar cells by spatially resolved photo- and electroluminescence imaging. *Nanoscale*. https://doi.org/10.1039/c5nr05308k

Matsui, T., Yamamoto, T., Nishihara, T., Morisawa, R., Yokoyama, T., Sekiguchi, T., & Negami, T. (2019). Compositional Engineering for Thermally Stable, Highly Efficient Perovskite Solar Cells Exceeding 20% Power Conversion Efficiency with 85 °C/85% 1000 h Stability. *Advanced Materials*. https://doi.org/10.1002/adma.201806823

Mazumdar, S., Zhao, Y., & Zhang, X. (2021). Stability of Perovskite Solar Cells: Degradation Mechanisms and Remedies. *Frontiers in Electronics*, *0*, 8. https://doi.org/10.3389/FELEC.2021.712785

Minemoto, T., & Murata, M. (n.d.). *Theoretical analysis on effect of band offsets in perovskite solar cells*. https://doi.org/10.1016/j.solmat.2014.10.036

Mori, D., Benten, H., Okada, I., Ohkita, H., & Ito, S. (2014). Highly efficient charge-carrier generation and collection in polymer/polymer blend solar cells with a power conversion efficiency of 5.7%. *Energy and Environmental Science*. https://doi.org/10.1039/c4ee01326c

Nelson, J. (2003). The Physics of Solar Cells. *The Physics of Solar Cells*. https://doi.org/10.1142/P276

Ono, L. K., Juarez-Perez, E. J., & Qi, Y. (2017). Progress on Perovskite Materials and Solar Cells with Mixed Cations and Halide Anions. In *ACS Applied Materials and Interfaces*. https://doi.org/10.1021/acsami.7b06001

Ou, Q., Bao, X., Zhang, Y., Shao, H., Xing, G., Li, X., Shao, L., & Bao, Q. (2019). Band structure engineering in metal halide perovskite nanostructures for optoelectronic applications. *Nano Materials Science*, *1*(4), 268–287. https://doi.org/10.1016/J.NANOMS.2019.10.004

Oyewole, D. O., Koech, R. K., Ichwani, R., Ahmed, R., Hinostroza Tamayo, J., Adeniji, S. A., Cromwell, J., Colin Ulloa, E., Oyewole, O. K., Agyei-Tuffour, B., Titova, L. V., Burnham, N. A., & Soboyejo, W. O. (2021). Annealing effects on interdiffusion in layered FA-rich perovskite solar cells. *AIP Advances*, *11*(6), 065327. https://doi.org/10.1063/5.0046205

Pascoe, A. R., Yang, M., Kopidakis, N., Zhu, K., Reese, M. O., Rumbles, G., Fekete, M., Duffy, N. W., & Cheng, Y. B. (2016). Planar versus mesoscopic perovskite microstructures: The influence of $CH_3NH_3PbI_3$ morphology on charge transport and recombination dynamics. *Nano Energy*. https://doi.org/10.1016/j.nanoen.2016.02.031

Phung, N., Al-Ashouri, A., Meloni, S., Mattoni, A., Albrecht, S., Unger, E. L., Merdasa, A., & Abate, A. (2020). The Role of Grain Boundaries on Ionic Defect Migration in Metal Halide Perovskites. *Advanced Energy Materials*. https://doi.org/10.1002/aenm.201903735

Pitchaiya, S., Natarajan, M., Santhanam, A., Asokan, V., Yuvapragasam, A., Madurai Ramakrishnan, V., Palanisamy, S. E., Sundaram, S., & Velauthapillai, D. (2020). A review on the classification of organic/inorganic/carbonaceous hole transporting materials for perovskite solar cell application. In *Arabian Journal of Chemistry*. https://doi.org/10.1016/j.arabjc.2018.06.006

Ponseca, C. S., Savenije, T. J., Abdellah, M., Zheng, K., Yartsev, A., Pascher, T., Harlang, T., Chabera, P., Pullerits, T., Stepanov, A., Wolf, J. P., & Sundström, V. (2014). Organometal halide perovskite solar cell materials rationalized: Ultrafast charge generation, high and microsecond-long balanced mobilities, and slow recombination. *Journal of the American Chemical Society*. https://doi.org/10.1021/ja412583t

Poorkazem, K., & Kelly, T. L. (2018). Compositional Engineering to Improve the Stability of Lead Halide Perovskites: A Comparative Study of Cationic and Anionic Dopants. *ACS Applied Energy Materials*. https://doi.org/10.1021/acsaem.7b00065

Qin, X., Zhao, Z., Wang, Y., Wu, J., Jiang, Q., & You, J. (2017). Recent progress in stability of perovskite solar cells. In *Journal of Semiconductors*. https://doi.org/10.1088/1674-4926/38/1/011002

Raga, S. R., Jung, M. C., Lee, M. V., Leyden, M. R., Kato, Y., & Qi, Y. (2015). Influence of air annealing on high efficiency planar structure perovskite solar cells. *Chemistry of Materials*. https://doi.org/10.1021/cm5041997

Rehman, W., McMeekin, D. P., Patel, J. B., Milot, R. L., Johnston, M. B., Snaith, H. J., & Herz, L. M. (2017). Photovoltaic mixed-cation lead mixed-halide perovskites: Links between crystallinity, photo-stability and electronic properties. *Energy and Environmental Science*. https://doi.org/10.1039/c6ee03014a

Richter, A., Glunz, S. W., Werner, F., Schmidt, J., & Cuevas, A. (2012). Improved quantitative description of Auger recombination in crystalline silicon. *Physical Review B - Condensed Matter and Materials Physics*, *86*(16), 165202. https://doi.org/10.1103/PHYSREVB.86.165202/FIGURES/10/MEDIUM

Rong, Y., Hu, Y., Mei, A., Tan, H., Saidaminov, M. I., Seok, S. Il, McGehee, M. D., Sargent, E. H., & Han, H. (2018). Challenges for commercializing perovskite solar cells. In *Science*. https://doi.org/10.1126/science.aat8235

Schloemer, T. H., Christians, J. A., Luther, J. M., & Sellinger, A. (2019). Doping strategies for small molecule organic hole-transport materials: impacts on perovskite solar cell performance and stability. *Chemical Science*. https://doi.org/10.1039/C8SC05284K

Schroder, D. K. (2005). Semiconductor Material and Device Characterization: Third Edition. In *Semiconductor Material and Device Characterization: Third Edition*. https://doi.org/10.1002/0471749095

Seo, J., Noh, J. H., & Seok, S. Il. (2016). Rational Strategies for Efficient Perovskite Solar Cells. In *Accounts of Chemical Research*. https://doi.org/10.1021/acs.accounts.5b00444

Shao, S., & Loi, M. A. (2020). The Role of the Interfaces in Perovskite Solar Cells. In *Advanced Materials Interfaces* (Vol. 7, Issue 1, p. 1901469). Wiley-VCH Verlag. https://doi.org/10.1002/admi.201901469

Shao, Y., Fang, Y., Li, T., Wang, Q., Dong, Q., Deng, Y., Yuan, Y., Wei, H., Wang, M., Gruverman, A., Shield, J., & Huang, J. (2016). Grain boundary dominated ion migration in polycrystalline organic-inorganic halide perovskite films. *Energy and Environmental Science*. https://doi.org/10.1039/c6ee00413j

Shockley, W., & Queisser, H. J. (1961). Detailed balance limit of efficiency of p-n junction solar cells. *Applied Physics*. https://doi.org/10.1063/1.1736034

Shockley, W., & Read, W. T. (1952). Statistics of the Recombinations of Holes and Electrons. *Physical Review*, *87*(5), 835. https://doi.org/10.1103/PhysRev.87.835

Singh, R., Singh, P. K., Bhattacharya, B., & Rhee, H. W. (2019). Review of current progress in inorganic hole-transport materials for perovskite solar cells. In *Applied Materials Today*. https://doi.org/10.1016/j.apmt.2018.12.011

Song, Z., Watthage, S. C., Phillips, A. B., & Heben, M. J. (2016). Pathways toward high-performance perovskite solar cells: review of recent advances in organo-metal halide perovskites for photovoltaic applications. *Journal of Photonics for Energy*. https://doi.org/10.1117/1.JPE.6.022001

Staub, F., Rau, U., & Kirchartz, T. (2018). Statistics of the Auger Recombination of Electrons and Holes via Defect Levels in the Band Gap—Application to Lead-Halide Perovskites. *ACS Omega*, *3*(7), 8009–8016. https://doi.org/10.1021/ACSOMEGA.8B00962

Stolterfoht, M., Wolff, C. M., Márquez, J. A., Zhang, S., Hages, C. J., Rothhardt, D., Albrecht, S., Burn, P. L., Meredith, P., Unold, T., & Neher, D. (2018). Visualization and suppression of interfacial recombination for high-efficiency large-area pin perovskite solar cells. *Nature Energy*. https://doi.org/10.1038/s41560-018-0219-8

Stranks, S. D., Eperon, G. E., Grancini, G., Menelaou, C., Alcocer, M. J. P., Leijtens, T., Herz, L. M., Petrozza, A., & Snaith, H. J. (2013). Electron-hole diffusion lengths exceeding 1 micrometer in an organometal trihalide perovskite absorber. *Science*. https://doi.org/10.1126/science.1243982

Tan, S., Yavuz, I., De Marco, N., Huang, T., Lee, S. J., Choi, C. S., Wang, M., Nuryyeva, S., Wang, R., Zhao, Y., Wang, H. C., Han, T. H., Dunn, B., Huang, Y., Lee, J. W., & Yang, Y. (2020). Steric Impediment of Ion Migration Contributes to Improved Operational Stability of Perovskite Solar Cells. *Advanced Materials*. https://doi.org/10.1002/adma.201906995

Tavakoli, M. M., Tavakoli, R., Hasanzadeh, S., & Mirfasih, M. H. (2016). Interface Engineering of Perovskite Solar Cell Using a Reduced-Graphene Scaffold. *Journal of Physical Chemistry C*. https://doi.org/10.1021/acs.jpcc.6b05667

Tavakoli, M. M., Tsui, K. H., Zhang, Q., He, J., Yao, Y., Li, D., & Fan, Z. (2015). Highly

Efficient Flexible Perovskite Solar Cells with Antireflection and Self-Cleaning Nanostructures. *ACS Nano*. https://doi.org/10.1021/acsnano.5b04284

Teresa, G., Simone, C., Mirko, P., Marco, S., Francesco, D. S., Alberto, A., Enzo, M., Aldo, D. C., & Francesco, B. (2016). Boosting Perovskite Solar Cells Performance and Stability through Doping a Poly-3(hexylthiophene) Hole Transporting Material with Organic Functionalized Carbon Nanostructures. *Advanced Functional Materials*. https://doi.org/doi:10.1002/adfm.201602803

Thakur, U., Kisslinger, R., & Shankar, K. (2017). One-Dimensional Electron Transport Layers for Perovskite Solar Cells. *Nanomaterials*. https://doi.org/10.3390/nano7050095

Tian, Y., Zhou, C., Worku, M., Wang, X., Ling, Y., Gao, H., Zhou, Y., Miao, Y., Guan, J., & Ma, B. (2018). Highly Efficient Spectrally Stable Red Perovskite Light-Emitting Diodes. *Advanced Materials*. https://doi.org/10.1002/adma.201707093

Ulfa, M., Zhu, T., Goubard, F., & Pauporté, T. (2018). Molecular: Versus polymeric hole transporting materials for perovskite solar cell application. *Journal of Materials Chemistry A*. https://doi.org/10.1039/c8ta03875a

Urieta-Mora, J., García-Benito, I., Molina-Ontoria, A., & Martín, N. (2018). Hole transporting materials for perovskite solar cells: a chemical approach. In *Chemical Society reviews*. https://doi.org/10.1039/c8cs00262b

Walsh, A. (2015). Principles of Chemical Bonding and Band Gap Engineering in Hybrid Organic–Inorganic Halide Perovskites. *The Journal of Physical Chemistry C*. https://doi.org/10.1021/jp512420b

Wang, H., Wang, Y., Xuan, Z., Chen, T., Zhang, J., Hao, X., Wu, L., Constantinou, I., & Zhao, D. (2021). Progress in Perovskite Solar Cells towards Commercialization—A Review. *Materials 2021, Vol. 14, Page 6569*, *14*(21), 6569. https://doi.org/10.3390/MA14216569

Wang, R., Mujahid, M., Duan, Y., Wang, Z. K., Xue, J., & Yang, Y. (2019). A Review of Perovskites Solar Cell Stability. In *Advanced Functional Materials*. https://doi.org/10.1002/adfm.201808843

Wang, S., Huang, Z., Wang, X., Li, Y., Günther, M., Valenzuela, S., Parikh, P., Cabreros, A., Xiong, W., & Meng, Y. S. (2018). Unveiling the Role of tBP-LiTFSI Complexes in Perovskite Solar Cells. *Journal of the American Chemical Society*. https://doi.org/10.1021/jacs.8b09809

Wang, Y. M., Bai, S., Cheng, L., Wang, N. N., Wang, J. P., Gao, F., & Huang, W. (2016). High-Efficiency Flexible Solar Cells Based on Organometal Halide Perovskites. *Advanced Materials*. https://doi.org/10.1002/adma.201504260

Wang, Z., Lin, Q., Chmiel, F. P., Sakai, N., Herz, L. M., & Snaith, H. J. (2017). Efficient ambient-air-stable solar cells with 2D-3D heterostructured butylammonium-caesium-formamidinium lead halide perovskites. *Nature Energy*.

https://doi.org/10.1038/nenergy.2017.135

Wang, Z., McMeekin, D. P., Sakai, N., van Reenen, S., Wojciechowski, K., Patel, J. B., Johnston, M. B., & Snaith, H. J. (2017). Efficient and Air-Stable Mixed-Cation Lead Mixed-Halide Perovskite Solar Cells with n-Doped Organic Electron Extraction Layers. *Advanced Materials*. https://doi.org/10.1002/adma.201604186

Weber, O. J., Ghosh, D., Gaines, S., Henry, P. F., Walker, A. B., Islam, M. S., & Weller, M. T. (2018). Phase Behavior and Polymorphism of Formamidinium Lead Iodide. *Chemistry of Materials*. https://doi.org/10.1021/acs.chemmater.8b00862

Wen, H., & Luo, X. (2021). Tuning Bandgaps of Mixed Halide and Oxide Perovskites $CsSnX_3$ (X=Cl, I), and $SrBO_3$ (B=Rh, Ti). *Applied Sciences 2021, Vol. 11, Page 6862*, *11*(15), 6862. https://doi.org/10.3390/APP11156862

Whitfield, P. S., Herron, N., Guise, W. E., Page, K., Cheng, Y. Q., Milas, I., & Crawford, M. K. (2016). Structures, Phase Transitions and Tricritical Behavior of the Hybrid Perovskite Methyl Ammonium Lead Iodide. *Scientific Reports*. https://doi.org/10.1038/srep35685

Wu, J., Liu, S. C., Li, Z., Wang, S., Xue, D. J., Lin, Y., & Hu, J. S. (2021). Strain in perovskite solar cells: origins, impacts and regulation. *National Science Review*, *8*(8). https://doi.org/10.1093/NSR/NWAB047

Wu, T., Cui, D., Liu, X., Luo, X., Su, H., Segawa, H., Zhang, Y., Wang, Y., & Han, L. (2021). Additive Engineering toward High-Performance Tin Perovskite Solar Cells. In *Solar RRL* (Vol. 5, Issue 5). https://doi.org/10.1002/solr.202100034

Wurfel, U., Cuevas, A., & Wurfel, P. (2015). Charge carrier separation in solar cells. *IEEE Journal of Photovoltaics*. https://doi.org/10.1109/JPHOTOV.2014.2363550

Xiao, J. W., Shi, C., Zhou, C., Zhang, D., Li, Y., & Chen, Q. (2017). Contact Engineering: Electrode Materials for Highly Efficient and Stable Perovskite Solar Cells. *Solar RRL*. https://doi.org/10.1002/solr.201700082

Xie, L., Song, P., Shen, L., Lu, J., Liu, K., Lin, K., Feng, W., Tian, C., & Wei, Z. (2020). Revealing the compositional effect on the intrinsic long-term stability of perovskite solar cells. *Journal of Materials Chemistry A*. https://doi.org/10.1039/d0ta01668c

Xu, Z., Wu, J., Wu, T., Bao, Q., He, X., Lan, Z., Lin, J., Huang, M., Huang, Y., & Fan, L. (2017). Tuning the Fermi Level of TiO_2 Electron Transport Layer through Europium Doping for Highly Efficient Perovskite Solar Cells. *Energy Technology*. https://doi.org/10.1002/ente.201700377

Yan, L., Xue, Q., Liu, M., Zhu, Z., Tian, J., Li, Z., Chen, Z., Chen, Z., Yan, H., Yip, H. L., & Cao, Y. (2018). Interface Engineering for All-Inorganic $CsPbI_2Br$ Perovskite Solar Cells with Efficiency over 14%. *Advanced Materials*. https://doi.org/10.1002/adma.201802509

Yang, H., Zhang, J., Zhang, C., Chang, J., Lin, Z., Chen, D., Xi, H., & Hao, Y. (2017). Effects of annealing conditions on mixed lead halide perovskite solar cells and their thermal

stability investigation. *Materials*. https://doi.org/10.3390/ma10070837

Yang, J., Chen, S., Xu, J., Zhang, Q., Liu, H., Liu, Z., & Yuan, M. (2019). A Review on Improving the Quality of Perovskite Films in Perovskite Solar Cells via the Weak Forces Induced by Additives. *Applied Sciences 2019, Vol. 9, Page 4393*, *9*(20), 4393. https://doi.org/10.3390/APP9204393

Yang, Y., Feng, S., Li, M., Xu, W., Yin, G., Wang, Z., Sun, B., & Gao, X. (2017). Annealing induced re-crystallization in $CH_3NH_3PbI_{3-x}Cl_x$ for high performance perovskite solar cells. *Scientific Reports*, *7*. https://doi.org/10.1038/srep46724

Yin, W., Pan, L., Yang, T., & Liang, Y. (2016). Recent advances in interface engineering for planar heterojunction perovskite solar cells. In *Molecules*. https://doi.org/10.3390/molecules21070837

Yin, X., Guo, Y., Xie, H., Que, W., & Kong, L. B. (2019). Nickel Oxide as Efficient Hole Transport Materials for Perovskite Solar Cells. In *Solar RRL*. https://doi.org/10.1002/solr.201900001

You, J., Hong, Z., Song, T. Bin, Meng, L., Liu, Y., Jiang, C., Zhou, H., Chang, W. H., Li, G., & Yang, Y. (2014). Moisture assisted perovskite film growth for high performance solar cells. *Applied Physics Letters*, *105*(18). https://doi.org/10.1063/1.4901510

You, P., Liu, Z., Tai, Q., Liu, S., & Yan, F. (2015). Efficient Semitransparent Perovskite Solar Cells with Graphene Electrodes. *Advanced Materials*. https://doi.org/10.1002/adma.201501145

Yu, M., Guo, Y., Yuan, S., Zhao, J. S., Qin, Y., & Ai, X. C. (2020). The influence of the electron transport layer on charge dynamics and trap-state properties in planar perovskite solar cells. *RSC Advances*, *10*(21), 12347–12353. https://doi.org/10.1039/d0ra00375a

Zarick, H. F., Soetan, N., Erwin, W. R., & Bardhan, R. (2018). Mixed halide hybrid perovskites: A paradigm shift in photovoltaics. In *Journal of Materials Chemistry A*. https://doi.org/10.1039/c7ta09122b

Zdanowicz, T., Rodziewicz, T., & Zabkowska-Waclawek, M. (2005). Theoretical analysis of the optimum energy band gap of semiconductors for fabrication of solar cells for applications in higher latitudes locations. *Solar Energy Materials and Solar Cells*. https://doi.org/10.1016/j.solmat.2004.07.049

Zhang, Fei, & Zhu, K. (2019). Additive Engineering for Efficient and Stable Perovskite Solar Cells. In *Advanced Energy Materials*. https://doi.org/10.1002/aenm.201902579

Zhang, Fengying, Yang, B., Li, Y., Deng, W., & He, R. (2017). Extra long electron-hole diffusion lengths in $CH_3NH_3PbI_{3-X}Cl_x$ perovskite single crystals. *Journal of Materials Chemistry C*. https://doi.org/10.1039/c7tc02802d

Zhang, L., Liu, X., Li, J., & McKechnie, S. (2018). Interactions between molecules and perovskites in halide perovskite solar cells. In *Solar Energy Materials and Solar Cells*. https://doi.org/10.1016/j.solmat.2017.09.038

Zhang, Q., Hao, F., Li, J., Zhou, Y., Wei, Y., & Lin, H. (2018). Perovskite solar cells: must lead be replaced–and can it be done? In *Science and Technology of Advanced Materials*. https://doi.org/10.1080/14686996.2018.1460176

Zhang, Y., Liu, M., Eperon, G. E., Leijtens, T. C., McMeekin, D., Saliba, M., Zhang, W., De Bastiani, M., Petrozza, A., Herz, L. M., Johnston, M. B., Lin, H., & Snaith, H. J. (2015). Charge selective contacts, mobile ions and anomalous hysteresis in organic-inorganic perovskite solar cells. *Materials Horizons*. https://doi.org/10.1039/c4mh00238e

Zhao, X., & Wang, M. (2018). Organic hole-transporting materials for efficient perovskite solar cells. In *Materials Today Energy*. https://doi.org/10.1016/j.mtener.2017.09.011

Zhao, Y., & Zhu, K. (2013). Charge transport and recombination in perovskite (CH_3NH_3)PbI_3sensitized TiO2Solar Cells. *Journal of Physical Chemistry Letters*. https://doi.org/10.1021/jz401527q

Zhen, C., Wu, T., Chen, R., Wang, L., Liu, G., & Cheng, H. M. (2019). Strategies for Modifying TiO_2 Based Electron Transport Layers to Boost Perovskite Solar Cells. *ACS Sustainable Chemistry & Engineering*, *7*(5), 4586–4618. https://doi.org/10.1021/ACSSUSCHEMENG.8B06580

Zheng, X., Chen, B., Dai, J., Fang, Y., Bai, Y., Lin, Y., Wei, H., Zeng, X. C., & Huang, J. (2017). Defect passivation in hybrid perovskite solar cells using quaternary ammonium halide anions and cations. *Nature Energy*. https://doi.org/10.1038/nenergy.2017.102

Zhou, H., Chen, Q., Li, G., Luo, S., Song, T. b., Duan, H. S., Hong, Z., You, J., Liu, Y., & Yang, Y. (2014). Interface engineering of highly efficient perovskite solar cells. *Science*. https://doi.org/10.1126/science.1254050

Zhou, X., Zhang, Y., Kong, W., Hu, M., Zhang, L., Liu, C., Li, X., Pan, C., Yu, G., Cheng, C., & Xu, B. (2018). Crystallization manipulation and morphology evolution for highly efficient perovskite solar cell fabrication: Via hydration water induced intermediate phase formation under heat assisted spin-coating. *Journal of Materials Chemistry A*. https://doi.org/10.1039/c7ta08947c

Zhou, Y., Zhou, Z., Chen, M., Zong, Y., Huang, J., Pang, S., & Padture, N. P. (2016). Doping and alloying for improved perovskite solar cells. In *Journal of Materials Chemistry A*. https://doi.org/10.1039/C6TA08699C

Zhu, Z., Ma, J., Wang, Z., Mu, C., Fan, Z., Du, L., Bai, Y., Fan, L., Yan, H., Phillips, D. L., & Yang, S. (2014). Efficiency enhancement of perovskite solar cells through fast electron extraction: The role of graphene quantum dots. *Journal of the American Chemical Society*. https://doi.org/10.1021/ja4132246

Zou, Y., Yu, W., Tang, Z., Li, X., Guo, H., Liu, G., Zhang, Q., Zhang, Y., Zhang, Z., Wu, C., Xiao, J., Qu, B., Chen, Z., & Xiao, L. (2021). Improving interfacial charge transfer by multi-functional additive for high-performance carbon-based perovskite solar cells. *Applied Physics Letters*, *119*(15). https://doi.org/10.1063/5.0061869

CHAPTER THREE

RESEARCH METHODOLOGY AND EXPERIMENTAL TECHNIQUES

3.1 Introduction

In this chapter, a summary of the different materials, research methods, and materials characterization techniques used to carry out this research is given. The general working principles of some of the characterization equipment used are also highlighted to enable the readers to acquire the basic knowledge behind their operation. The specific details of the materials, experimental procedures, and characterization techniques used for the different experiments carried out to achieve the objectives of this research work are given in the materials and methods section in each of the subsequent chapters.

3.2 Materials

The materials used in this work were mainly purchased from Sigma Aldrich and they were used without any further purification unless otherwise stated. They include lead (II) Iodide (PbI_2, 99.99%), Formamidinium Iodide (FAI), Methyl ammonium Chloride (MACl), Methyl ammonium Bromide (MABr), Cesium Bromide (CsBr), Polyethylene oxide, 2,2',7,7'-tetrakis(N,N-di-p-methoxyphenylamine)-9,9-spirobifluorene (Spiro-OMeTAD), lithium *bis*-(*tri*-fluoromethanesulfonyl)imide (Li-TSFI), Fullerine-C60 and 4-*tert*-butylpyridine (*t*BP) which all existed as solutes.

The other chemicals such as Acetone, Acetonitrile (99.8%), Butanol, Chlorobenzene, Dimethyl sulfoxide (DMSO; 99.9%), Isopropyl alcohol (IPA), and N,N-dimethylformamide

(DMF; 99.8%) existed as solvents. Titanium diisopropoxide bis(acetylacetonate) (75% wt in isopranol) and Tin (IV) Oxide nano-particle ink (2.5% wt in butanol) existed as suspensions. Pure gold (99.999%) was purchased from Kurt J. Lesker Company and they existed mainly in form of pellets. The Fluorine-doped tin oxide (FTO)-coated glasses were also purchased from Sigma Aldrich either in the pre-etched form or without any etching.

3.3 Experimental methods

3.3.1 Substrate preparation

The FTO-coated glass substrate existed in un-etched and etched forms. For the un-etched substrate, the preparation process began by cutting the substrate into the required dimensions of 12.5 mm by 25 mm followed by etching using zinc powder and 2M Hydrochloric acid (HCl) solution. This was then followed by sequential cleaning in a detergent, deionized water, acetone, and IPA; each for 15 min. For the pre-etched FTO-coated glass substrates, sequential cleaning was carried out after cutting the substrates to the required dimensions. After cleaning, the substrates were dried in Nitrogen gas and finally exposed to UV Ozone so as to rid off any form of organic matter that may have remained on their surfaces during the cleaning process.

3.3.2 Preparation of the ETL thin films

The ETL thin films were formed on the cleaned FTO-coated glass substrates by spin-coating 0.15 M and 0.3 M solutions of Titanium dioxide (TiO_2) in Butanol; mixed with an appropriate proportion of Tin oxide (SnO_2) nano-particle ink; in a two-step process. In the first step, the 0.15 M TiO_2 solution (mixed with SnO_2) was spin-coated on the substrate followed by thermal annealing at 150 °C for 5 minutes. In the second step; which was done

after the first film had cooled to room temperature; the mixture containing the 0.3 M TiO_2 solution was spin-coated, sintered at 500 °C for 30 minutes then allowed to cool to form the ETL thin film.

3.3.3 Preparation of perovskite thin films

Except for perovskite films incorporating a thin layer of CsBr, the thin films of the AL were prepared via a two-step spin-coating process where a layer of PbI_2 was first deposited followed by a layer of the mixed organic components (FAI, MACl, and MABr). The details of the perovskite film preparation process are explained in each of the subsequent chapters.

3.3.4 Fabrication of PSC

A Planar PSCs; with a regular architecture; was fabricated by sequential deposition of the thin films of the different components (ETL, AL, HTL & electrode) on FTO-coated glass substrate. Apart from the gold electrode which was formed via thermal evaporation, the other layers were formed via spin-coating. The different layers were however subjected to different thermal annealing temperatures as explained in the experimental section of the subsequent chapters.

3.4 Materials characterization techniques

3.4.1 Scanning electron microscopy

This is a non-destructive materials characterization technique that involves creating a magnified image of a sample surface that reveals different information about its microscopic features (Inkson, 2016). A scanning electron microscope (SEM) works on the principle of directing a highly collimated beam of high-energy electrons on the surface of the sample so as to acquire information about its physical and chemical properties on a microscopic scale. In a

nutshell, the electrons which are generated from a source are accelerated to high energies and focused into a beam with the help of apertures and lenses. The electrons then interact with the sample and undergo reflection or scattering from different regions of the sample depending on their energies. The reflected or scattered electrons are finally collected by different detectors to obtain information about the different features of the sample such as the topography, morphology, crystallography, and elemental composition. The other features such as grain size can be obtained from a SEM image with the help of a computer software such as imageJ.

3.4.2 X-Ray diffractometry

This is a non-destructive materials characterization technique that provides information about the crystallinity and the phases present in a material. The basic operating principles of X-ray diffraction (XRD) involve the production of monochromatic X-rays, diffraction of the X-rays from a sample surface, and angle-resolved detection of the diffracted signals by a detector (Epp, 2016; Snyder & Jenkins, 2012). Depending on the nature of the crystalline sample, the diffracted X-rays undergo either constructive or destructive interference which is recorded as diffraction patterns in the detector. A diffraction peak intensity is recorded when the X-rays impinging on the sample satisfy the Bragg relation given in eqn (3.1).

$$n\lambda = 2d \sin\theta \tag{3.1}$$

Where n, λ, d and θ denotes the diffraction order, the wavelength of X-rays, the inter-planar spacing, and diffraction angle respectively. A plot of the XRD peak intensity as a function of the peak position (2θ) generates a spectrum that provides information about the crystalline nature of the sample and the crystalline phases present. The XRD patterns of crystalline

materials are characterized by well-defined or sharp diffraction peaks while those of non-crystalline ones are characterized by broad humped peaks. Figure 3.1 indicates the XRD patterns of crystalline and amorphous materials.

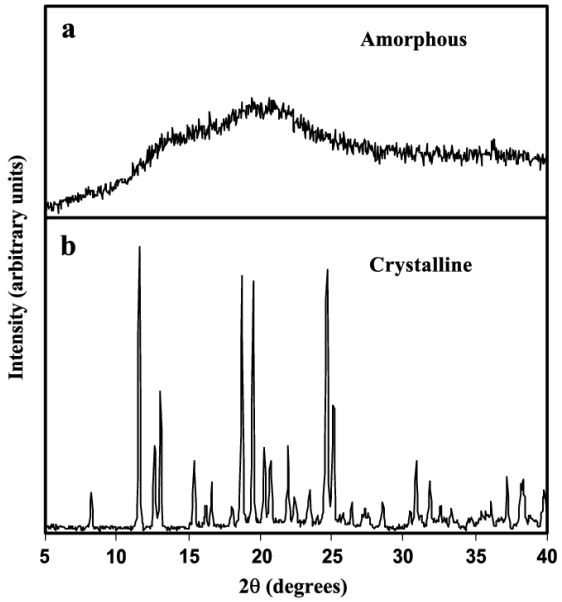

Figure 3.1: XRD patterns of amorphous and crystalline materials (Source: Nunes et al., 2005)

In the XRD spectra, a shift in the position of the peaks is an indication of a change in the inter-atomic distance or the lattice parameter which may be caused by either substitutional doping, temperature change, or lattice strain. Information about crystallite size (D) can be determined from the full-width at half maximum (β), the wavelength of the X-rays (λ), and the Bragg angle (θ) using the Scherrer formula given by eqn (3.2) (Valério & Morelhão, 2019).

$$D = \frac{k\lambda}{\beta \cos\theta} \tag{3.2}$$

Where k is the geometrical factor. Some softwares such as High score PANalytical are very helpful in phase identification and indexing of the XRD spectra.

3.4.3 Ultraviolet-visible (UV-Vis) spectroscopy

This is a quantitative technique that measures the extent of attenuation of a beam of light from a UV or visible source after passing through a given sample. Basically, it involves passing a light beam through a sample and measuring the intensity of the transmitted beam over an extended spectral range relative to a reference sample (Manivannan, 1997). By comparing the intensities of the incident and transmitted light beam, the physical and chemical properties of the sample can be obtained. According to Beer Lambert's law (eqn 3.3), the intensity of the transmitted beam (I) is related to the intensity of the incident beam (I_o) through:

$$I = I_o \exp\left(-c \in L\right) \tag{3.3}$$

Where $c, \in$ and L denote the concentration, molar extinction coefficient and the path length respectively. The transmittance (T) and absorbance (A) of the sample are related to the intensities I_o and I according to eqns (3.4) and (3.5).

$$T = \frac{I}{I_o} \tag{3.4}$$

$$A = \log \frac{I_o}{I} = -\log T \tag{3.5}$$

In a UV-Vis spectrum, a plot of T or A as a function of the wavelength can be used to obtain information on the optoelectronic properties of semiconductor material. From absorbance data, the optical bandgap of the semiconductor can be estimated from a Tauc plot (Makuła et al., 2018). Another parameter called Urbach energy; which quantifies the degree of structural disorder in the semiconductor; can also be obtained from absorbance (Ikhmayies & Ahmad-Bitar, 2013).

3.4.4 Photoluminescence measurement

Photoluminescence (PL) is the phenomenon of light emission in semiconductors when photoelectrons make a transition from excited states to the ground state. As a materials characterization technique, PL is a contactless, non-destructive method that provides important insights for understanding the optoelectronic properties of semiconducting materials (Bishop, 1981). It involves shining light on a material to cause photo-excitation and measuring the intensity (energy) of the emitted photons as the photo-excited electrons relax back to the ground state. The energy of the emitted photons is a direct measure of the energy difference between the conduction band and valence band edges (i.e the optical band gap) in a semiconductor. A plot of the intensity of the emitted photon as a function of the wavelength of light used can be used to understand the optical properties and defect characteristics of a semiconductor material (Higgs et al., 2000). The PL intensity can be considered as an indication of the density of defects in semiconductor thin films or the charge extraction (PL quenching) ability of CTLs in solar cells. For perovskite films deposited on bare substrates (without the CTLs), the PL intensity is inversely proportional to the density of defects. Figure 3.2 shows the PL spectra of Cesium formamidinium (CsFA)-based perovskite films, one containing methyl-ammonium (MA) additive and one without. The PL intensity of the MA-containing film is higher since its reduced defect density compared to pristine CsFA-based film (Tan et al., 2018). Time-resolved PL (TRPL) studies can be used to obtain information regarding the radiative and non-radiative recombination dynamics in semiconductor thin films (Weiss et al., 2019).

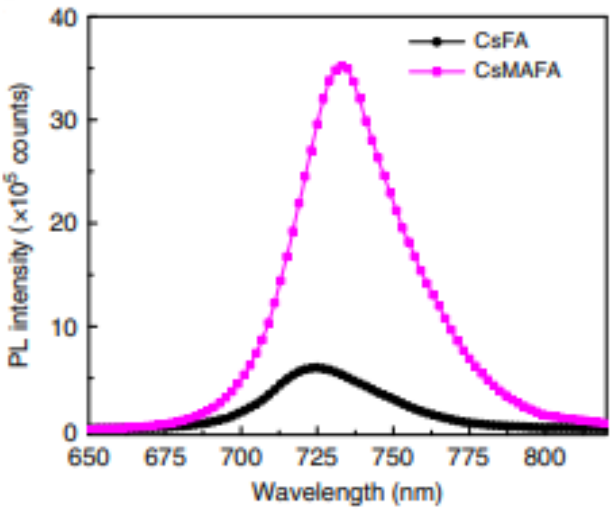

Figure 3.2: PL spectra of perovskite films with different defect densities (Source: Tan et al., 2018)

3.4.5 X-ray photoelectron spectroscopy and Ultraviolet photoelectron spectroscopy

X-ray photoelectron spectroscopy (XPS) and Ultraviolet photoelectron spectroscopy are surface-sensitive analytical techniques that rely on the principles of the photoelectric effect to obtain information on the materials' surface chemistry and electronic band structure respectively (Nascente, 2005; Stevie & Donley, 2020; Zatsepin & Zatsepin, 2021). They both involve measuring the kinetic energy ($K.E$) or the number of photoelectrons emitted when the surface of a sample is bombarded with photons of certain energies. In XPS analysis, the surface of a sample is bombarded with X-rays while in UPS, UV radiations are used. The $K.E$ of photoelectrons is used to determine the binding energy (E_B) of the electrons using eqn (3.6).

$$E_B = h\nu - K.E - \phi \qquad (3.6)$$

Where $h\nu$ and ϕ are the energy of the incident photons and material's work function respectively.

In XPS, the number of electrons detected at a given E_B is used to obtain useful information about the elemental composition and chemical states on the surface of a sample. A plot of the number of electrons at a given E_B is termed as XPS spectrum and each peak in the spectrum is a signature of a particular element or functional group present in the sample. In UPS, the photoelectron count as a function of E_B is used to get some insights into the electronic band structure of a material.

3.4.6 Fourier transform infra-red (FTIR) spectroscopy

This is a spectroscopic technique that uses a beam of infra-red (IR) radiation to identify the functional groups present in a material (Dutta, 2017; Faix, 1992). Atoms in a molecule always undergo vibrational motions which cause a change in their dipole moments. These vibrations absorb IR only at specific wavelengths. In FTIR spectroscopy, IR radiation is passed through a sample and the resulting absorption or transmission spectra are recorded. The spectra create a molecular fingerprint that is unique to the functional groups present in a given material. The IR radiation emanating from the source is first passed through an interferometer for encoding before it passes through the sample. The IR beam from the sample is then sent to a detector to generate a signal which undergoes Fourier transformation in the computer for easy interpretation. The signal is displayed in the form of a spectrum where the intensity of absorption/transmission is plotted as a function of the wavenumber (*k*). Depending on the vibrations of the different functional groups present and the concentration of molecules in a sample, the intensity of the peaks will differ. Different functional groups absorb IR radiation at the same *k* values regardless of the structure of the material under consideration.

3.4.7 Transient absorption spectroscopy

This spectroscopic technique is used to quantitatively characterize the time-dependent photo-excited state absorption dynamics of an optically active sample. In transient absorption spectroscopy (TAS), a high-intensity pump laser and low-intensity probe laser are passed through the sample with a certain delay time (t) so that the difference between their absorption spectra (ΔA) is recorded. By varying the delay time t between the pump and the probe lasers and recording ΔA, a spectrum that provides information on the nature and the dynamics of the excited states occurring in the sample is generated (Berera et al., 2009). In perovskite films, the technique helps in understanding the charge carrier relaxation and recombination dynamics, charge carrier lifetimes, the strength of electronic coupling between the AL and the CTLs as well as the defect passivation effects of additives (Kulshreshtha et al., 2020; Pasanen et al., 2020; Wang et al., 2014)

3.4.8 Current-Voltage (I-V) measurement

The current-voltage (I-V) measurement is another characterization technique that is usually applied to semiconductor structures in order to get some insights into their electrical properties. The I-V curve of a semiconductor device; also represented as the J-V (current density-voltage) curve; is a graphical representation of the relationship between the current and the potential difference across it. It is very important in determining the values of the electrical parameters such as electrical conductivity, charge carrier density, charge carrier mobility, series resistance, shunt resistance, and diode ideality factor. The J-V characterization of a semiconductor material is usually carried out by applying a current (I) through the material and measuring the potential difference (V) developed across it. This can be done in

the dark or under illumination either in forward bias or reverse bias modes depending on the parameters of interest.

For semiconductor thin films, the J-V curves in the dark are usually linear in the low voltage regimes due to the dominance of Ohmic conduction. However, they deviate from linearity at higher voltage regimes where the space charge limited conduction dominates (Wetzelaer, 2018). The point where the curves deviate from linearity is referred to as the trap-filled voltage limit (V_{TFL}) and is dependent on the trap density state of the material (see figure 3.3(a)) (Khan et al., 2020). For a solar cell, the J-V curve is important in understanding its PV performance characteristics and the power loss mechanisms taking place within the solar cell (Wang et al., 2019). Figure 3.3(b) shows the J-V curves of a screen-printed n-type silicon solar cell both in the dark and under illumination. Under illumination, the J-V curve is useful in determining PV parameters while that in the dark is useful in determining power losses in solar cells.

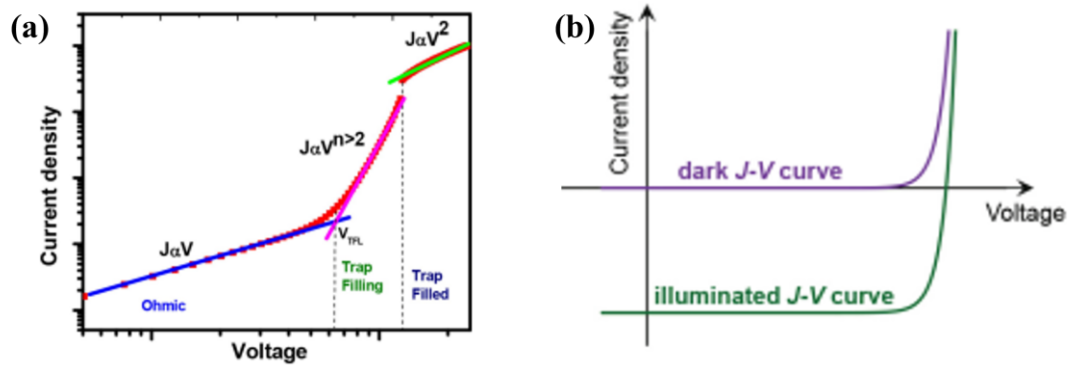

Figure 3.3: The J-V curves of (a) Perovskite semiconductor film under dark in log scale (b) n-type silicon solar cell (Sources: Tao, 2016; Khan et al., 2020)

3.4.9 Electrochemical impedance spectroscopy

This is a quantitative materials characterization technique that involves the application of small-signal alternating current (AC) to a sample in order to probe its impedance characteristics. In electrochemical impedance spectroscopy (EIS), the impedance (Z) of a sample is plotted as a function of the frequency of the AC signal either in the form of a Nyquist plot or Bode plot so as to understand the various electrochemical processes that occur at different time scales. The electrochemical impedance spectra are usually interpreted by fitting the data to an equivalent electrical circuit that consists of different combinations of resistors, capacitors, or inductors in order to extract the values of the parameters of interest. This characterization technique was commonly used in the study of DSSCs and has recently been applied in the study of PSCs (Guerrero et al., 2021). The technique is useful in understanding how the modification of any component of PSC influences the charge transport kinetics.

3.4.10 External quantum efficiency measurement

The external quantum efficiency (EQE) measurement is a fundamental characterization technique that is usually applied to any PV system to understand how efficient it is in converting the incident light photons to electric current. It specifies the ratio of the number of charge carriers collected from a PV device under the short circuit condition to the number of light photons incident on it (Slami & Benramdane, 2021). The EQE measurement is carried out by shining light of known wavelength to a PV device and recording the number of charge carriers collected at a given wavelength. A plot of the ratio of charge carriers collected to the number of the incident light photons; expressed as a function of the wavelength of the incident light; gives the EQE curve of the given PV device. The EQE curve of an ideal PV device is

equal to unity and has a profile shown by the dotted line in Figure 3.4. However, due to charge carrier recombination, low carrier diffusion lengths, and optical loss effects, the EQE of a PV is reduced and usually assumes a profile that depends on the charge carrier collection efficiency at each wavelength region of the solar spectrum (Nakane et al., 2016). Figure 3.4 shows a typical EQE of a solar cell device and how it is shaped by the various charge carrier loss mechanisms that occur at each wavelength region.

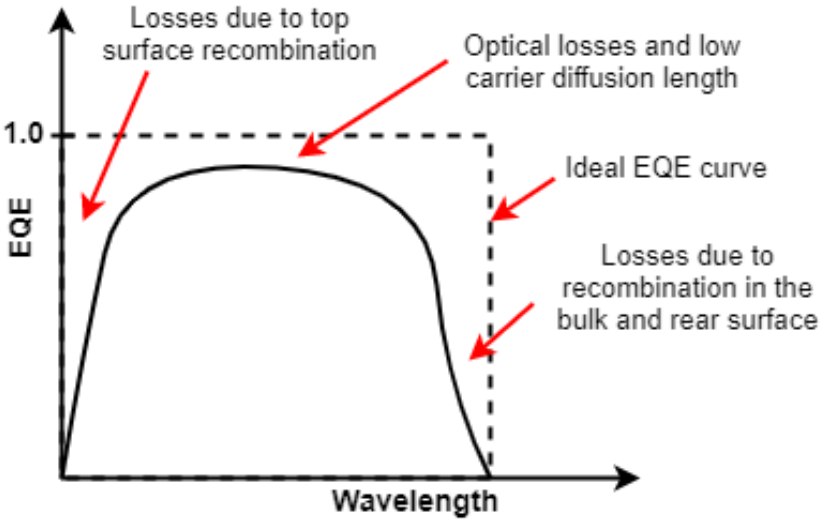

Figure 3.4: External quantum efficiency curve of a PV device

3.5 References

Berera, R., van Grondelle, R., & Kennis, J. T. M. (2009). Ultrafast transient absorption spectroscopy: principles and application to photosynthetic systems. Photosynthesis Research, 101(2–3), 105. https://doi.org/10.1007/S11120-009-9454-Y

Bishop, S. G. (1981). Characterization Of Semiconductors By Photoluminescence And Photoluminescence Excitation Spectroscopy. Https://Doi.Org/10.1117/12.931681, 0276, 2–10. https://doi.org/10.1117/12.931681

Dutta, A. (2017). Fourier Transform Infrared Spectroscopy. Spectroscopic Methods for Nanomaterials Characterization, 2, 73–93. https://doi.org/10.1016/B978-0-323-46140-5.00004-2

Epp, J. (2016). X-ray diffraction (XRD) techniques for materials characterization. Materials Characterization Using Nondestructive Evaluation (NDE) Methods, 81–124. https://doi.org/10.1016/B978-0-08-100040-3.00004-3

Faix, O. (1992). Fourier Transform Infrared Spectroscopy. 83–109. https://doi.org/10.1007/978-3-642-74065-7_7

Guerrero, A., Bisquert, J., & Garcia-Belmonte, G. (2021). Impedance Spectroscopy of Metal Halide Perovskite Solar Cells from the Perspective of Equivalent Circuits. Chemical Reviews, 121(23), 14430–14484. https://doi.org/10.1021/ACS.CHEMREV.1C00214

Higgs, V., Chin, F., Wang, X., Mosalski, J., & Beanland, R. (2000). Photoluminescence characterization of defects in Si and SiGestructures. Journal of Physics: Condensed Matter, 12(49), 10105. https://doi.org/10.1088/0953-8984/12/49/310

Ikhmayies, S. J., & Ahmad-Bitar, R. N. (2013). A study of the optical bandgap energy and Urbach tail of spray-deposited CdS:In thin films. Journal of Materials Research and Technology, 2(3), 221–227. https://doi.org/10.1016/J.JMRT.2013.02.012

Inkson, B. J. (2016). Scanning electron microscopy (SEM) and transmission electron microscopy (TEM) for materials characterization. Materials Characterization Using Nondestructive Evaluation (NDE) Methods, 17–43. https://doi.org/10.1016/B978-0-08-100040-3.00002-X

Kulshreshtha, C., Clement, A., Pascher, T., Sundström, V., & Matyba, P. (2020). Investigating ultrafast carrier dynamics in perovskite solar cells with an extended π-conjugated polymeric diketopyrrolopyrrole layer for hole transportation. RSC Advances, 10(11), 6618–6624. https://doi.org/10.1039/C9RA10009A

Makuła, P., Pacia, M., & Macyk, W. (2018). How To Correctly Determine the Band Gap Energy of Modified Semiconductor Photocatalysts Based on UV-Vis Spectra. Journal of Physical Chemistry Letters, 9(23), 6814–6817.

https://doi.org/10.1021/ACS.JPCLETT.8B02892/SUPPL_FILE/JZ8B02892_LIVESLIDES.

Manivannan, G. (1997). UV-vis spectroscopy as an analytical tool for the characterization of polymers. Materials Characterization and Optical Probe Techniques: A Critical Review, 10291, 1029107. https://doi.org/10.1117/12.279857

Nascente, P. A. P. (2005). Materials characterization by X-ray photoelectron spectroscopy. Journal of Molecular Catalysis A: Chemical, 228(1–2), 145–150. https://doi.org/10.1016/J.MOLCATA.2004.09.075

Pasanen, H. P., Vivo, P., Canil, L., Hempel, H., Unold, T., Abate, A., & Tkachenko, N. V. (2020). Monitoring Charge Carrier Diffusion across a Perovskite Film with Transient Absorption Spectroscopy. Journal of Physical Chemistry Letters, 11(2), 445–450. https://doi.org/10.1021/ACS.JPCLETT.9B03427/SUPPL_FILE/JZ9B03427_SI_002.ZIP

Snyder, R., & Jenkins, R. (2012). Introduction to X-Ray Powder Diffractometry. 428. https://books.google.com/books/about/Introduction_to_X_Ray_Powder_Diffractome.html?id=khDCUhKV788C

Stevie, F. A., & Donley, C. L. (2020). Introduction to x-ray photoelectron spectroscopy. Journal of Vacuum Science & Technology A: Vacuum, Surfaces, and Films, 38(6), 063204. https://doi.org/10.1116/6.0000412

Valério, A., & Morelhão, S. L. (2019). Usage of Scherrer's formula in X-ray diffraction analysis of size distribution in systems of monocrystalline nanoparticles. http://arxiv.org/abs/1911.00701

Wang, Lei, Liu, F., Zhang, Z., Shao, X., Zhu, Z., & Deng, S. (2019). Micro-Mismatch Loss Analysis Based on Solar Cell IV Curve. Journal of Physics: Conference Series, 1346(1). https://doi.org/10.1088/1742-6596/1346/1/012006

Wang, Lili, McCleese, C., Kovalsky, A., Zhao, Y., & Burda, C. (2014). Femtosecond time-resolved transient absorption spectroscopy of CH 3NH3PbI3 perovskite films: Evidence for passivation effect of pbi2. Journal of the American Chemical Society, 136(35), 12205–12208. https://doi.org/10.1021/JA504632Z

Weiss, T. P., Bissig, B., Feurer, T., Carron, R., Buecheler, S., & Tiwari, A. N. (2019). Bulk and surface recombination properties in thin film semiconductors with different surface treatments from time-resolved photoluminescence measurements. Scientific Reports 2019 9:1, 9(1), 1–13. https://doi.org/10.1038/s41598-019-41716-x

Zatsepin, D. A., & Zatsepin, A. F. (2021). Ultraviolet Photoelectron Spectroscopy – Materials Science Technique. Spectroscopy for Materials Characterization, 383–403. https://doi.org/10.1002/9781119698029.CH13

CHAPTER FOUR

TIN OXIDE MODIFIED TITANIUM DIOXIDE AS ELECTRON TRANSPORT LAYER IN FORMAMIDINIUM-RICH PEROVSKITE SOLAR CELLS

4.1 Introduction

In this chapter, we incorporated tin oxide (SnO_2) into titanium dioxide (TiO_2) thin film and studied the evolution of its microstructural and optoelectronic properties with SnO_2 loading. The thin films were then integrated as ETLs in a regular planar Formamidinium (FA)-rich mixed lead halide PSCs so as to assess the overall effect of SnO_2 proportion on their charge transport and PV characteristics.

Perovskite solar cells (PSCs) have emerged as one of the low-cost photovoltaic (PV) technologies with photoconversion efficiencies comparable to those of the conventional crystalline silicon-based solar cells (Even et al., 2016; Koech et al., 2019). They consist of photoactive perovskite layers that are sandwiched between two oppositely doped CTLs to form regular (n-i-p) or inverted (p-i-n) device architectures with electrodes on either side (Mali & Hong, 2016; You et al., 2016). Within these architectures, the perovskite layer absorbs light and generates charge carriers that are injected into the CTLs before being transported in opposite directions to their respective electrodes where they are collected as electric current (Thakur et al., 2017).

The charge carrier collection efficiency and hence the overall PCE of PSCs depends on the effectiveness of light absorption (Yue et al., 2016) and the accompanying charge carrier

dynamics (Shi et al., 2018) that occur within the PSC structure. Owing to the exceptional optoelectronic properties of the perovskite AL such as high light absorption ability (Yue et al., 2016), low exciton binding energies (Hsiao et al., 2015), balanced ambipolar charge carrier transport (Giorgi & Yamashita, 2015; Shi et al., 2018), high defect tolerance and long carrier diffusion lengths (Zhang et al., 2017), the charge carriers in the AL are effectively generated, separated and transported to the interface with CTLs when PSCs are illuminated (Tailor, Abdi-Jalebi, Gupta, Lu, et al., 2020).

One of the main hindrances to achieving high PCEs in PSCs is the low charge carrier collection efficiency that is associated with non-radiative recombination losses arising from inadequate extraction and transportation of photo-generated charge carriers through the CTLs to the electrodes (Grill et al., 2017; Le Corre, Stolterfoht, Perdigo, et al., 2019; Wolff et al., 2019; N. Wu et al., 2017). These processes are mainly governed by the material properties of the CTLs and the nature of the interface they form with the AL (Courtier et al., 2019; Stolterfoht et al., 2019a). In order to further improve the performance of PSCs, the CTLs ought to be designed to achieve good optical transparency, excellent carrier selectivity, good electrical conductivity, and band energy levels that align well with those of the AL (Mahmood et al., 2017; Ren et al., 2019).

In planar PSCs with n-i-p configurations, the ETL not only plays a key role in the extraction and transportation of photo-generated electrons (Yu et al., 2020) but also in the light absorption and the crystallization dynamics of the AL (Nimens et al., 2018). Hence, different materials have been explored for use as ETLs in PSCs with those based on metal oxide semiconductors; either in mesoporous and/or compact forms, proving to be attractive in terms of PCE and stability (Mahmood et al., 2017; Shin et al., 2019; Zheng et al., 2019; Yu

Zhou et al., 2020). Among the metal oxide semiconductors, titanium dioxide (TiO_2) is the most commonly used ETL due to its high transmittance in the visible light regime, low cost, good chemical stability, non-toxicity, and the ease with which its properties can be tuned with minimal impact on its structure (Chen, 2009; Chen & Mao, 2007). However, TiO_2 has a low electrical conductivity that increases the series resistance (R_s) and causes power losses in PSCs (Pan et al., 2013; Yu et al., 2018).

Modification of TiO_2 through strategies such as doping with cations/anions (Nwankwo et al., 2020), hybridization with graphene derivatives (Belchi et al., 2019; Saleem et al., 2018), forming core-shell nanostructures (Li et al., 2018), and coupling with other n-type semiconductors (Akurati et al., 2005; Apostolopoulou et al., 2017) is an effective method to improve its optoelectronic properties which consequently leads to an improvement in the PCEs and stability of PSCs (Zhen et al., 2019a). Tin (IV) Oxide (SnO_2) is one of the n-type metal oxide semiconductors that has successfully been used to tune the optoelectronic properties of TiO_2 for applications in photocatalysis (Akurati et al., 2005), gas sensing (Larin et al., 2016), and in dye-sensitized solar cells (Desai et al., 2013; Duan et al., 2012). It has a similar crystal structure with TiO_2 but exhibits higher optical transmittance, higher electrical conductivity, better UV stability and is more favorable for the growth of perovskite films than TiO_2 (Dou & Persson, 2013; Yu et al., 2020).

The synergetic effects that arise from the combination of SnO_2 and TiO_2 to form either a bi-layered or composite ETL structure have been utilized to improve the PCE and stability of PSCs (Guo et al., 2018; Li et al., 2020; Liu et al., 2018; Martínez-Denegri et al., 2018; Song et al., 2017; Tavakoli et al., 2018; Wan et al., 2018). The improvement has mainly been attributed to suppression of charge carrier recombination and accelerated extraction of the

photo-generated electrons resulting from better energy level alignment and defect passivation at the ETL/perovskite interface (Wan et al., 2018). Though the few studies that have been done on the use of SnO_2-TiO_2 nano-composite as ETLs in PSCs have shown that they help to improve the performance (Guo et al., 2018; Liu et al., 2020; Mohammadbeigi et al., 2020), the underlying physical and intrinsic phenomena that are responsible for the reported improvement are not clear, necessitating the need for more research in this area. In particular, the evolution of the properties of TiO_2 with SnO_2 loading, its possible impacts on the optoelectronic properties of the perovskite film, and how it influences the overall charge transport kinetics and performance metrics of PSC requires further investigation.

This chapter presents the results of the effects of SnO_2 incorporation in TiO_2-based ETL on the charge carrier dynamics and performance characteristics of planar Formamidium (FA)-rich mixed lead halide PSCs. First, we processed the ETL thin films on FTO-coated glass substrates and studied the evolution of their structural, morphological, and optoelectronic properties with the proportion of SnO_2 in TiO_2. We then fabricated a series of planar regular PSCs that incorporated the SnO_2-TiO_2 and pristine TiO_2 thin films as ETLs and compared their performance parameters. The results are then discussed for the design of efficient PSCs.

4.2 Materials and methods

4.2.1 Materials

Unless otherwise stated, all the materials and reagents used in this work were purchased from Sigma Aldrich and used in the as-received condition. They include Titanium diisopropoxide, Tin (IV) Oxide nanoparticles (2.5% weight in butanol, nanoparticle size < 20 nm), Formamidinium iodide (FAI), Methylammonium Chloride (MACl), Methylammonium

Bromide (MABr), Lead (II) Iodide, Spiro-OMeTAD, and Fullerene C60. Dimethyl sulfoxide (DMSO), anhydrous N,N-dimethylformamide (DMF), Chlorobenzene were among the solvents used. Gold pellets (99.999%) were purchased from Kurt J. Lesker Company.

4.2.2 Processing of ETL thin films

FTO-coated glass substrates were patterned using zinc powder and 2M Hydrochloric acid and cleaned sequentially in an ultrasonic bath using detergent, deionized water, acetone, and IPA for 15 min each. The substrates were then blow-dried using nitrogen gas before being treated with UV ozone for 15 min in order to remove any residual organic matter. Solutions of 0.15 M and 0.3 M of compact TiO_2 were then prepared by dissolving 55 µL and 110 µL of titanium diisopropoxide bis(acetylacetonate) respectively in 1ml of 1-butanol. SnO_2 nano-particle ink (2.5% in butanol, particle size < 20 nm) was then incorporated into the 0.15 M and 0.3 M TiO_2 solutions in different volume fractions of 0.1, 0.2 and 0.3 to obtain SnO_2-TiO_2 mixed solutions. The mixed solutions were sonicated for 30 min before being spin-coated onto the FTO-coated glass substrates. The solutions containing 0.15M were first spin-coated onto the FTO coated glass at 2000 rpm for 30 s, annealed at 150 °C for 5 min, and allowed to cool to room temperature. This was followed by spin-coating of the mixed solution containing 0.3M TiO_2 at 2000 rpm for 30 s before sintering at 500 °C for 30 min on a hot plate under ambient conditions. The thin film of pristine TiO_2 was also prepared following the same protocol. Figure 4.1(a)–(f) presents the schematics of the processing procedure of the ETL thin films.

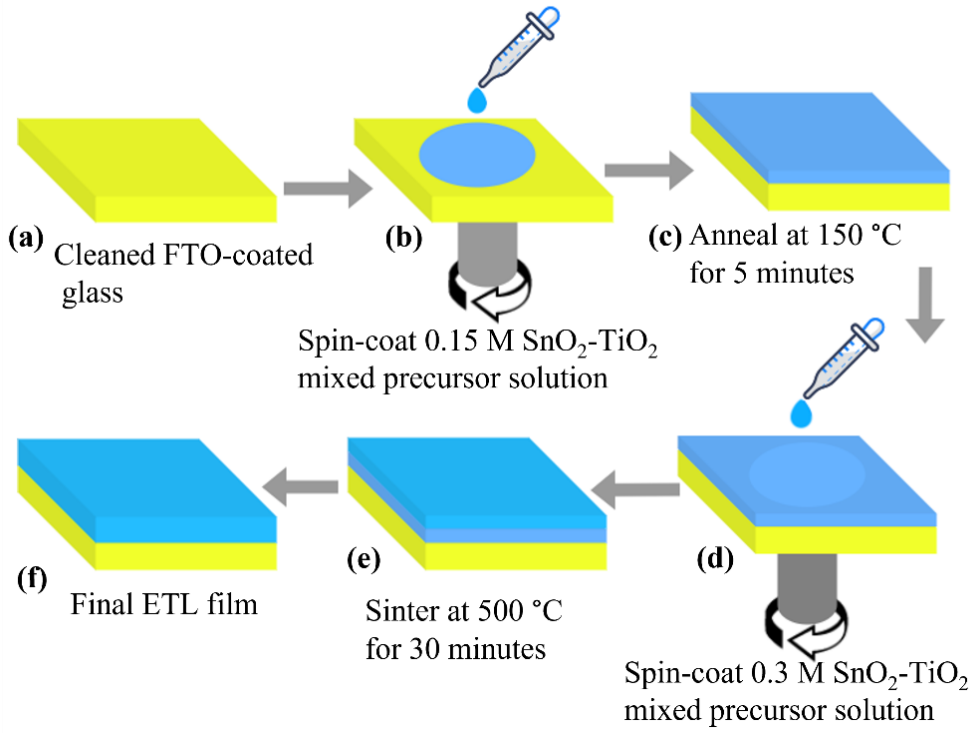

Figure 4.1: (a)–(f): Schematics of the ETL preparation procedure.

4.2.3 Fabrication of PSCs

Planar PSCs were prepared based on the modified and pristine TiO_2 as ETLs via a spin-coating technique. First, the ETLs were prepared on cleaned FTO-coated glass substrate as per the procedure summarized in Figure 4.1(a)–(f). Perovskite films were then deposited on the ETLs via a two-step spin-coating process described elsewhere (Oyewole, Koech, Ichwani, Ahmed, Tamayo, et al., 2021). The films were annealed at 130 °C for 15 min before the Spiro-OMeTAD solution was spin-coated onto it at 4000 rpm for 30 s. A thin layer of gold (90 nm) was deposited on the Spiro-OMeTAD film to form an electrode using a thermal evaporator (Edward E306A, UK).

4.3 Characterization of materials

The morphological, structural, optical, and electrical properties of the ETL thin films were investigated using various characterization techniques. The micro-structural images of the films and elemental composition were obtained using a field emission scanning electron microscope (SEM) (JEOL JSM-700F, Hollingsworth & Vose, MA, USA) that was instrumented with an energy dispersive X-ray spectrometer (EDS) (Oxford Instrument). The X-ray diffraction (XRD) patterns of the films were obtained using an X-ray diffractometer (Malvern PANalytical, Westborough, MA, USA) under Cu Kα radiation source at a voltage of 40 kV, current of 40 mA. This was done with a scanning step size of 0.01° and 2θ angles in the range of 20–90°. The optical properties of the thin films were measured using an ultraviolet-visible (UV-Vis) spectrometer (AVANTES Starline, Avaspec-2048) in the wavelength range of 200 nm to 1100 nm.

The current density-voltage (J-V) characteristics of the films and PSC devices were studied using a Keithley 2400 source meter unit (Keithley, Tektronix, Newark, NJ, USA) interfaced with a computer. In the case of PSC devices, the Keithley system was connected to an Oriel solar simulator (Oriel, Newport Corporation, Irvine, CA, USA) and the J-V curves were obtained under AM1.5G illumination of 100 mW/cm^2. The J-V measurement for the PSC device was carried out on a device area of 0.1 cm^2 with a voltage scan range of -0.4 to 1.2 V. The electrochemical impedance spectroscopy (EIS) of the fabricated PSCs was measured under illumination using a potentiostat (SP-300, BioLogic Instrument). The impedance measurements were performed at a bias voltage of 0.1 V with an AC signal of amplitude 10mV in the frequency range 1 MHz to 1 Hz while the external quantum efficiency measurement was carried out with Quantx-300 quantum efficiency measurement system.

4.4 Results and discussion

4.4.1 Structure and morphology of the ETL and perovskite thin Films

The microstructural characteristics of the ETL and perovskite films play an important role in the charge carrier dynamics and the overall performance of PSCs. Compact morphologies with fewer pinholes and grain boundaries are essentially needed to form good interfacial contacts with adjacent layers and to reduce power losses due to series resistance, current leakage, and charge carrier trapping (Noh et al., 2018). The SEM images of the ETL thin films with different proportions of SnO_2 are presented in Figure 4.2(a)–(d). As seen in the figure, the SEM images of the ETLs with 0, 0.1, and 0.2 proportions of SnO_2 (Figure 4.2(a)–(c)) are smooth and more compact when compared to the one with 0.3 proportion of SnO_2 which appears to be porous and with more pinholes (Figure 4.2(d)). The formation of pinholes at higher SnO_2 content can be associated with the agglomeration of SnO_2 nanoparticles or the degradation of SnO_2 at higher annealing temperatures (Ke et al., 2015). The presence of the pinholes in these films can provide shunting paths that cause current leakage from the AL to the FTO thus reducing the fill factor (*FF*) and the overall PCEs of PSC devices.

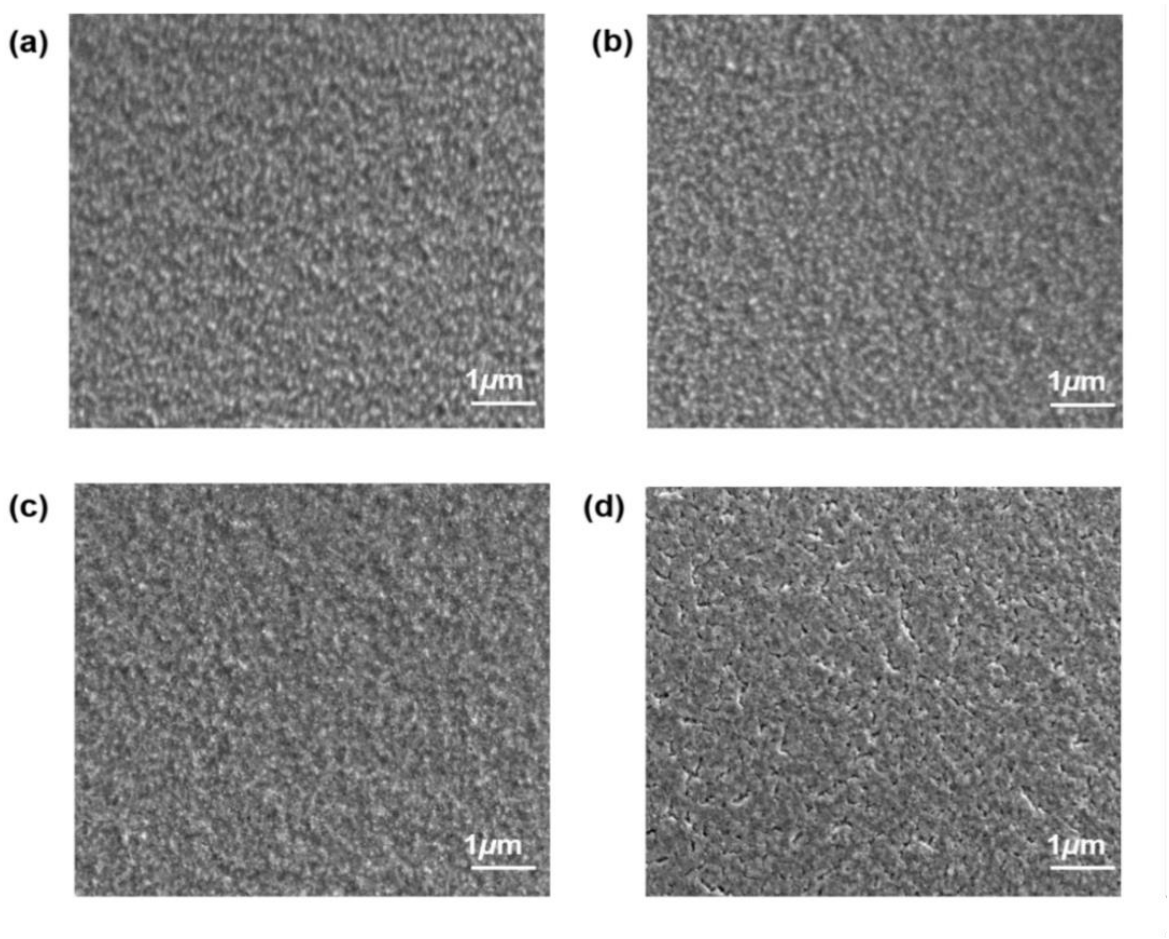

Figure 4.2: SEM images of ETL with (a) TiO_2 (b) 0.1 (c) 0.2 and (d) 0.3 proportions of SnO_2.

The elemental composition of the ETLs was studied by taking the EDS cross-sectional images. Figure 4.3 (a)-(b) shows the SEM and EDS cross-sectional images of the representative SnO_2-TiO_2 ETL film deposited on the FTO-coated glass substrate. From the figure, a thin layer of the ETL (around 100 nm in thickness) is visible on top of the FTO with an even distribution of Sn (Green) and Ti (Red). The EDS spectra of the ETLs at different SnO_2 content are presented in Figure 4.4 (a)-(d). From the figure, we see that Sn, Ti, and O are present in all the ETL films with different weight percentages. The SnO_2-TiO_2 based ETLs showed a higher Sn content relative to the TiO_2-based ETL and the percentage weight of Sn increased with the SnO_2 content. This confirms the successful incorporation of SnO_2 in TiO_2.

The Sn signals detected in the pristine TiO_2 ETL possibly diffused from the underlying FTO layer during the sintering process. The other elements detected such as Si, Mg, and Cu, originated from glass substrate and the copper tape that was used to attach the samples to the sample holder while Pd and Au came from the coating film used.

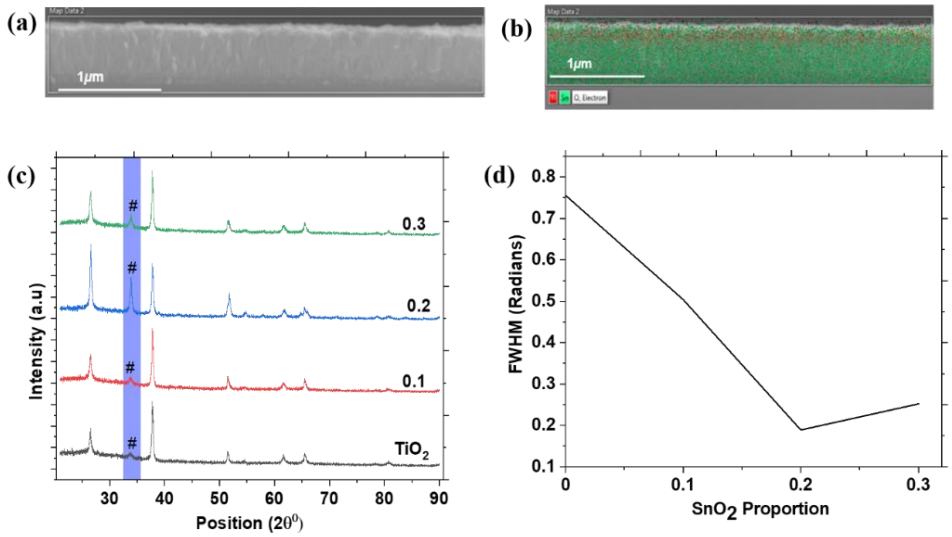

Figure 4.3: (a) SEM and (b) EDS Cross-sectional image of representative ETL film on FTO-coated glass; (c) XRD patterns of the ETL films (d) FWHM for the ETLs at different SnO_2 content.

To investigate the possible impact of SnO_2 incorporation on the structural properties of the ETL films, the XRD patterns of the different films were recorded at room temperature (25 °C). Figure 4.3 (c) shows the XRD patterns of all the ETL films at different proportions of SnO_2. The result shows that the diffraction peaks of all the ETL films occur at 2θ angles of 26.5°, 33.8°, 37.8°, 51.8°, 61.6° and 66° which can respectively be indexed to the planes (110), (011), (020), (121), (130) and (031) for tetragonal titanium tin oxide composite (ICSD 98-009-0868). The (020) plane is the preferred crystal orientation in nearly all the ETL films except the one containing 0.2 SnO_2 proportion whose preferred crystal orientation is the plane

(110). Another observable difference in the diffractograms of the ETL films lies in the intensity of the diffraction peaks. The intensity of the peak corresponding to the plane (011) (labeled #) is observed to increase with the content of SnO_2 in the ETL and reaches the highest value at SnO_2 proportion of 0.2. The full-width at half maximum (FWHM) of the peak was also found to decrease with increasing SnO_2 content attaining a minimum value at the same SnO_2 proportion (Figure 4.3(d)). This shows that the ETL film with the 0.2 proportion of SnO_2 had better crystallinity relative to the rest.

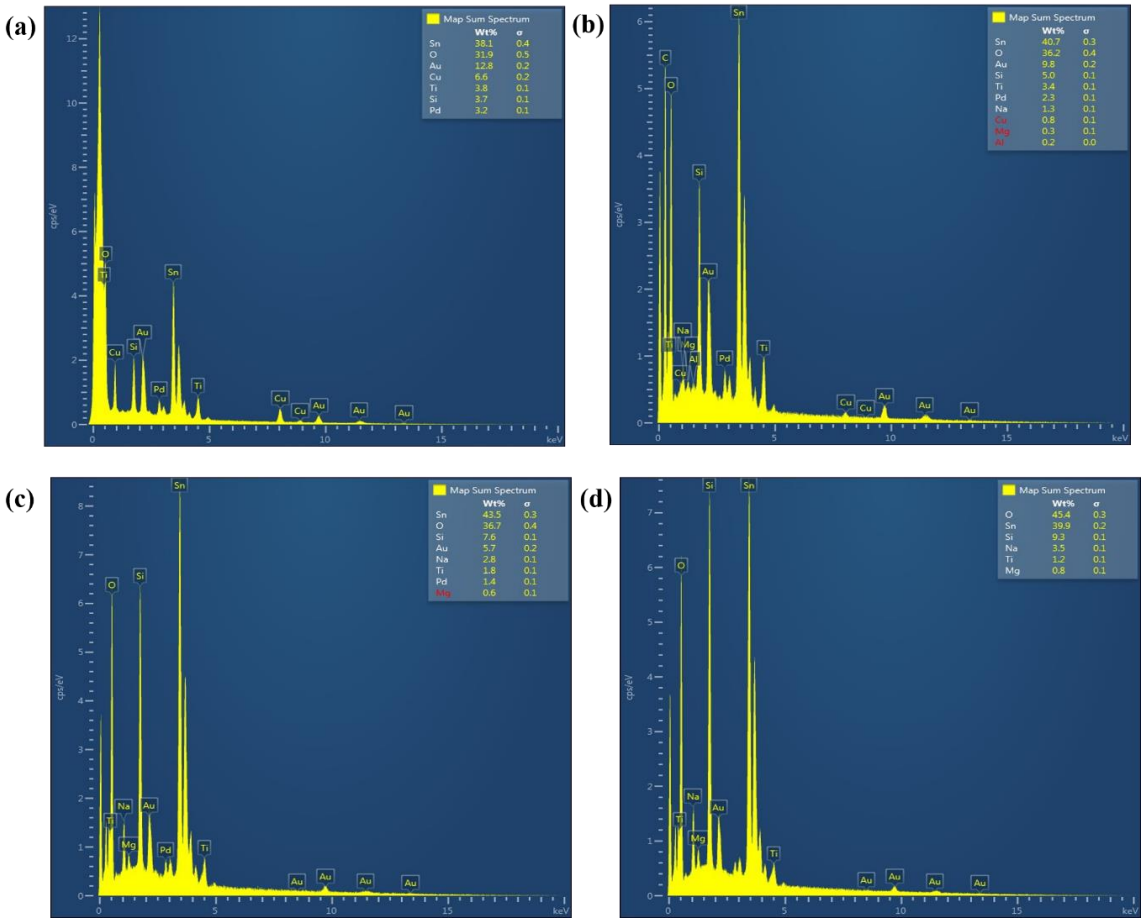

Figure 4.4: EDS spectra of ETL films for (a) TiO_2 and SnO_2-TiO_2 with (b) 0.1 (c) 0.2 (d) 0.3 proportion of SnO_2

In regular planar PSCs, the ETL forms the base over which the perovskite layer is deposited. This means that any variation in its surface characteristics can influence the crystallization dynamics and morphology of the perovskite films. We studied the effect of the ETL modification on the morphological properties of the perovskite films deposited on them by taking the SEM images of the top surface. The SEM images of the perovskite films formed on pristine TiO_2 and SnO_2-TiO_2 based ETLs are presented in Figure 4.5(a)–(d).

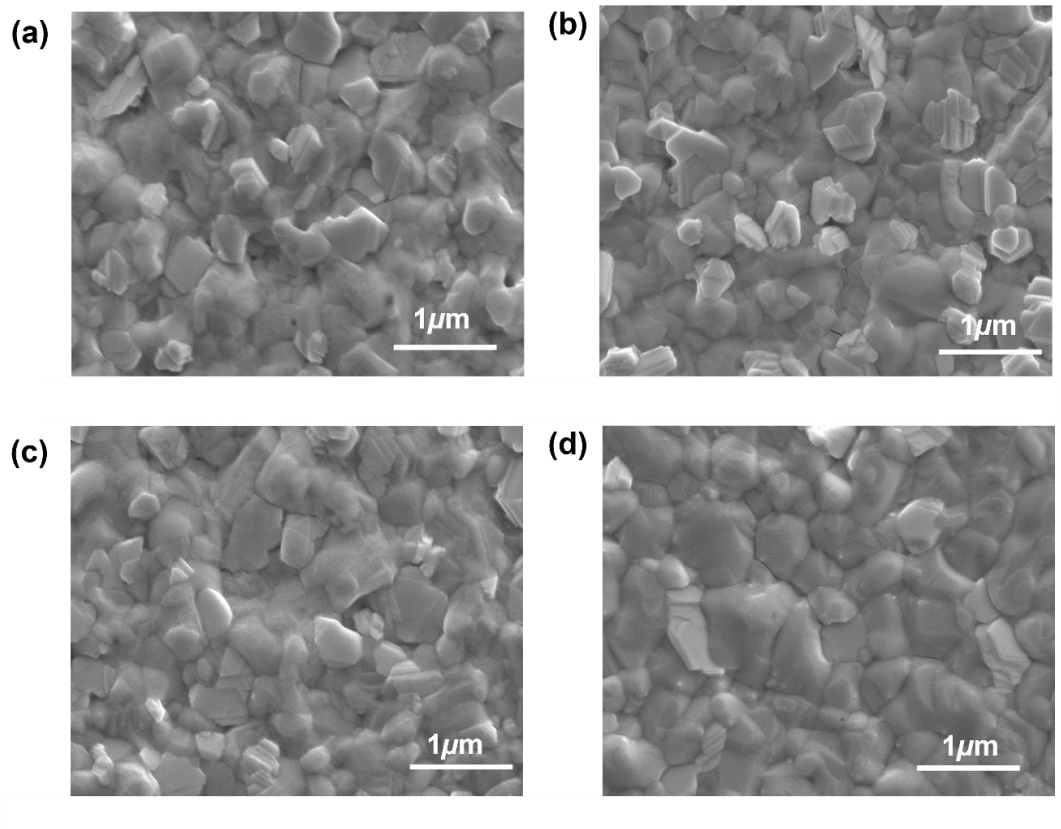

Figure 4.5: SEM images of perovskite films deposited on the different ETLs: (a) TiO_2 (b) 0.1 (c) 0.2 and (d) 0.3 proportion of SnO_2.

From the figure, we observe a slight change in the morphology for the perovskite films deposited on the ETL containing 0.3 volume proportion of SnO_2. At this proportion, the perovskite film appears to have larger interconnected grains with fewer grain boundaries when

compared to the rest. This implies that higher SnO_2 content in the ETL resulted in the growth of perovskite films with improved morphologies. This observation is in agreement with what has been reported by other researchers (Yu et al., 2020).

4.4.2 Optoelectronic properties of the thin Films

The optical properties of the ETL in PSCs can influence the amount of light reaching the photoactive perovskite layer, thus affecting the charge carrier generation. We studied the effect of SnO_2 incorporation on the optical properties of the ETL films by measuring their transmittance and absorbance at different proportions of SnO_2. The transmittance and absorption spectra of the different ETL films were measured in the range of 200 nm to 1100 nm using the UV-Vis spectrometer. The optical transmittance spectra (Figure 4.6(a)) indicate that all the ETL films had high transmittance within the visible spectrum which makes them suitable for PV application. The ETL films modified with 0.2 and 0.3 SnO_2 proportion exhibited higher transmittance relative to TiO_2. The optical band gaps (E_g) of the ETL films at different proportions of SnO_2 were determined from absorbance by plotting αhv versus the photon energy hv and fitting the linear section of the resulting curve to the Tauc relation given in Eqn. (4.1) (Makuła et al., 2018; Tauc & Menth, 1972).

$$(\alpha hv)^{\frac{1}{\gamma}} = B\left(hv - E_g\right) \tag{4.1}$$

In Equation (4.1), α is the absorption coefficient of the ETL films, *B* is the edge width parameter and γ is a parameter that specifies the nature of the optical transition and usually takes a value of 2 for indirect optical transitions (Makuła et al., 2018). As shown in Figure 4.6(b), we see a general blue-shift in the band gaps of ETL films as the SnO_2 content increases. The bandgap increased from 3.58 eV to 3.70 eV when the volume proportion of

SnO_2 increased from 0 to 0.3. The increase in bandgap explains the observed increase in transmittance of the ETL films with the content of SnO_2 in TiO_2.

The electrical properties of the ETL films are also very important as they influence their electron transport function in PSCs. Good electrical conductivity ensures proper extraction of the photo-generated electrons and reduces the series resistance (R_s) of PSC devices. We determined the electrical conductivity (σ) of the ETL films at room temperature from the Ohmic region of their dark I-V curves (Figure 4.6(c)) which were obtained by applying a voltage to the films sandwiched between two electrodes (FTO/ETLs/Au). The results show that σ increases with the SnO_2 content in TiO_2 and the highest value was obtained for the film modified with 0.2 volume proportion of SnO_2. Beyond the 0.2 proportion of SnO_2, the value of σ was found to decrease slightly (Figure 4.6 (d)). The decrease in σ is attributed to the microstructural changes of the ETL at 0.3 proportion of SnO_2 revealed by the SEM image in Figure 4.2(d). The evolution of the bandgap and σ with SnO_2 content in the ETL are summarized in Table 4.1.

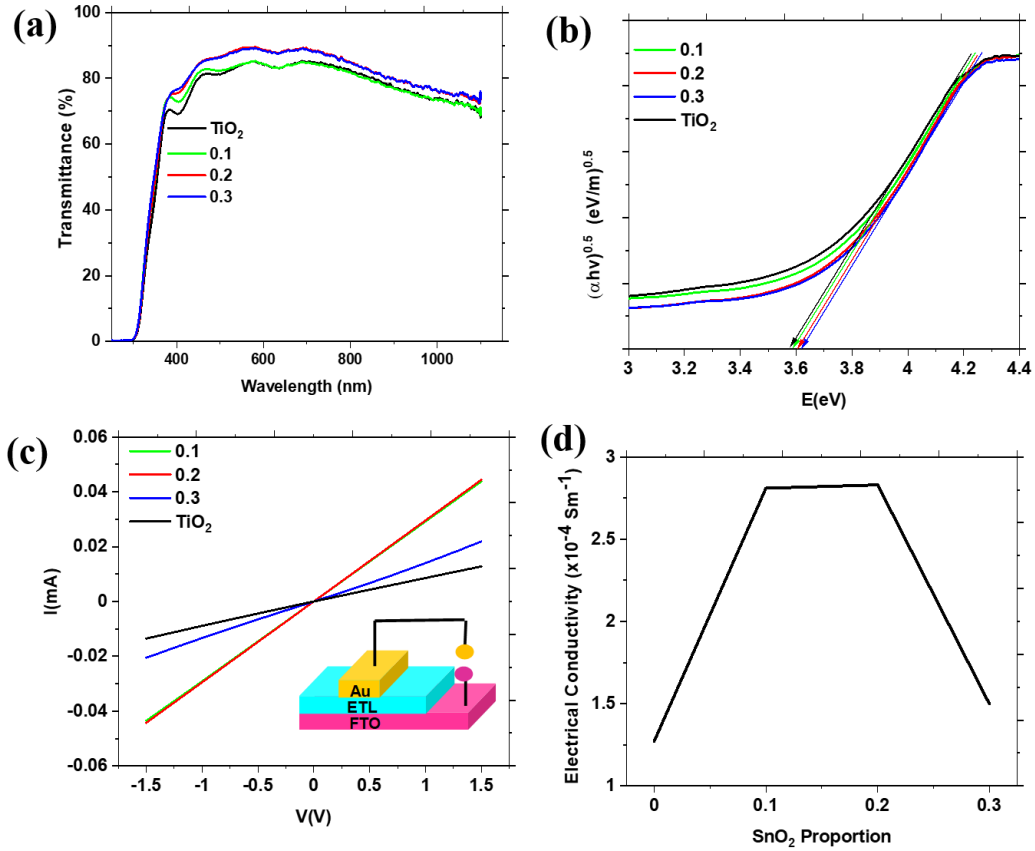

Figure 4.6: Optoelectronic Behavior of ETLs films: (a) Transmittance, (b) Tauc plot from absorbance (c) Dark I-V curves of the films, and (d) Electrical conductivity.

Table 4.1: Bandgap and electrical conductivity of the ETL at different SnO_2 content

SnO_2 Proportion	**0**	**0.1**	**0.2**	**0.3**
Band gap (eV)	3.58±0.030	3.59±0.027	3.62±0.046	3.70±0.059
Conductivity, σ ($\times 10^{-4}$) (S/m)	1.27±0.69	2.81±0.81	2.83±0.81	1.37±0.34

To understand the effect of ETL modification on the electron transport dynamics of the PSCs, we investigated the variation of the optoelectronic properties of perovskite films

deposited on pristine TiO_2 and SnO_2-TiO_2 ETLs through UV-Vis, steady-state photoluminescence (PL), time-resolved photoluminescence (TRPL), and space charge limited conduction (SCLC) techniques. The UV-Vis spectra of the perovskite films (Figure 4.7(a)) show that all the films had nearly equal absorption onsets (~800 nm) with a slight variation in their absorption intensities. This shows that the different proportions of SnO_2 in the ETL layer did not alter the bandgap of the perovskite films. The PL spectra of the perovskite films (Figure 4.7(b)) also show one major peak, all centered at ~800 nm, with small variations being observed only in their emission intensities. In particular, the PL emission peak for the perovskite film deposited on TiO_2 modified with 0.3 volume proportion of SnO_2 is stronger than those of the perovskite films deposited on pristine TiO_2, and composite SnO_2-TiO_2 ETL with 0.1 and 0.2 SnO_2 contents. This change in the PL intensity of perovskite film is usually associated with the variation in the crystal quality of the perovskite films or changes in the PL quenching capability of the CTLs (Fassl et al., 2019; Handa et al., 2017). In our case, the stronger PL emission peak for the perovskite film on the ETL with 0.3 SnO_2 proportion is most likely to be an indication of reduced non-radiative recombination resulting from the improvement in the film morphology as seen from the SEM images in Figure 4.5(d).

To ascertain the above observation, the electron trap densities of the perovskite films were determined using the SCLC method from the dark J-V curves of the electron-only devices with the structure FTO/ETLs/perovskite/C_{60}/Au. Figure 4.6(c) shows the dark J-V curves of the electron-only devices with TiO_2 and SnO_2-TiO_2 ETLs containing different proportions of SnO_2. The J-V curves kink upwards at different bias voltages indicating a variation in their electron trap densities. The bias voltage at which the J-V curves kink upwards corresponds to the threshold voltage (trap-filled voltage limit, V_{TFL}) at which the electron traps in the

perovskite films are filled. Figure 4.7(c) shows that the perovskite films on the different ETLs have different values of V_{TFL}, which implies that they have different trap densities. The trap density (N_t) of the perovskite films was determined from the values of V_{TFL} from the J-V curves by applying Equation (4.2) (Jain et al., 2007).

$$N_t = \frac{2\varepsilon_r \varepsilon_o}{eL^2} V_{TFL} \quad (4.2)$$

The constants ε_r, ε_o, e and L are the relative permittivity, permittivity of free space, electronic charge, and the thickness of the perovskite films, respectively. From Figure 4.7(c), the V_{TFL} values of the perovskite films on TiO_2 and SnO_2-TiO_2 ETLs with 0.1, 0.2, and 0.3 volume proportion of SnO_2 were respectively determined to be 0.67V, 0.81V, 0.59V, and 0.28V. The corresponding values of N_t were calculated and the perovskite film on the ETL with 0.3 SnO_2 content was found to have the least N_t value of 1.10 x 10^{16} cm^{-3}. The perovskite films deposited on pristine TiO_2 and SnO_2-TiO_2 ETLs with 0.1 and 0.2 SnO_2 content had N_t values of 2.63 x 10^{16} cm^{-3}, 3.18 x 10^{16} cm^{-3} and 2.23 x 10^{16} cm^{-3} respectively. Thus, the N_t values of all the perovskite films were all in the order of 10^{16} cm^{-3} with those of the perovskite film deposited on the ETL with 0.3 SnO_2 proportion being nearly 2.5 folds lower than those of the control device. The electron mobilities corresponding to the calculated N_t were respectively determined to be 2.63 x 10^{-4} Vcm^{-2}, 5.93 x 10^{-5} Vcm^{-2} and, 2.71 x 10^{-4} Vcm^{-2} while that of the films on the ETL with 0.3 SnO_2 proportion was 3.53 x 10^{-4} Vcm^{-2}.

Although perovskite films are known to be defect-tolerant, the presence of deep defects in the bulk and on the surface will hinder proper extraction and transportation of charge carriers leading to their loss through recombination (Jin et al., 2020). To probe the electron extraction dynamics at the ETL/perovskite interface, the TRPL decay curves of the perovskite films (Figure 4.7(d)) were recorded. The TRPL results were fitted to a bi-

exponential decay function and the electron decay lifetimes (τ_1 and τ_2) were extracted and the values obtained are tabulated in Table 4.2. The fast decay lifetime (τ_1) reflects the loss of carriers due to trap-mediated non-radiative recombination or charge extraction at perovskite/ETL interface while the slow decay lifetime (τ_2) indicates radiative recombination in the perovskite film (Liang et al., 2014). The perovskite films on the ETLs with 0.2 and 0.3 SnO_2 contents exhibited smaller τ_1 values of 0.541 ± 0.013 ns and 0.636 ± 0.022 ns respectively compared to 2.775 ± 0.0133 ns and 2.926 ± 0.129 ns for perovskite films deposited on ETL consisting of pure TiO_2 and SnO_2 -modified $TiO_2$with 0.1 proportion of SnO_2. The reduction in the τ_1 values for the perovskite film on the ETL modified with 0.3 volume proportion of SnO_2 agrees well with the calculated value of the electron trap densities which was found to be tenfold lower than those on the other ETLs. The least value obtained for the ETL with 0.2 SnO_2 proportion reflects its good electron extraction ability arising from its good electrical conductivity. The values of τ_2 were also observed to decrease with SnO_2 proportion in the ETL from a value of 16.38 ± 0.761 ns for perovskite films with undoped ETL to a value of 2.63 ± 0.149 ns for the films on the ETL with 0.3 SnO_2 content. This shows that the perovskite film on the ETL with 0.3 SnO_2 content had fewer defects, which agrees well with the SCLC results and is also evident in the UV-Vis spectra (Figure 4.7(a)).

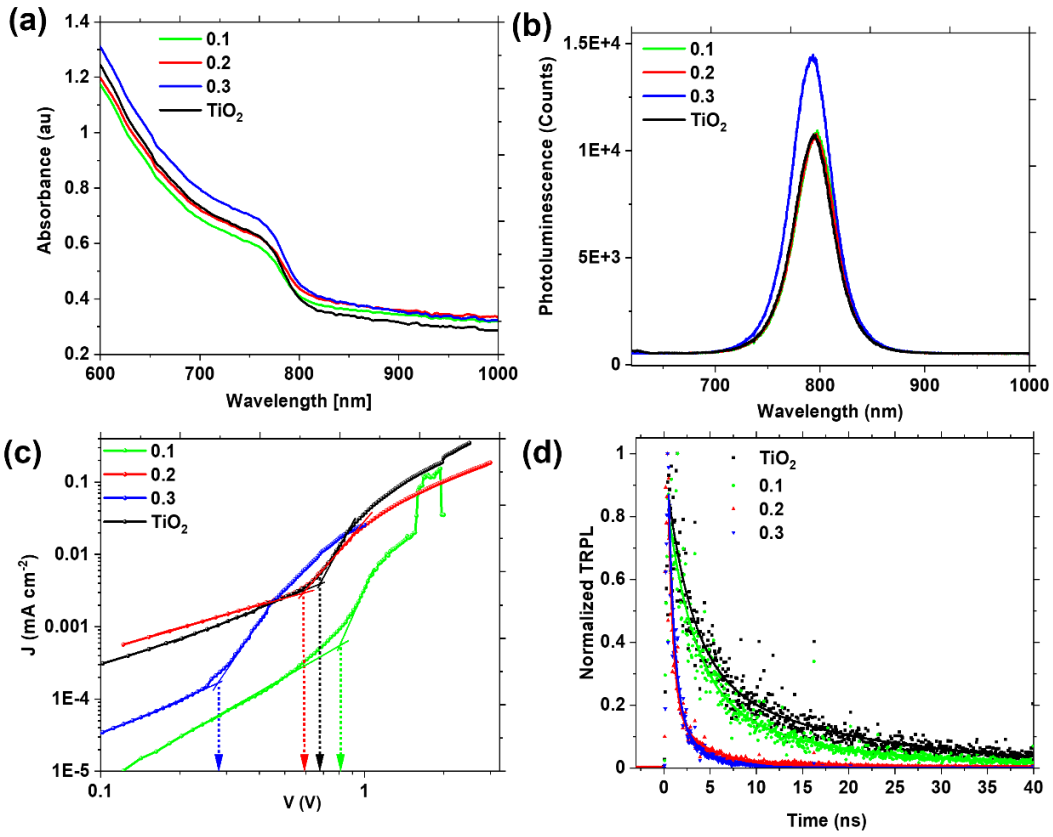

Figure 4.7: Optical properties of perovskite films for different volume proportions of SnO_2: (a) UV-Vis absorbance spectra (b) PL spectra, (c) J-V curves of electron-only devices, and (d) TRPL spectra of perovskite films on different ETL.

Table 4.2: TRPL Bi-exponential fitting parameters

Vol. fraction of SnO_2	**0**	**0.1**	**0.2**	**0.3**
A1	0.650 ± 0.016	0.676 ± 0.037	1.646 ± 0.037	1.476 ± 0.028
τ_1	2.774 ± 0.133	2.926 ± 0.129	0.541 ± 0.013	0.636 ± 0.022
A2	0.322 ± 0.016	0.245 ± 0.020	0.20 ± 0.008	0.255 ± 0.025
τ_2	16.38 ± 0.761	13.47 ± 0.82	3.97 ± 0.136	2.63 ± 0.149

4.4.3 Performance characteristics of PSCs

The photovoltaic performance of a solar cell is quantified by its PCE which is a function of J_{sc}, $V_{oc,}$ and *FF*. The PV performance parameters of the fabricated PSCs were determined from their J-V curves measured under illumination using a solar simulator (AM1.5, 100 mW/cm^2). Figure 4.8(a)–(c) compares the J-V curves, Nyquist plots, and the EQE curves of the control and best-performing devices while Figure 4.8(d) shows the SEM cross-sectional image of the fabricated planar PSC device. It is seen from Figure 4.8(a) that the best performing device based on SnO_2-TiO_2 ETL with 0.2 SnO_2 content had higher J_{sc} when compared to the control device based on TiO_2. To find out the reason for the observed increase in J_{sc}, we carried out EIS studies on the control and the best performing PSC devices under illumination and the results are displayed by Nyquist plots shown in Figure 4.8(b).

The Nyquist plots show two semicircles, one in the high-frequency region that is associated with the charge transfer resistance (R_{tr}) from perovskite to the ETL and one in the low-frequency region which is associated with recombination resistance (R_{rec}) at the ETL/perovskite interface in the PSC device (Zhang et al., 2015). The Nyquist curves were fitted with an equivalent RC circuit (inset of Figure 4.8(b)) to allow for the extraction of R_s, $R_{ct,}$ and R_{rec}. It is noticeable from Figure 4.8(b) that the incorporation of SnO_2 into TiO_2 leads to a reduction in both the R_s and R_{ct} values while the value of R_{rec} increases. For the device area under consideration, R_s and R_{ct} decreased from 5.23 Ω cm^2 to 3.67 Ω cm^2 and from 14.54 Ω cm^2 to 12.27 Ω cm^2, respectively for the control and the best performing SnO_2-TiO_2 based devices. On the other hand, R_{rec} increased from 5.37 Ω cm^2 for the control device to 13.07 Ω cm^2 for the SnO_2-TiO_2 based device. The decrease in R_s agrees with the observed

improvement in σ of the ETL with SnO_2 incorporation (Figure 4.6(d)). The reduction in the value of R_s in the SnO_2-TiO_2 based device led to an improvement in its electron transport properties. Consequently, the charge carrier collection efficiency of the PSC device based on SnO_2-TiO_2 ETL improved, as shown by the EQE measurement in Figure 4.8(c).

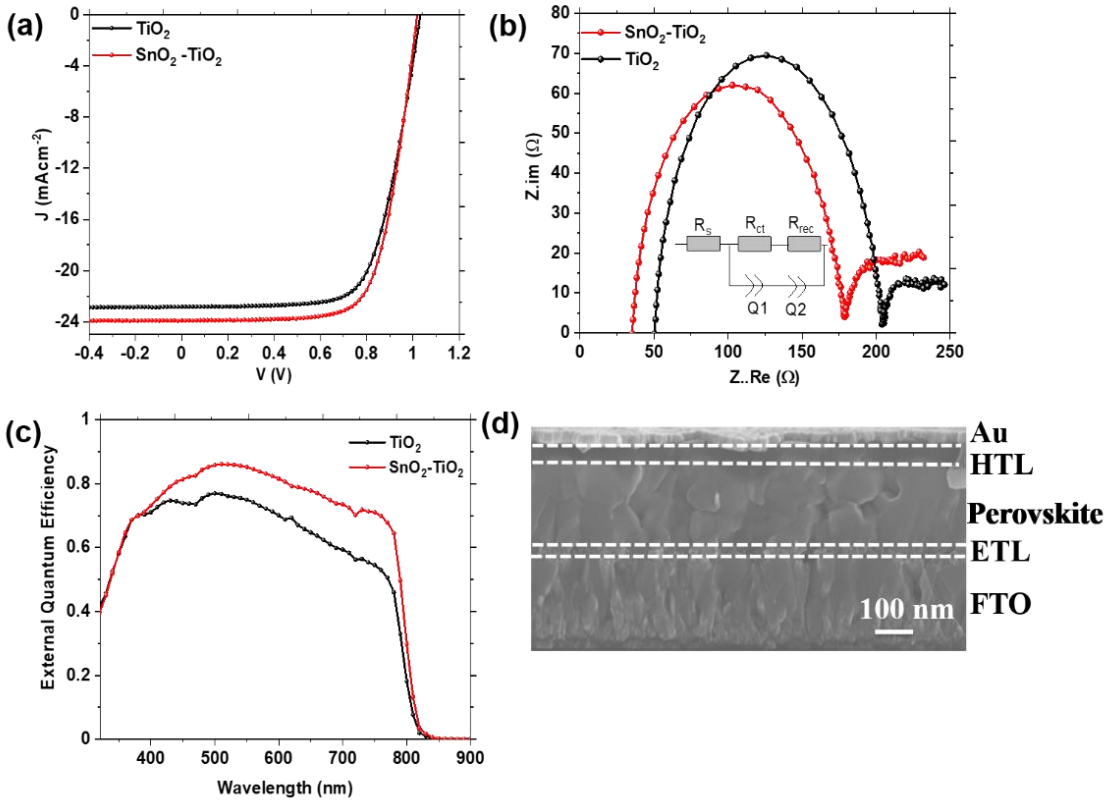

Figure 4.8: (a) J-V curves; (b) Nyquist curves and (c) EQE curves of the control and the best performing PSC devices (d) Cross-sectional image of the fabricated planar PSC.

For the different sets of PSCs fabricated, the PV performance parameters (J_{sc}, V_{oc}, *FF*, and PCE) were determined from their J-V curves and expressed as a function of the proportion of SnO_2 in the ETL by means of the statistical box plots as shown in Figure 4.9(a)–(d).

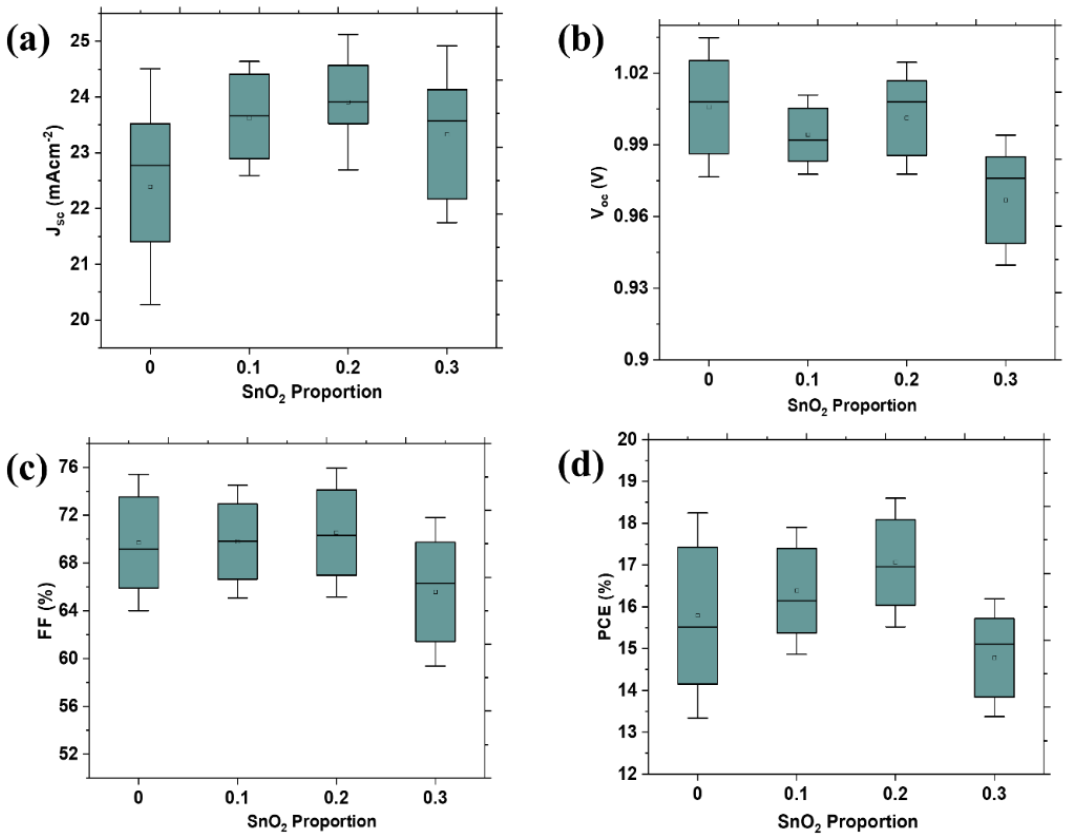

Figure 4.9: Box plots showing the variation of (a) J_{sc} (b) V_{oc} (c) *FF* and (d) PCE with SnO_2 content in the ETL.

From Figure 4.9, we observe an increase in the mean values of J_{sc}, *FF*, and PCE of the PSCs as the proportion of SnO_2 in the ETL increase from 0 to 0.2. Beyond this proportion, the mean values of these PV parameters decreased. The trend observed in the variation of these parameters with the proportion of SnO_2 in the ETL follows the same trend displayed by the σ of the ETL (Figure 4.6(d)). This indicates that σ of the ETL played a role in shaping the performance of the overall PSC device. However, the mean values of the V_{oc} showed a general decrease with the SnO_2 content in the ETL due to a possible downward shift in the conduction band edge of TiO_2 when modified with SnO_2 (Ranjan et al., 2018).

4.5 Summary and concluding remarks

Pristine TiO_2 and SnO_2-modified TiO_2 thin films with different proportions of SnO_2 have been studied as ETLs in FA-rich planar PSCs. The results show that incorporating SnO_2 in TiO_2 in the right proportion improves its electrical conductivity and optical transmission of the ETL film which consequently increases the PCE of PSC. By introducing 0.2 volume proportion of SnO_2 in TiO_2, the PCE of the PSC increased by 7.17%. The improvement is mainly attributed to the enhancement in the electrical conductivity of the ETL and the accompanying reduction in R_s of PSC that increases the charge carrier collection efficiency and hence the PCE. The EIS results show that the values of R_s of the PSCs decrease from 5.23 Ω cm^2 to 3.67 Ω cm^2 when TiO_2 ETL is modified with 0.2 volume proportion of SnO_2. From this study, we conclude that the strategies geared towards reducing R_s in PSCs are beneficial in improving the PCE.

4.6 References

Akurati, K. K., Vital, A., Hany, R., Bommer, B., Graule, T., & Winterer, M. (2005). One-step flame synthesis of SnO_2/TiO_2 composite nanoparticles for photocatalytic applications. *International Journal of Photoenergy*. https://doi.org/10.1155/S1110662X05000231

Apostolopoulou, A., Sygkridou, D., Rapsomanikis, A., Kalarakis, A. N., & Stathatos, E. (2017). Enhanced performance of mesostructured perovskite solar cells in ambient conditions with a composite TiO_2–In_2O_3 electron transport layer. *Solar Energy Materials and Solar Cells*. https://doi.org/10.1016/j.solmat.2017.03.024

Belchi, R., Habert, A., Foy, E., Gheno, A., Vedraine, S., Antony, R., Ratier, B., Bouclé, J., & Herlin-Boime, N. (2019). One-Step Synthesis of TiO_2/Graphene Nanocomposites by Laser Pyrolysis with Well-Controlled Properties and Application in Perovskite Solar Cells. *ACS Omega*. https://doi.org/10.1021/acsomega.9b01352

Chen, X. (2009). Titanium dioxide nanomaterials and their energy applications. In *Cuihua Xuebao / Chinese Journal of Catalysis*. https://doi.org/10.1016/s1872-2067(08)60126-6

Chen, X., & Mao, S. S. (2007). Titanium dioxide nanomaterials: Synthesis, properties, modifications and applications. In *Chemical Reviews*. https://doi.org/10.1021/cr0500535

Courtier, N. E., Cave, J. M., Foster, J. M., Walker, A. B., & Richardson, G. (2019). How transport layer properties affect perovskite solar cell performance: Insights from a coupled charge transport/ion migration model. *Energy and Environmental Science*. https://doi.org/10.1039/c8ee01576g

Desai, U. V., Xu, C., Wu, J., & Gao, D. (2013). Hybrid TiO_2-SnO_2 nanotube arrays for dye-sensitized solar cells. *Journal of Physical Chemistry C*. https://doi.org/10.1021/jp3096727

Dou, M., & Persson, C. (2013). Comparative study of rutile and anatase SnO_2 and TiO_2: Band-edge structures, dielectric functions, and polaron effects. *Journal of Applied Physics*. https://doi.org/10.1063/1.4793273

Duan, Y., Fu, N., Liu, Q., Fang, Y., Zhou, X., Zhang, J., & Lin, Y. (2012). Sn-doped TiO_2 photoanode for dye-sensitized solar cells. *Journal of Physical Chemistry C*. https://doi.org/10.1021/jp212517k

Even, J., Boyer-Richard, S., Carignano, M., Pedesseau, L., Jancu, J.-M., & Katan, C. (2016). Theoretical insights into hybrid perovskites for photovoltaic applications. *Proceedings of SPIE*. https://doi.org/10.1117/12.2213135

Fassl, P., Zakharko, Y., Falk, L. M., Goetz, K. P., Paulus, F., Taylor, A. D., Zaumseil, J., & Vaynzof, Y. (2019). Effect of density of surface defects on photoluminescence properties in $MAPbI_3$ perovskite films. *Journal of Materials Chemistry C*.

https://doi.org/10.1039/c8tc05998e

Giorgi, G., & Yamashita, K. (2015). Organic-inorganic halide perovskites: An ambipolar class of materials with enhanced photovoltaic performances. *Journal of Materials Chemistry A*. https://doi.org/10.1039/c4ta05046k

Grill, I., Aygüler, M. F., Bein, T., Docampo, P., Hartmann, N. F., Handloser, M., & Hartschuh, A. (2017). Charge Transport Limitations in Perovskite Solar Cells: The Effect of Charge Extraction Layers. *ACS Applied Materials and Interfaces*. https://doi.org/10.1021/acsami.7b09567

Guo, H., Zhang, H., Yang, J., Chen, H., Li, Y., Wang, L., & Niu, X. (2018). TiO_2/SnO_2 Nanocomposites as Electron Transporting Layer for Efficiency Enhancement in Planar $CH_3NH_3PbI_3$-Based Perovskite Solar Cells. *ACS Applied Energy Materials*. https://doi.org/10.1021/acsaem.8b01331

Handa, T., Tex, D. M., Shimazaki, A., Wakamiya, A., & Kanemitsu, Y. (2017). Charge Injection Mechanism at Heterointerfaces in $CH_3NH_3PbI_3$ Perovskite Solar Cells Revealed by Simultaneous Time-Resolved Photoluminescence and Photocurrent Measurements. *Journal of Physical Chemistry Letters*. https://doi.org/10.1021/acs.jpclett.6b02847

Hsiao, Y. C., Wu, T., Li, M., Liu, Q., Qin, W., & Hu, B. (2015). Fundamental physics behind high-efficiency organo-metal halide perovskite solar cells. *Journal of Materials Chemistry A*. https://doi.org/10.1039/c5ta01376c

Jain, A., Kumar, P., Jain, S. C., Kumar, V., Kaur, R., & Mehra, R. M. (2007). Trap filled limit voltage (V_{TFL}) and V^2 law in space charge limited currents. *Journal of Applied Physics*. https://doi.org/10.1063/1.2802553

Jin, H., Debroye, E., Keshavarz, M., Scheblykin, I. G., Roeffaers, M. B. J., Hofkens, J., & Steele, J. A. (2020). It's a trap! on the nature of localised states and charge trapping in lead halide perovskites. In *Materials Horizons*. https://doi.org/10.1039/c9mh00500e

Ke, W., Zhao, D., Cimaroli, A. J., Grice, C. R., Qin, P., Liu, Q., Xiong, L., Yan, Y., & Fang, G. (2015). Effects of annealing temperature of tin oxide electron selective layers on the performance of perovskite solar cells. *Journal of Materials Chemistry A*. https://doi.org/10.1039/c5ta06574g

Koech, R. K., Kigozi, M., Bello, A., Onwualu, P. A., & Soboyejo, W. O. (2019). Recent advances in solar energy harvesting materials with particular emphasis on photovoltaic materials. *IEEE PES/IAS PowerAfrica Conference: Power Economics and Energy Innovation in Africa, PowerAfrica 2019*, 627–632. https://doi.org/10.1109/PowerAfrica.2019.8928859

Larin, A., Womble, P. C., & Dobrokhotov, V. (2016). Hybrid SnO_2/TiO_2 nanocomposites for selective detection of ultra-low hydrogen sulfide concentrations in complex backgrounds. *Sensors (Switzerland)*. https://doi.org/10.3390/s16091373

Le Corre, V. M., Stolterfoht, M., Perdigo, L., Feuerstein, M., Wolff, C., Bolink, H. J., Neher, D., & Jan Anton Koster, L. (2019). Charge Transport Layers Limiting the Efficiency of Perovskite Solar Cells: How To Optimize Conductivity, Doping, and Thickness. *29*, 40. https://doi.org/10.1021/acsaem.9b00856

Li, N., Yan, J., Ai, Y., Jiang, E., Lin, L., Shou, C., Yan, B., Sheng, J., & Ye, J. (2020). A low-temperature TiO_2/SnO_2 electron transport layer for high-performance planar perovskite solar cells. *Science China Materials*, *63*(2), 207–215. https://doi.org/10.1007/s40843-019-9586-x

Li, W., Elzatahry, A., Aldhayan, D., & Zhao, D. (2018). Core-shell structured titanium dioxide nanomaterials for solar energy utilization. In *Chemical Society Reviews*. https://doi.org/10.1039/c8cs00443a

Liang, P. W., Liao, C. Y., Chueh, C. C., Zuo, F., Williams, S. T., Xin, X. K., Lin, J., & Jen, A. K. Y. (2014). Additive enhanced crystallization of solution-processed perovskite for highly efficient planar-heterojunction solar cells. *Advanced Materials*. https://doi.org/10.1002/adma.201400231

Liu, N., Chen, M., Yang, H., Ran, M., Zhang, C., Luo, X., Lu, H., & Yang, Y. (2020). TiO_2 /Mg-SnO_2 nanoparticle composite compact layer for enhancing the performance of perovskite solar cells . *Optical Materials Express*. https://doi.org/10.1364/ome.380354

Liu, Z., Sun, B., Liu, X., Han, J., Ye, H., Tu, Y., Chen, C., Shi, T., Tang, Z., & Liao, G. (2018). 15% efficient carbon based planar-heterojunction perovskite solar cells using a TiO_2/SnO_2 bilayer as the electron transport layer. *Journal of Materials Chemistry A*. https://doi.org/10.1039/c8ta00526e

Mahmood, K., Sarwar, S., & Mehran, M. T. (2017). Current status of electron transport layers in perovskite solar cells: materials and properties. In *RSC Advances*. https://doi.org/10.1039/c7ra00002b

Makuła, P., Pacia, M., & Macyk, W. (2018). How To Correctly Determine the Band Gap Energy of Modified Semiconductor Photocatalysts Based on UV-Vis Spectra. In *Journal of Physical Chemistry Letters*. https://doi.org/10.1021/acs.jpclett.8b02892

Mali, S. S., & Hong, C. K. (2016). P-i-n/n-i-p type planar hybrid structure of highly efficient perovskite solar cells towards improved air stability: Synthetic strategies and the role of p-type hole transport layer (HTL) and n-type electron transport layer (ETL) metal oxides. In *Nanoscale*. https://doi.org/10.1039/c6nr02276f

Martínez-Denegri, G., Colodrero, S., Kramarenko, M., & Martorell, J. (2018). All-Nanoparticle SnO_2/TiO_2 Electron-Transporting Layers Processed at Low Temperature for Efficient Thin-Film Perovskite Solar Cells. *ACS Applied Energy Materials*. https://doi.org/10.1021/acsaem.8b01118

Mohamad Noh, M. F., Teh, C. H., Daik, R., Lim, E. L., Yap, C. C., Ibrahim, M. A., Ahmad Ludin, N., Mohd Yusoff, A. R. Bin, Jang, J., & Mat Teridi, M. A. (2018). The architecture of the electron transport layer for a perovskite solar cell. In *Journal of*

Materials Chemistry C. https://doi.org/10.1039/c7tc04649a

Mohammadbeigi, A., Mozaffari, S., & Ghorashi, S. M. B. (2020). Yolk-shell SnO_2@TiO_2 nanospheres as electron transport layer in mesoscopic perovskite solar cell. *Journal of Sol-Gel Science and Technology*. https://doi.org/10.1007/s10971-020-05221-2

Nimens, W. J., Ogle, J., Caruso, A., Jonely, M., Simon, C., Smilgies, D., Noriega, R., Scarpulla, M., & Whittaker-Brooks, L. (2018). Morphology and Optoelectronic Variations Underlying the Nature of the Electron Transport Layer in Perovskite Solar Cells. *ACS Applied Energy Materials*. https://doi.org/10.1021/acsaem.7b00147

Nwankwo, U., Ngqoloda, S., Nkele, A. C., Arendse, C. J., Ozoemena, K. I., Ekwealor, A. B. C., Jose, R., Maaza, M., & Ezema, F. I. (2020). Effects of alkali and transition metal-doped TiO_2 hole blocking layers on the perovskite solar cells obtained by a two-step sequential deposition method in air and under vacuum. *RSC Advances*. https://doi.org/10.1039/d0ra01532f

Oyewole, D. O., Koech, R. K., Ichwani, R., Ahmed, R., Tamayo, J. H., Adeniji, S. A., Cromwell, J., Ulloa, E. C., Oyewole, O. K., Agyei-Tuffour, B., Titova, L. V, Burnham, N. A., & Soboyejo, W. O. (2021). Annealing effects on interdiffusion in layered FA-rich perovskite solar cells Annealing effects on interdiffusion in layered FA-rich perovskite solar cells AIP Advances. *AIP Advances*, *11*, 65327. https://doi.org/10.1063/5.0046205

Pan, X., Yang, M. Q., Fu, X., Zhang, N., & Xu, Y. J. (2013). Defective TiO_2 with oxygen vacancies: Synthesis, properties and photocatalytic applications. In *Nanoscale*. https://doi.org/10.1039/c3nr00476g

Ranjan, R., Prakash, A., Singh, A., Singh, A., Garg, A., & Gupta, R. K. (2018). Effect of tantalum doping in a TiO_2 compact layer on the performance of planar spiro-OMeTAD free perovskite solar cells. *Journal of Materials Chemistry A*. https://doi.org/10.1039/c7ta09193a

Ren, X., Wang, Z. S., & Choy, W. C. H. (2019). Device Physics of the Carrier Transporting Layer in Planar Perovskite Solar Cells. In *Advanced Optical Materials*. https://doi.org/10.1002/adom.201900407

Saleem, A., Ullah, N., Khursheed, K., Iqbal, T., Shah, S. A., Asjad, M., Sarwar, N., Saleem, M., & Arshad, M. (2018). Graphene Oxide–TiO_2 Nanocomposite Films for Electron Transport Applications. *Journal of Electronic Materials*. https://doi.org/10.1007/s11664-018-6235-4

Shi, J., Li, Y., Li, Y., Li, D., Luo, Y., Wu, H., & Meng, Q. (2018). From Ultrafast to Ultraslow: Charge-Carrier Dynamics of Perovskite Solar Cells. In *Joule*. https://doi.org/10.1016/j.joule.2018.04.010

Shin, S. S., Lee, S. J., & Seok, S. Il. (2019). Metal Oxide Charge Transport Layers for Efficient and Stable Perovskite Solar Cells. In *Advanced Functional Materials*. https://doi.org/10.1002/adfm.201900455

Song, S., Kang, G., Pyeon, L., Lim, C., Lee, G. Y., Park, T., & Choi, J. (2017). Systematically Optimized Bilayered Electron Transport Layer for Highly Efficient Planar Perovskite Solar Cells (η = 21.1%). *ACS Energy Letters*. https://doi.org/10.1021/acsenergylett.7b00888

Stolterfoht, M., Caprioglio, P., Wolff, C. M., Márquez, J. A., Nordmann, J., Zhang, S., Rothhardt, D., Hörmann, U., Amir, Y., Redinger, A., Kegelmann, L., Zu, F., Albrecht, S., Koch, N., Kirchartz, T., Saliba, M., Unold, T., & Neher, D. (2019). The impact of energy alignment and interfacial recombination on the internal and external open-circuit voltage of perovskite solar cells. *Energy and Environmental Science*. https://doi.org/10.1039/c9ee02020a

Tailor, N. K., Abdi-Jalebi, M., Gupta, V., Lu, H., Dar, M. I., Li, G., & Satapathi, S. (2020). Recent progress in morphology optimization in perovskite solar cells. *Journal of Materials Chemistry A*. https://doi.org/10.1039/d0ta00143k

Tauc, J., & Menth, A. (1972). States in the gap. *Journal of Non-Crystalline Solids*, *8*, 569–585.

Tavakoli, M. M., Yadav, P., Tavakoli, R., & Kong, J. (2018). Surface Engineering of TiO_2 ETL for Highly Efficient and Hysteresis-Less Planar Perovskite Solar Cell (21.4%) with Enhanced Open-Circuit Voltage and Stability. *Advanced Energy Materials*. https://doi.org/10.1002/aenm.201800794

Thakur, U., Kisslinger, R., & Shankar, K. (2017). One-Dimensional Electron Transport Layers for Perovskite Solar Cells. *Nanomaterials*. https://doi.org/10.3390/nano7050095

Wan, F., Qiu, X., Chen, H., Liu, Y., Xie, H., Shi, J., Huang, H., Yuan, Y., Gao, Y., & Zhou, C. (2018). Accelerated electron extraction and improved UV stability of TiO_2 based perovskite solar cells by SnO_2 based surface passivation. *Organic Electronics*. https://doi.org/10.1016/j.orgel.2018.05.008

Wolff, C. M., Caprioglio, P., Stolterfoht, M., & Neher, D. (2019). Nonradiative Recombination in Perovskite Solar Cells: The Role of Interfaces. *Advanced Materials*. https://doi.org/10.1002/adma.201902762

Wu, N., Wu, Y., Walter, D., Shen, H., Duong, T., Grant, D., Barugkin, C., Fu, X., Peng, J., White, T., Catchpole, K., & Weber, K. (2017). Identifying the Cause of Voltage and Fill Factor Losses in Perovskite Solar Cells by Using Luminescence Measurements. *Energy Technology*. https://doi.org/10.1002/ente.201700374

You, J., Meng, L., Hong, Z., Li, G., & Yang, Y. (2016). Inverted planar structure of perovskite solar cells. In *Organic-Inorganic Halide Perovskite Photovoltaics: From Fundamentals to Device Architectures*. https://doi.org/10.1007/978-3-319-35114-8_12

Yu, J. C., Hong, J. A., Jung, E. D., Kim, D. Bin, Baek, S. M., Lee, S., Cho, S., Park, S. S., Choi, K. J., & Song, M. H. (2018). Highly efficient and stable inverted perovskite solar cell employing PEDOT:GO composite layer as a hole transport layer. *Scientific Reports*. https://doi.org/10.1038/s41598-018-19612-7

Yu, M., Guo, Y., Yuan, S., Zhao, J. S., Qin, Y., & Ai, X. C. (2020). The influence of the electron transport layer on charge dynamics and trap-state properties in planar perovskite solar cells. *RSC Advances*, *10*(21), 12347–12353. https://doi.org/10.1039/d0ra00375a

Yue, L., Yan, B., Attridge, M., & Wang, Z. (2016). Light absorption in perovskite solar cell: Fundamentals and plasmonic enhancement of infrared band absorption. *Solar Energy*. https://doi.org/10.1016/j.solener.2015.11.028

Zhang, F., Yang, B., Li, Y., Deng, W., & He, R. (2017). Extra long electron-hole diffusion lengths in $CH_3NH_3PbI_{3-X}Clx$ perovskite single crystals. *Journal of Materials Chemistry C*. https://doi.org/10.1039/c7tc02802d

Zhang, J., Juárez-Pérez, E. J., Mora-Seró, I., Viana, B., & Pauporté, T. (2015). Fast and low temperature growth of electron transport layers for efficient perovskite solar cells. *Journal of Materials Chemistry A*. https://doi.org/10.1039/c4ta06416j

Zhen, C., Wu, T., Chen, R., Wang, L., Liu, G., & Cheng, H. M. (2019). Strategies for Modifying TiO_2 Based Electron Transport Layers to Boost Perovskite Solar Cells. *ACS Sustainable Chemistry and Engineering*. https://doi.org/10.1021/acssuschemeng.8b06580

Zheng, S., Wang, G., Liu, T., Lou, L., Xiao, S., & Yang, S. (2019). Materials and structures for the electron transport layer of efficient and stable perovskite solar cells. In *Science China Chemistry*. https://doi.org/10.1007/s11426-019-9469-1

Zhou, Y., Li, X., & Lin, H. (2020). To Be Higher and Stronger—Metal Oxide Electron Transport Materials for Perovskite Solar Cells. In *Small*. https://doi.org/10.1002/smll.201902579

CHAPTER FIVE

A STUDY OF THE EFFECTS OF A THERMALLY EVAPORATED NANOSCALE CsBr LAYER ON THE OPTOELECTRONIC PROPERTIES AND STABILITY OF FORMAMIDINIUM-RICH PEROVSKITE SOLAR CELLS

5.1 Introduction

In this chapter, a nanoscale Cesium Bromide (CsBr) layer of varying thicknesses was introduced into FA-rich mixed halide perovskite film via thermal evaporation technique. The effects of the thickness of the CsBr layer on the optoelectronic properties of the perovskite film and the performance characteristics of the resulting PSC are discussed.

Perovskite solar cells (PSCs) are emerging solar cells with unique optoelectronic properties and simple processing routes that make them stand out from other PV technologies in the pursuit of high performance and low-cost solar energy harnessing systems (Assadi et al., 2018; Shi & Jayatissa, 2018; Tai et al., 2019). Within a short period, PSCs have achieved remarkable progress in their power conversion efficiencies (PCEs) and are currently almost at par with the conventional PV technologies based on crystalline silicon (Green et al., 2018). This progress was a culmination of many concerted efforts from researchers drawn from different disciplines that yielded a better understanding of their structure, optoelectronic properties, and their working principles (Chouhan et al., 2020; Hussain et al., 2018). However, the PSC technology is still faced with myriads of challenges which; amongst others; include non-radiative recombination power losses and performance degradation under real outdoor operating conditions (Kundu & Kelly, 2020; Wali et al., 2020).

Various studies that have been carried out to probe the origin of the above-mentioned challenges have pointed out that they are majorly caused by perovskite phase instability and the presence of defects in the bulk of the AL and at the interfaces with the CTLs (Asghar et al., 2017; Chen et al., 2016; Fu et al., 2020). The morphology of the perovskite film plays a big role in controlling the defect states in the bulk and at the interfaces. Therefore, research efforts have been expended to improve the morphology of the perovskite AL through compositional engineering (Kim et al., 2019), solvent engineering (Liu & Xu, 2020), optimization of perovskite precursors (Yakiangngam et al., 2019), additive engineering (Zhang & Zhu, 2019), improving deposition conditions (Zeng et al., 2017) and optimization of post-treatment techniques (Xiao et al., 2020). These strategies are aimed at controlling the nucleation and crystallization dynamics of the perovskite film to passivate the defects at grain boundaries which are the genesis of most problems in PSCs (Landi et al., 2017; Sherkar et al., 2017; Wang et al., 2019). The tunability of the perovskite (ABX_3) structure through elemental substitution and mixing has given rise to perovskite films with mixed cations and mixed halides which have better morphologies and superior photophysical properties (Kim et al., 2019; Zhen Li et al., 2016; Tailor, Abdi-Jalebi, Gupta, Lu, et al., 2020). The elemental substitution/mixing also tunes the tolerance factor that stabilizes the perovskite phase and improves its stability (Li et al., 2016; Xu et al., 2020).

In an effort to enhance PCEs and stability of PSCs, Cesium (Cs)-based mixed cation-mixed halide PSCs have been explored (Bella et al., 2018; Liu et al., 2018; Tang et al., 2020). The Cs atom occupies the A-site in the ABX_3 structure of perovskite which is important in the formation of the closed packed structure and in improving charge carrier mobility in perovskite films (Myung et al., 2018). The ionic radii of the A-site cations control the B-X

bond length in the perovskite structure which dictates the band gap of the resulting perovskite film (Li et al., 2008). The smaller ionic radius of Cs^+ (1.81 Å) can cause lattice contraction or octahedral tilting which increases the bandgap of the perovskite film (Bush et al., 2018; Prasanna et al., 2017). In spite of this, the presence of Cs^+ in the right proportion is beneficial in stabilizing the perovskite α-phase, reducing the defect density as well as improving optical absorption and carrier lifetimes in the perovskite layer which in turn improves the stability, reproducibility, and PCE of PSC (Bella et al., 2018; Saliba et al., 2016; Tang et al., 2020).

The Cs^+ is incorporated into the perovskite film from Cesium halides (CsX, X = I, Br, Cl) which are usually added directly into the precursor solutions or via interfacial interdiffusion method (Chavan et al., 2019; Li et al., 2018; Liu et al., 2018). Recent studies have found the interfacial interdiffusion method to be a good strategy to incorporate Cs^+ into the perovskite absorber layer while simultaneously tuning the interface energetics (Xue et al., 2018). The technique can allow for localized incorporation of Cs^+ within the vicinity of the interface between the perovskite layer and the CTLs which helps to mitigate the expected blueshift in the absorption edge of the perovskite film while boosting its crystallization dynamics. Among the Cs halides, CsBr has been shown to be more effective in improving both the PCE and stability of PSCs (Chen et al., 2019; Li et al., 2016; Ueoka et al., 2018). Pang and co-workers (Pang et al., 2021) incorporated CsBr into the perovskite film via interfacial interdiffusion method and they found that CsBr is essential in passivating the defects in perovskite bulk, promoting charge extraction through better band alignment at the CTL/perovskite interface and improving the asymmetric charge transport due to gradient distribution of CsBr in the perovskite bulk. It is, therefore, very important to have an in-depth understanding of the effect of CsBr on the microstructural and optoelectronic properties of

perovskite film as well as the long-term stability of the ensuing PSCs. Furthermore, a suitable, low-cost, and scalable CsBr deposition approach needs to be sought since CsBr has limited solubility in most solvents.

Herein, we present a novel Cs incorporation process where a thin layer of CsBr is thermally evaporated between the lead (II) Iodide (PbI_2) and the organic components. In other words, the perovskite film is formed via a three-step process where PbI_2 is first deposited followed by thermal evaporation of CsBr and finally the organic mixed solution (FAI, MABr, MACl). The effect of the CsBr layer thickness on the microstructural properties, surface chemical states, and electronic structure of the perovskite film is studied. The thickness of the CsBr layer was varied from 0 nm (control), 30 nm, 50 nm to 100 nm, and the different perovskite films were respectively labeled as CsBr0, CsBr30, CsBr50, and CsBr100. We see an improvement in the crystal quality and the surface properties of the perovskite films, with the incorporation of CsBr. The resulting PSC based on the CsBr50 perovskite film showed 15% improvement in PCE and was able to retain over 70% of its PCE for over 120 days in an un-encapsulated state. The results of this study demonstrate the importance of the thermally evaporated CsBr layer in improving the long-term stability of PSC.

5.2 Materials and methods

5.2.1 Materials

Materials used in this work were purchased from Sigma Aldrich and they were used as received unless otherwise indicated. Chemicals include: lead (II) Iodide (PbI_2, 99.99%); Methyl ammonium Bromide (MABr); Methyl ammonium Chloride (MACl); Formamidinium Iodide (FAI); Cesium Bromide (CsBr), Titanium diisopropoxide bis(acetylacetonate) (75% wt in isopranol), 2,2',7,7'-tetrakis(N,N-di-p-methoxyphenylamine)-9,9-spirobifluorene (Spiro-

OMeTAD); Fullerine-C60, 4-*tert*-butylpyridine (*t*BP); lithium *bis*-(*tri*-fluoromethanesulfonyl)imide (Li-TSFI), and Tin (IV) Oxide nano-particle ink (2.5% wt in butanol). Fluorine-doped tin oxide (FTO)-coated glass and solvents such as Acetonitrile (99.8%), Acetone, Isopropyl alcohol (IPA), N,N-dimethylformamide (DMF; 99.8%), Dimethyl sulfoxide (DMSO; 99.9%), Chlorobenzene and Butanol solvents were also purchased from the Sigma Aldrich while pure gold (99.999%, Lesker) was purchased from Kurt J. Lesker Company.

5.2.2 Materials processing

Pre-patterned FTO-coated glass substrates were cut into dimensions of 12.5 mm by 25 mm and sequentially cleaned in an ultrasonic bath using detergent, deionized water, acetone, and IPA for 15 min each. The substrates were tried in nitrogen gas before being treated with UV ozone for 15 minutes to remove any residual organic matter. An ETL was formed from precursor solutions consisting of 0.15 M and 0.3 M solutions of TiO_2 as described elsewhere (Oyewole, Koech, Ichwani, Ahmed, Tamayo, et al., 2021). However, the 0.3 M TiO_2 solution was modified with SnO_2 nanoparticles to obtain SnO_2-TiO_2 mixed solutions with a volume fraction of 0.2 before being spin-coated. The perovskite film was processed via a three-step deposition process where PbI_2 was first spin-coated on the ETL, followed by thermal evaporation of CsBr and a final spin coating of the organic components. The PbI_2 was spin-coated at 1500 rpm for 30 seconds; from a precursor solution containing 599.3 mg of PbI_2 in 1 ml of DMF: DMSO (19:1, v/v); followed by annealing at 70 ^{0}C for 1 minute. Different thicknesses of CsBr were then deposited onto the PbI_2 thin film using a thermal evaporator (Edward E306A, UK). It is important to note that the deposition of CsBr on PbI_2 thin film was

not immediate due to the waiting period for a high vacuum to build after loading the samples in the thermal evaporator.

Subsequently, the organic solution containing a mixture of FAI, MABr, and MACl (60 mg, 6 mg, 6 mg) in 1 ml of IPA was spin-coated onto CsBr at 1300 rpm for 30 seconds. This was then annealed at 130 ^{0}C for 20 minutes to allow for the formation of perovskite crystals. The summary of the perovskite film preparation procedure is indicated in the schematics of Figure 5.1. A layer of the hole transport layer (HTL) was formed by spin coating Spiro-OMeTAD solution onto the perovskite film at 4000 rpm for 30 s. The Spiro-OMeTAD solution was prepared by adding 30 μL of *t*BP and 35 μL of a solution containing 260 mg of Li-TSFI salt in 1ml of acetonitrile into a solution containing 72 mg of Spiro-OMeTAD in 1ml of chlorobenzene. Finally, a 90 nm thick layer of gold was thermally evaporated onto the Spiro-OMeTAD film under a high vacuum (pressure of ~10^{-6} Torr) at an average deposition rate of 1.1 Å/s. All depositions were done under ambient conditions (~25-30^{o}C, 25-55 %RH).

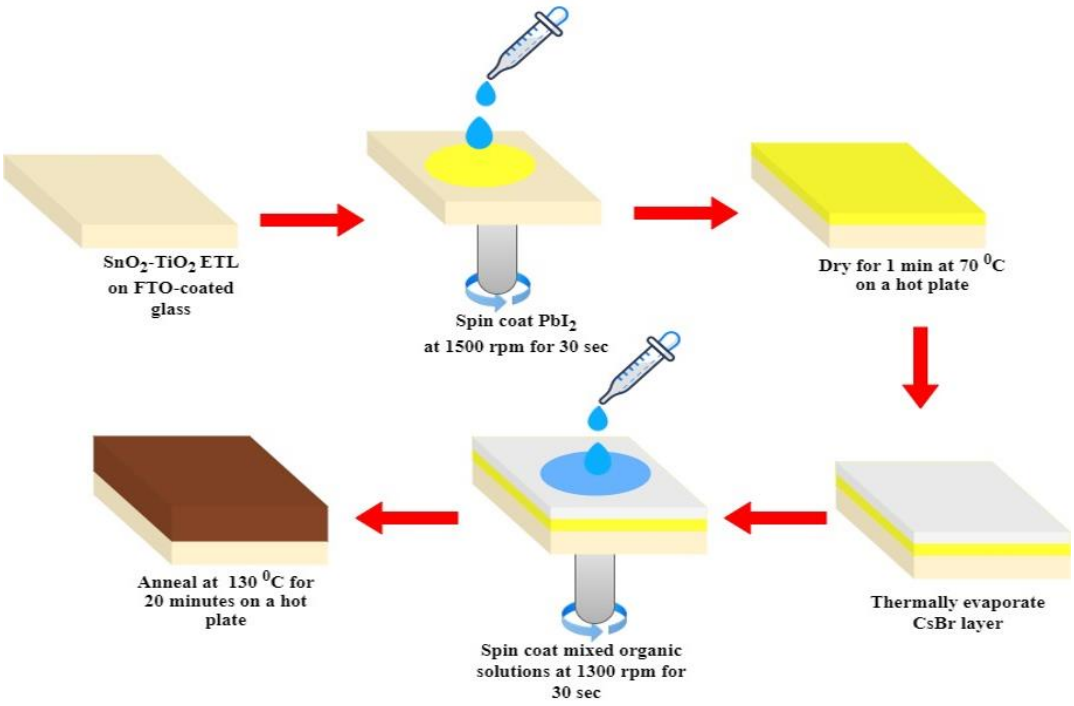

Figure 5.1: Schematic diagram showing the perovskite film preparation procedure

5.2.3 Materials characterization

The microstructural studies of the films were carried out by taking their top view images using a field emission scanning electron microscope (SEM) (JEOL JSM-700F, Hollingsworth & Vose, MA, USA). The structural properties were probed using an X-ray diffractometer (Malvern PANalytical, Westborough, MA, USA) under Cu Kα radiation source with 2θ angles from 5-70^0. The optical properties were measured in the wavelength range of 200 nm to 1100 nm using an Ultraviolet-Visible (UV-Vis) spectrometer (AVANTES Starline, Avaspec-2048) while the photoluminescence (PL) measurement was done with an excitation wavelength of 450 nm using laser light. The X-ray photoelectron spectroscopy (XPS) and ultraviolet photoelectron spectroscopy (UPS) studies were carried out using a PHI5600 XPS system following the method described elsewhere (Carl et al., 2017). The PV performance

and electrochemical impedance (EI) characteristics of the fabricated PSC devices were studied under AM1.5G illumination of 100 mW/cm^2 using Keithley 2400 source meter unit (Keithley, Tektronix, Newark, NJ, USA) and potentiostat (SP-300, BioLogic Instrument) each connected to a solar simulator (Oriel, Newport Corporation, Irvine, CA, USA). The *J–V* measurement for the PSC device was carried out on a device area of 0.1 cm^2 with a voltage scan range of -0.4 to 1.2 V while the EI studies were performed with an AC amplitude of 10 mV in the frequency range 1 MHz to 10 Hz.

5.3 Results and discussion

The morphology of perovskite film is controlled by its crystallization dynamics which is a function of many variables such as perovskite stoichiometry, fabrication conditions, and post-treatment techniques (Abbas et al., 2020; Guo et al., 2019). Proper control of perovskite film morphology is the best route to achieve compact and pinhole-free films that have better light absorption and longer charge carrier diffusion lengths. Figures 5.2(a-d) present the SEM images of the perovskite films for different thicknesses of the CsBr layer. We observe a change in the morphology of perovskite films with the incorporation of CsBr, which implies that the thickness of the CsBr layer affected their crystallization dynamics. The top surface SEM image of the CsBr0 film shows more pronounced grain boundaries when compared to the CsBr-modified perovskite films. The CsBr30 and CsBr50 show surfaces with no distinct boundaries between adjacent grains while the CsBr100 shows some grain boundaries but they are not as pronounced as those of CsBr0. This shows that the CsBr-modified perovskite films had more compact films with well-passivated grain boundaries. This grain boundary passivation effect of CsBr is important in addressing the problems in PSCs that are caused by the presence of defects.

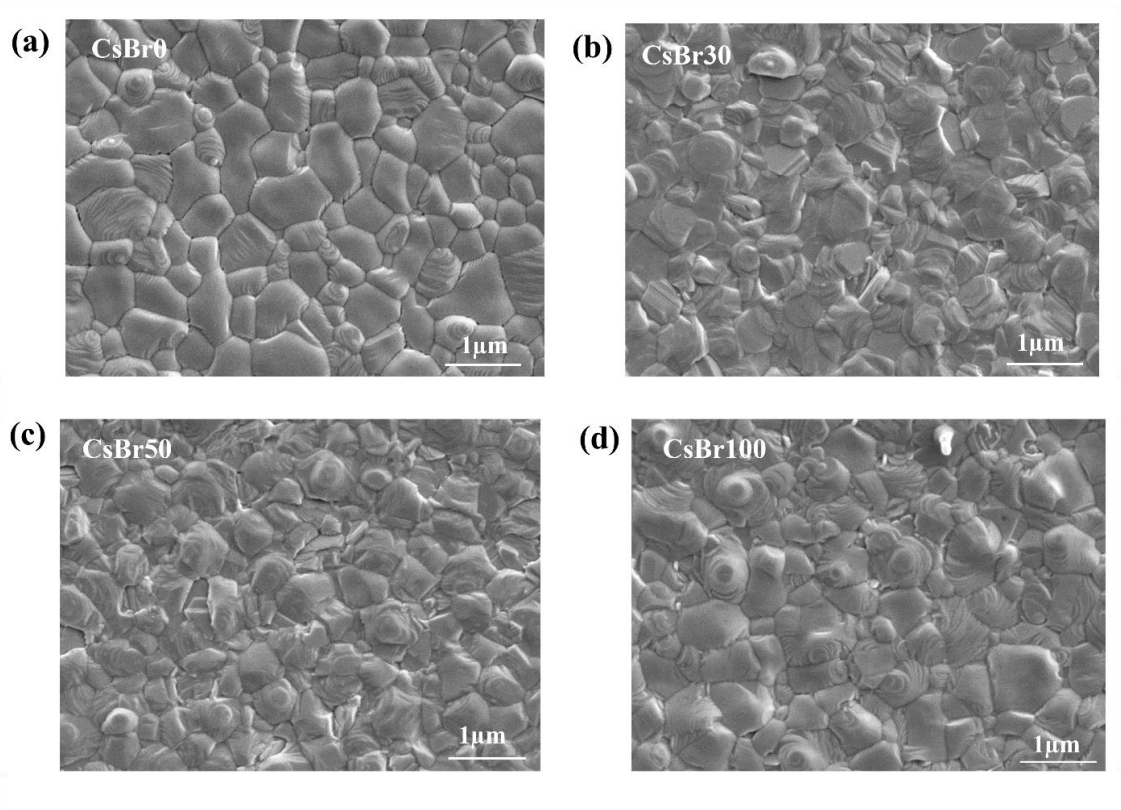

Figure 5.2: SEM images of perovskite films at different thicknesses of CsBr layer: (a) control, (b) 30 nm, (c) 50 nm and (d) 100 nm

The structural properties of the perovskite films were also studied to gain an understanding of the possible effects of the CsBr layer on their crystal quality. The XRD patterns of the CsBr0, CsBr30, CsBr50 and CsBr100 perovskite films are depicted in Figures 5.3(a-b). All the films showed diffraction peaks at 2θ angles around 14.0°, 19.9°, 24.4°, 28.2°, 31.5°, 40.2°, and 42.8° that shows the formation of black (alpha) perovskite phase (Dong et al., 2018). The intensities of the main peaks at 14.0° and 28.2° were found to increase with the thickness of the CsBr doping layer up to 50 nm and decreased thereafter. The increase in peak intensities between CsBr0 and CsBr50 shows that the CsBr layer up to 50 nm improves the crystallinity of the perovskite film. Beyond 50 nm, the crystallinity decreases slightly as seen by the reduction in the intensity of the main peak. It is also evident from Figure 5.3(b) that the

major peak at 14.0° shifts towards higher angles as the thickness of the CsBr layer increases, indicating a decrease in the lattice parameter. This decrease in the lattice parameter is a confirmation that Cs; which has a smaller ionic radius; has successfully been incorporated into the perovskite film. Figure 5.3(c) shows the variation of the position and d-spacing of the major peak at 14.0° with the thickness of the CsBr layer. In agreement with the shift in the peak position to higher angles, the d-spacing decreases as the thickness of the CsBr layer increases. The peak seen at 12.6° in the perovskite films CsBr0 and CsBr30 can be indexed to the (001) plane of hexagonal lead iodide (PbI_2) (Acuña et al., 2016). The presence of this peak in these films shows the existence of some unreacted lead iodide. The intensity of this peak is lower in the perovskite film CsBr30 when compared to that in CsBr0 film and is invisible in the films CsBr50 and CsBr100. This shows that the presence of CsBr layer is likely to have facilitated the reaction of PbI_2 with the organic components to form perovskite.

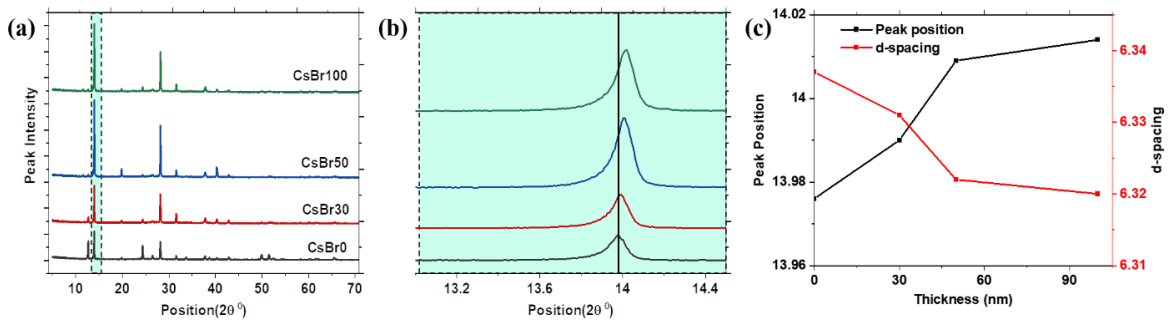

Figure 5.3: (a) XRD patterns of the perovskite films with different CsBr layer thicknesses (b) Zoomed-in view of the major peak (c) Variation of peak position and d-spacing with the thickness of CsBr layer.

The surface chemistry of a semiconductor is quite sensitive to the fabrication conditions and the presence of any substance that may induce changes in the lattice discontinuities and periodicity of chemical bonds (Ono & Qi, 2016). A change in the surface

states of perovskite film affects its electronic structure and its interfacial interaction with adjacent CTLs which influences its charge transport dynamics (Shao & Loi, 2020; Zu et al., 2017). To understand the influence of CsBr on the surface states of the perovskite films, X-ray photoelectron spectroscopy study of the different films was carried out. The XP results complemented the XRD results by revealing near-interfacial concentration changes in the perovskite films as a function of CsBr deposition thickness. For perovskites with 0 nm-, 30 nm-, 50 nm-, and 100-nm-thick initial CsBr layers, Figure 5.4 presents the high-resolution XP spectra of the Cs $3d_{5/2}$ regions that are each normalized to the corresponding I $3d_{5/2}$ feature intensity.

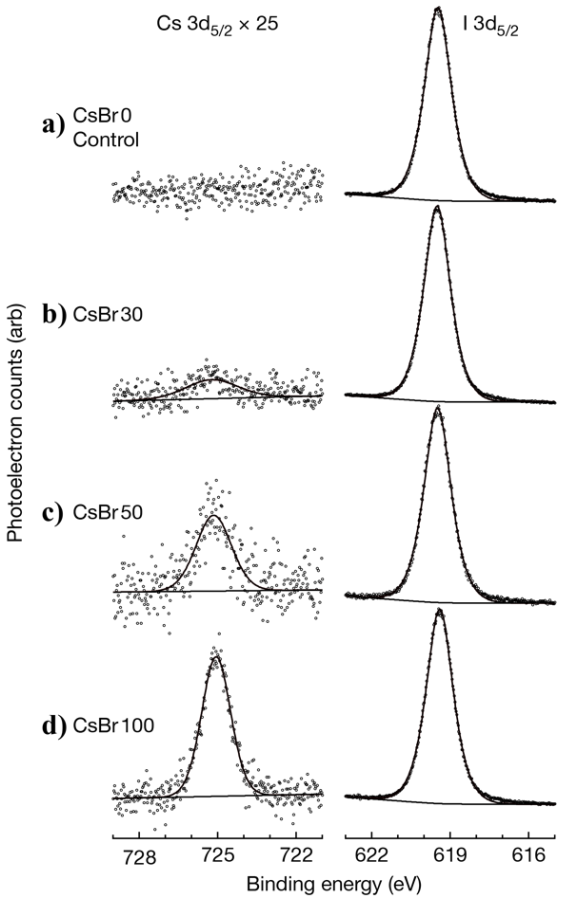

Figure 5.4: High-resolution XP spectra of the Cs $3d_{5/2}$ and I $3d_{5/2}$ regions for perovskite samples as a function of CsBr thickness.

The figure demonstrates that thicker CsBr films yield successively increasing relative concentrations of Cs^+ cations in the near-interfacial region of the resulting perovskite films. This indicates that varying the thickness of the CsBr layer effectively regulates the amount of Cs that can diffuse towards the surface of the perovskite film. The atomic mass ratios of different elements at the surface of the films CsBr0, CsBr30, CsBr50, and CsBr100 were determined from their XP core-level spectra and tabulated in Table 5.1. The atomic mass ratios of Cs to I and Cs to oxidized Pb at the surface of the perovskite film were found to increase with the thickness of the CsBr layer. This is a clear indication that the concentration of Cs at the surface increased with the thickness of the CsBr layer. We also employed the EDS cross-sectional analysis to study the distribution of Cs and Br within the bulk of the perovskite films and the underlying components.

Table 5.1: Atomic ratios of different elements on the surface of perovskite films with different thicknesses of CsBr layer

Sample ID	I:oxidized Pb	Cs:I	Cs:oxidized Pb	red. Pb:ox. Pb
CsBr0	1.98	0.00	0.00	0.06
CsBr30	2.19	0.01	0.02	0.27
CsBr50	3.05	0.02	0.06	0.32
CsBr100	2.13	0.06	0.14	0.17

The EDS cross-sectional maps of the CsBr30- and CsBr100-modified perovskite films are displayed in Figure 5.5. The maps reveal the presence of Cs and Br in the bulk of the perovskite films and some traces of Cs and Br were also detected in the components below the

perovskite films, possibly due to diffusion that occurs during annealing (Oyewole, Koech, Ichwani, Ahmed, Tamayo, et al., 2021).

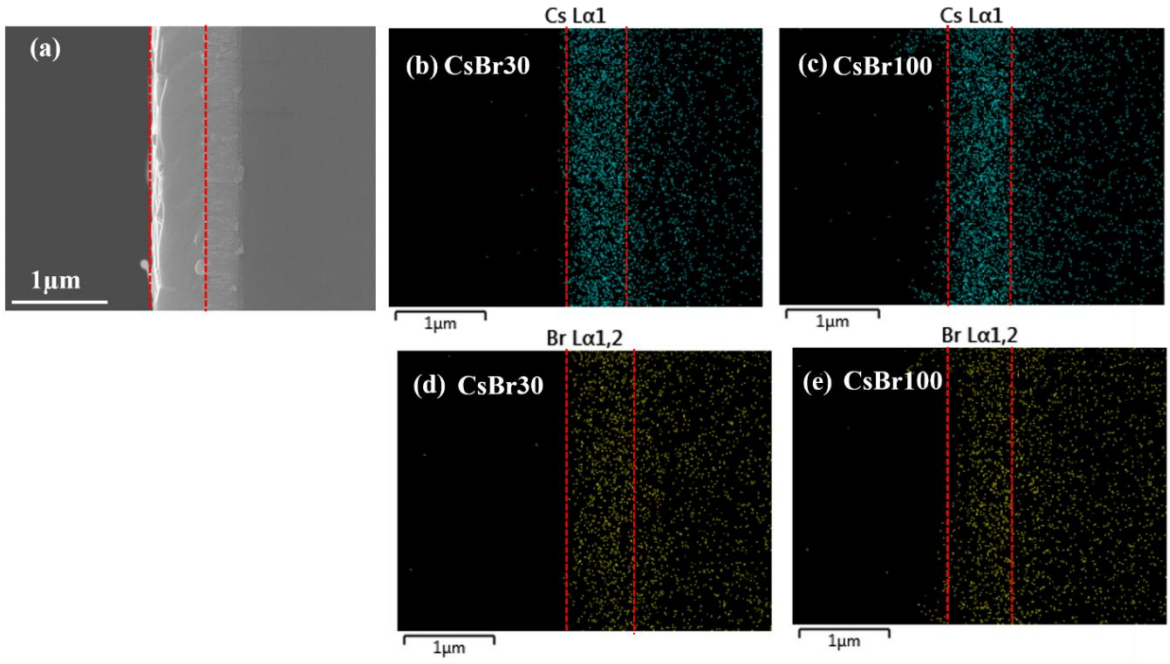

Figure 5.5: (a) Cross-sectional SEM image and (b-e) Cross-sectional EDS maps of the CsBr-modified perovskite films showing Cs and Br distribution

The perovskite AL is the most important component of PSC due to its intrinsic function of light absorption and photogeneration. The light absorption capability of perovskite film determines the number of photons that can be absorbed to generate the charge carriers and is usually influenced by its thickness, defect density state, and bandgap (Ezealigo et al., 2020; Wang et al., 2016). To understand the effects of the CsBr layer on the photo-physical properties of perovskite films, we carried out UV-Vis and PL studies on the different films. Figure 5.6(a) shows the light absorption spectra of the perovskite films at different thicknesses of CsBr. We observe a small blueshift in the absorption onset of the perovskite films as the CsBr layer thickness increases, which signifies an increase in the optical bandgap. The

bandgaps of the perovskite films at different CsBr thicknesses were estimated from absorbance using the Tauc plot as shown in Figure 5.6(b). The mean values of the bandgap were slightly blue-shifted from 1.547 ± 0.015 eV to 1.565 ± 0.021 eV as the thickness of the CsBr layer increased from 0 to 100 nm, which is also evident in the shift in the normalized PL peaks shown in Figure 5.6(c).

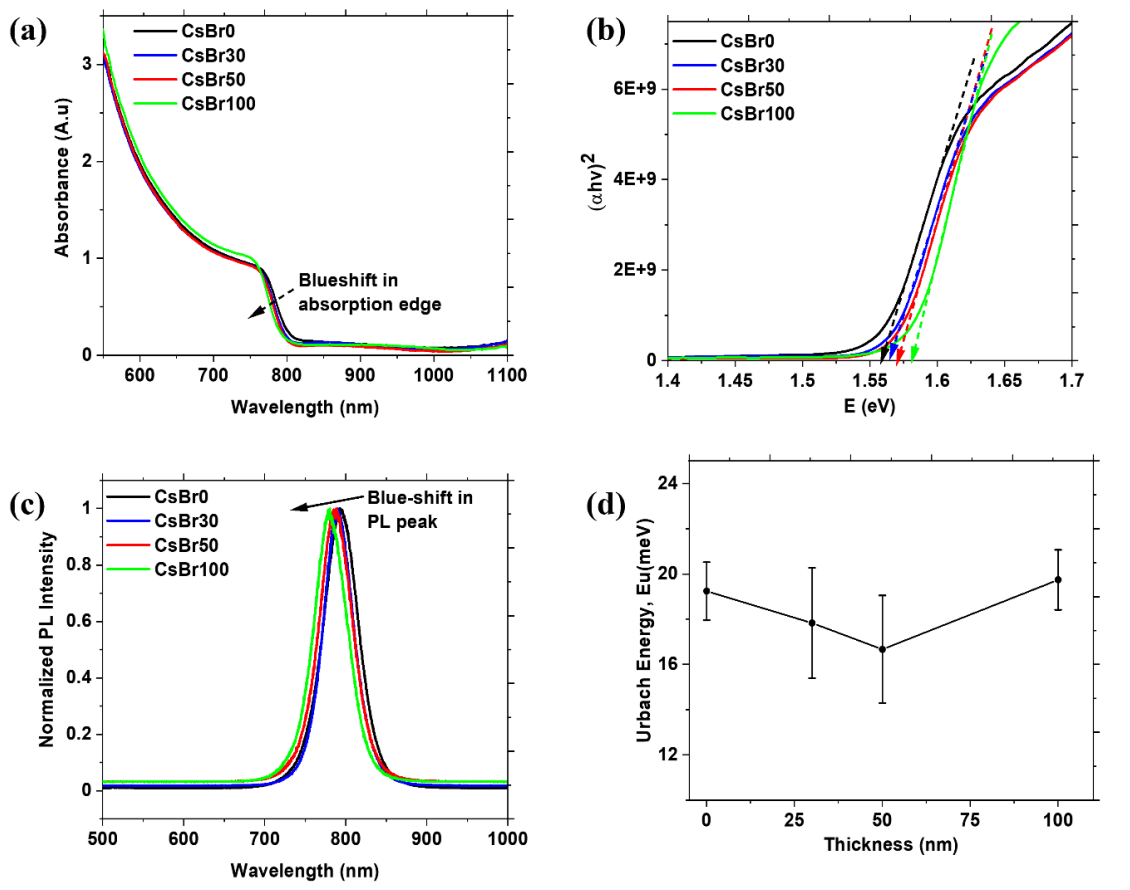

Figure 5.6: (a) Absorption spectra of perovskite films (b) Tauc plot (c) Normalized PL curves (d) Eu values of the different perovskite films

The shift in bandgap could be an indication of changes in the electronic band structure or reduction in the band tail states of the perovskite films with increasing CsBr layer thickness.

The distribution of band tail states within the bandgap of perovskite film can be studied by estimating the Urbach energy (Eu), a parameter that indicates the level of structural disorder in the film (Chantana et al., 2020). The Eu values of the different perovskite films were determined from the inverse slope of a plot of lnα vs photon energy (hν). The calculated values of Eu were observed to decrease from 19.24 ± 1.28 meV for CsBr0 to 16.67 ± 2.44 meV for CsBr50 but thereafter increased to 19.74 ± 1.32 meV for CsBr100 perovskite films (Figure 5.6(d)). The lower Eu values for CsBr30 and CsBr50 films signify a decrease in structural disorder in these perovskite films (Caselli et al., 2020). The relative position of the band edges is also important in the charge injection and extraction dynamics in PSC devices since it controls the band offsets at the interface with the CTLs (Wolff et al., 2017). To investigate the impact of the CsBr layer on the electronic band structure of perovskite films, we carried out UPS study on the different perovskite films. Figure 5.7 shows the variation of the secondary photoemission cut-off energies ($\mathbf{E}_{SEC}$) for CsBr0, CsBr30, CsBr50, and CsBr100 perovskite films. The figure shows that $\mathbf{E}_{SEC}$ values shifted towards lower binding energies as the CsBr layer thickness increased from 0 to 50 nm and shifted towards higher binding energies thereafter. This led to a slight increase in the work function ($\mathbf{\Phi}_{WF}$) of the top surface of the perovskite films from 3.95 eV for CsBr0 to 4.12 eV for CsBr50 and later decreased to 3.99 eV for CsBr100. The increase in the $\mathbf{\Phi}_{WF}$ of the surface of perovskite film signifies a downward shift in the Fermi level (E_f) which may arise due to reduction in the donor-type defect states such as iodine vacancies or Pb^0 that are known to make the films exhibit n-type conductivity (Frolova et al., 2015).

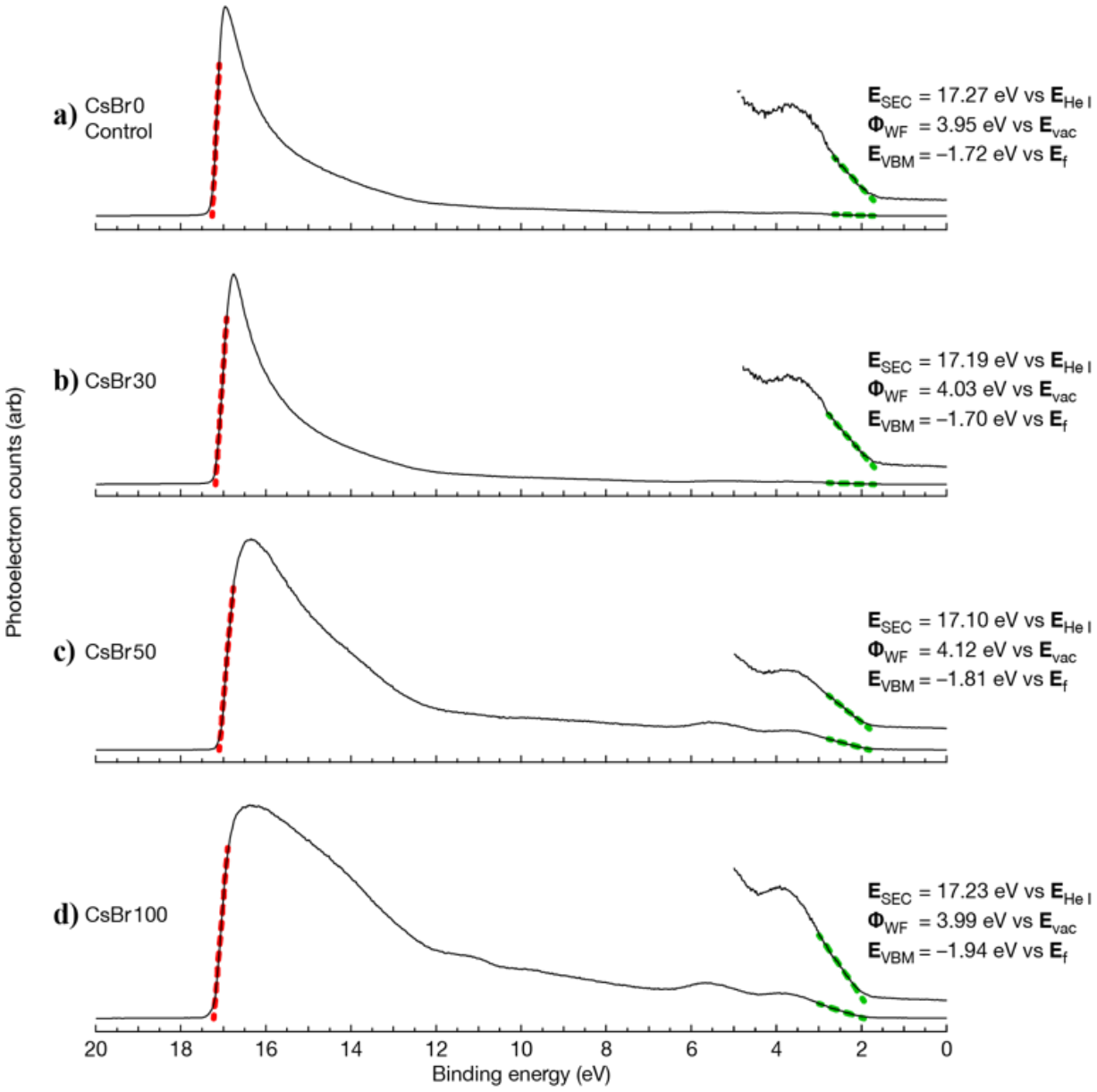

Figure 5.7: UPS spectra of different perovskite films: (a) CsBr0 (b) CsBr30 (c) CsBr50 and, (d) CsBr100

The electronic band edge positions were determined from the combined UPS and UV-Vis data for the different perovskite films. Table 5.2 summarizes the experimentally determined and interpreted values of $\mathbf{\Phi}_{WF}$ and the band edge positions relative to the vacuum

level (E_{vac}). From these values, we drew the electronic band structure of the different perovskite films as depicted in Figure 5.8(a). The figure indicates that the CsBr layer thickness played a role in tuning the band edge positions in the perovskite film which control the interfacial band alignment and the charge carrier injection dynamics of the ensuing PSC structure shown in Figure 5.8(b). Higher interfacial band offsets between the perovskite layer and the CTL may cause thermionic power losses that contribute to a reduction in V_{oc} (Stolterfoht et al., 2019b). Considering the planar PSC architecture we fabricated, the downward shift in $\mathbf{E}_{CBM}$ of the perovskite film with CsBr thickness leads to a reduction of the interfacial energy barrier at ETL/perovskite interface which favors electron injection.

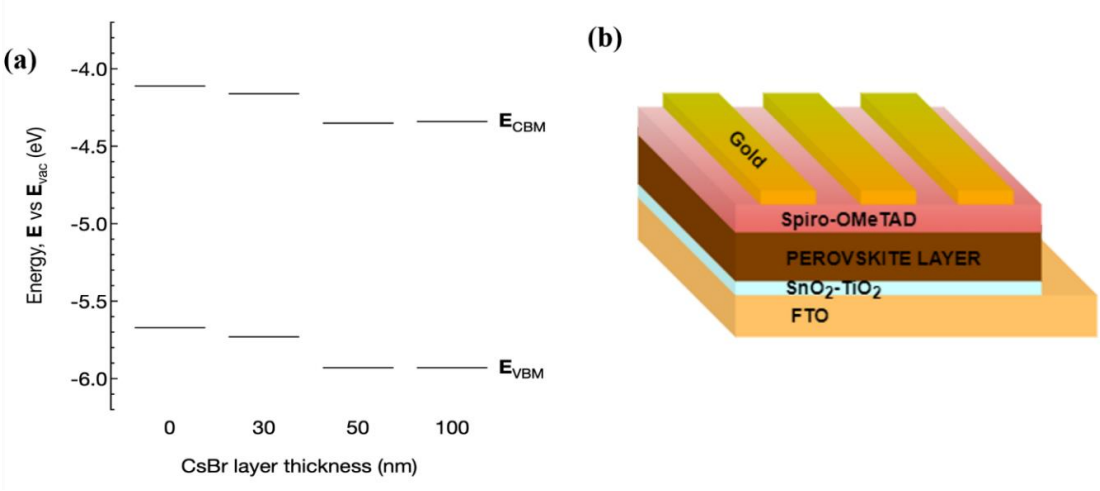

Figure 5.8: (a) Band structure of perovskite film at different CsBr thickness (b) Planar PSC fabricated

Table 5.2: Electronic band structure parameters based on UPS and UV-Vis data.

Sample	Experimental data			Interpreted Results	
	Φ_{WF}	E_{VB} vs E_f	E_g	E_{VBM} vs E_{vac}	E_{CBM} vs vs E_{vac}
CsBr0	3.95	–1.72	1.547 ± 0.015	–5.67	–4.12
CsBr30	4.03	–1.70	1.552 ± 0.025	–5.73	–4.16
CsBr50	4.12	–1.81	1.559 ± 0.016	–5.93	–4.36
CsBr100	3.99	–1.94	1.565 ± 0.021	–5.93	–4.35

The performance of PSC is a function of many variables which are strongly influenced by the device fabrication conditions (Roy et al., 2020b). To understand the impacts of the thermally evaporated CsBr layer on the PV parameters, we recorded the J-V curves of the PSCs fabricated with CsBr0, CsBr30, CsBr50, and CsBr100 perovskite films as absorber layers. Figure 5.9(a) compares the J-V curves of the control and the best performing CsBr-modified PSC devices from which we observe an improvement in both the short circuit current (J_{sc}) and the open-circuit voltage (V_{oc}) in the CsBr-modified device. The PV performance parameters for the different PSCs are summarized in Table 5.3. It is seen that the parameters varied with the thickness of the CsBr layer in the AL. The PSC device with CsBr50 perovskite film showed better PCE when compared to the rest. The improved PCE for the device with CsBr50 perovskite film as absorber layer can be associated with the improved perovskite film morphology or better interface band alignment that led to improved charge carrier collection efficiency as shown by the EQE curves in Figure 5.9(b).

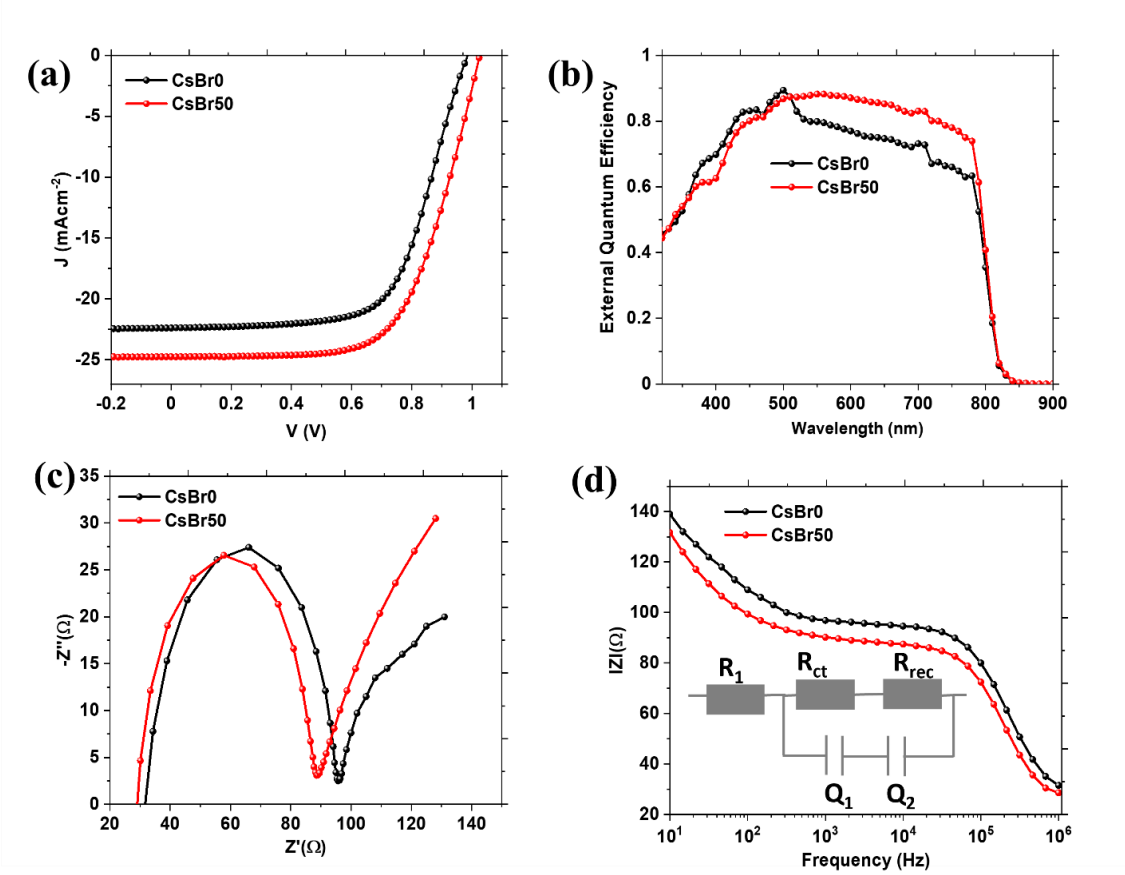

Figure 5.9: (a) J-V Curves (b) EQE Curves (c) Nyquist plots (d) Bode plots for control and best performing PSCs

To establish the real cause of the observed PCE improvement in PSC device with CsBr50 perovskite absorber, we probed the charge transport and recombination dynamics of the device relative to the control device using EI spectroscopy. The EI spectra for both PSC devices were represented in the form of Nyquist and bode plots as shown in Figure 5.9(c)-(d). The plots indicate that the devices exhibit two relaxation processes that are usually associated with charge transport dynamics. In the Nyquist plots of Figure 5.9(c), we see two arcs; one in the low-frequency regime and the other in the high-frequency regime; that are respectively associated with recombination and charge carrier transfer resistances within the layered PSC

structure (Juarez-Perez et al., 2014b). The Nyquist plots were fitted with an equivalent circuit consisting of resistors and constant phase elements; shown in the inset of Figure 5.9(d); in order to obtain the values of the parameters of interest such as the series resistance (R_1) and the charge transfer resistance (R_{ct}). The values of R_1 were determined to be 34.12 Ω and 33.46 Ω for the control and CsBr-modified PSC devices respectively while the R_{ct} values were 66.84 Ω and 62.02 Ω. Thus, R_1 and R_{ct} values were lower for the CsBr-modified PSC device when compared to the control device which led to a reduction in the charge carrier recombination.

Table 5.3: Summary of the PV performance parameters for PSCs with different perovskite layers

Perovskite film	**PCE**	**J_{sc}**	**V_{oc}**	**FF**
CsBr0	14.86(14.07±0.98)	22.77(22.4±0.71)	1.008(0.992±0.018)	64.73(63.33±3.39)
CsBr30	16.49(15.78±0.84)	24.36(23.76±1.02)	1.008(0.992±0.009)	67.16(66.96±1.96)
CsBr50	16.78(16.19±0.17)	24.85(24.76±1.02)	1.04(1.024±0.021)	64.93(63.84±2.92)
CsBr100	15.11(13.37±1.41)	23.26(21.62±1.77)	0.96 (0.944±0.015)	67.67(65.52±2.08)

The long-term stability of PSCs under ambient conditions is another important parameter for consideration in the efforts to accelerate the commercialization of this PV technology. To understand the role of the CsBr layer on the degradation behavior of PSCs, we monitored the PV performance characteristics of the control and the best performing CsBr-modified PSC devices left to age in an un-encapsulated state for 4 months under the ambient conditions by periodically recording their J-V and EQE curves. The PV parameters were determined from the J-V curves and normalized to clearly show their degradation rate. The

evolution of the normalized PV performance parameters with time (days) is depicted in Figure 5.10(a)-(d).

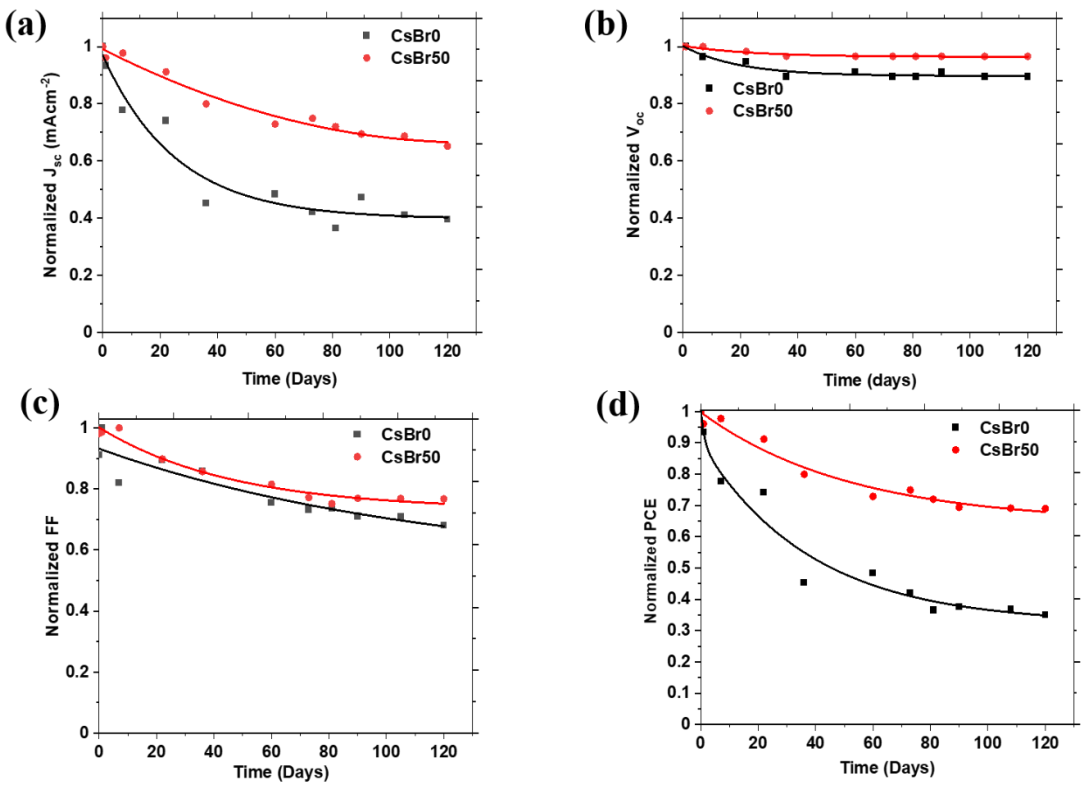

Figure 5.10: Variation of the normalized PV performance parameters of PSC with time (a) J_{sc} (b) V_{oc} (c) *FF* and, (d) PCE

The figure shows that the PV performance parameters of the control and best performing PSC based on the CsBr50 perovskite absorber decreased gradually with time. It is important to note that the decrease in the PV parameters of the PSC device with the CsBr-modified absorber layer was slower than that of the control device. The PSC with CsBr50 perovskite film as the light-absorbing layer was able to retain over 70% of its PCE for over 120 days.

The EQE of a solar cell is a parameter that quantifies the charge carrier collection efficiency of the device at a given wavelength region of the solar spectrum and provides

useful information on the degradation behavior of PSCs (Hierrezuelo-Cardet et al., 2020). Figure 5.11(a)-(b) depicts the EQE curves of the control and best performing CsBr-modified PSCs. From the figure, we observe that the EQEs of both PSC devices decreased with the aging time and that the decrease is more pronounced in the long-wavelength region of the solar spectrum. The decrease in the EQE is also seen to be faster for the control device than that of the CsBr-modified counterpart.

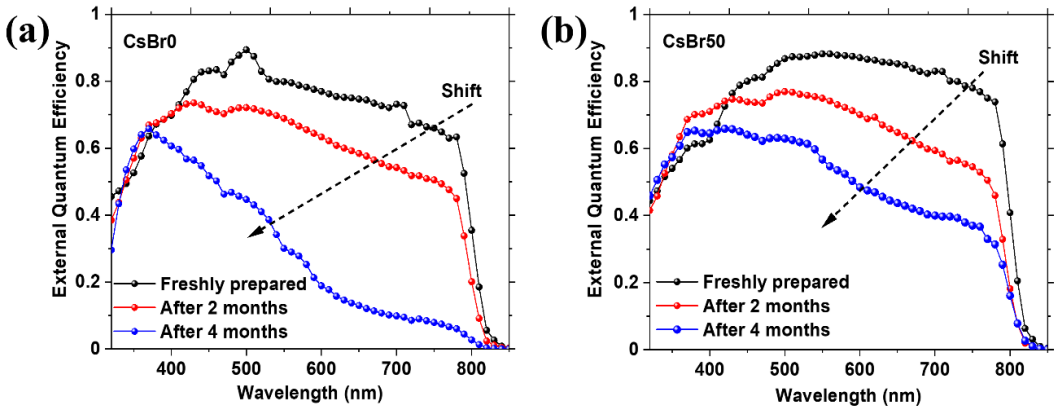

Figure 5.11: EQE Curves of (a) the control and (b) best performing CsBr-Modified PSC at different times

The faster EQE decay in the long-wavelength region is an indication that the charge carrier collection from the bulk and at the back surface of the devices is impaired as they age (Hierrezuelo-Cardet et al., 2020; Xu et al., 2017). This means that the charge transfer properties at the perovskite/Spiro-OMeTAD interface become poor as the devices age.

To establish the real cause of this observation, we compared the SEM cross-sectional images of freshly prepared devices and those that have been aged for 2 and 4 months under ambient conditions for both the control and the CsBr-modified PSC devices. Figure 5.12(a)-

(f) shows the SEM images from which we observe voids (marked with arrows) in the Spiro-OMeTAD (HTL) in both the control and CsBr-modified devices after being aged. This shows that the HTL undergoes degradation faster than the other components of the device possibly because it is more exposed to the ambient conditions when compared to the other components. The degradation in the Spiro-OMeTAD will affect the interfacial energetics at the perovskite/HTL interface of PSC which reduces the charge carrier collection efficiency. The degradation of Spiro-OMeTAD will finally expose the perovskite layer to the ambient conditions causing it to degrade as seen in the SEM cross-sectional images after aging the devices for a period of 4 months. The perovskite film CsBr0 appears to be degraded more than the perovskite film CsBr50 for the CsBr-modified device. This shows that the CsBr layer has an important effect of suppressing the degradation of PSCs.

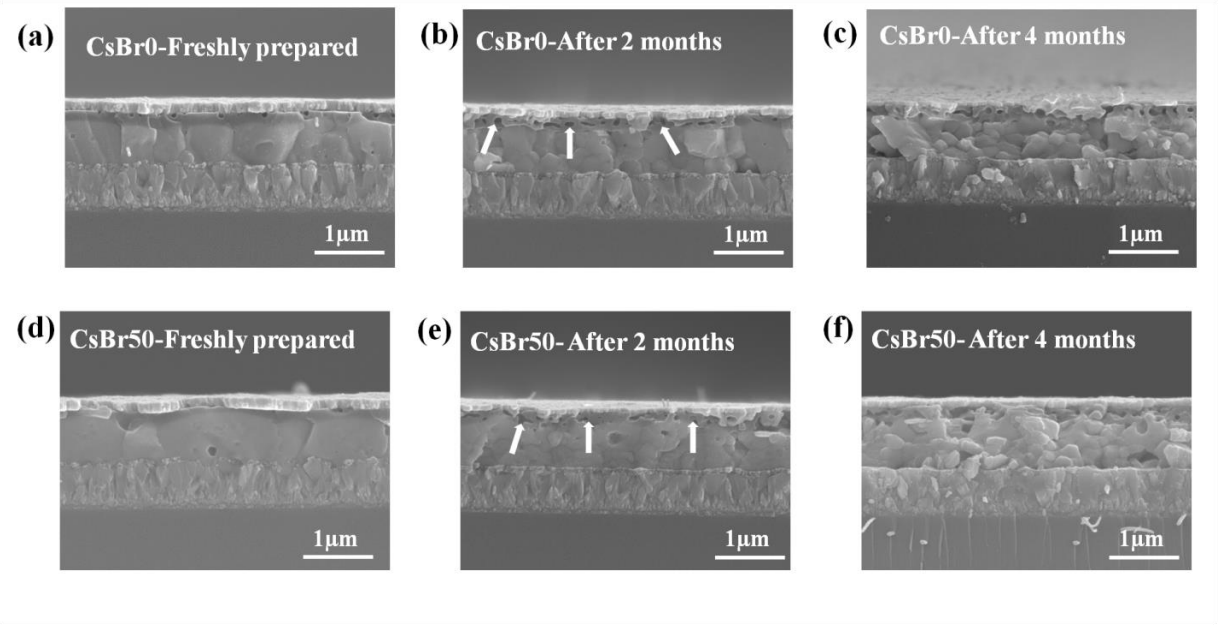

Figure 5.12: SEM Cross-sectional images of PSCs at different aging times (a) CsBr0-Freshly prepared (b) CsBr0 film after 2 months (c) CsBr0 film after 4 months (d) CsBr50-Freshly prepared (e) CsBr50 film after 2 months (f) CsBr50 film after 4 months

5.4 Summary and concluding remarks

A thermally evaporated CsBr layer of appropriate thickness in FA-rich perovskite film passivates the grain boundaries and modifies the interfacial energetics with adjacent CTLs. This improves the charge transport and PV performance characteristics of PSC while simultaneously suppressing the degradation of the perovskite layer when exposed to ambient conditions. We have shown that the incorporation of a 50 nm thick CsBr layer in the absorber layer helps to improve the PCE and long-term stability of PSC. The CsBr-modified PSC showed a 15 % improvement in the PCE when compared to the control device and was able to retain about 70 % of its initial PCE for over 120 days. The improvement in PCE and stability resulted from defect passivation and band structure modulation effects of CsBr as revealed by the SEM and UPS studies.

5.5 References

Abbas, M., Zeng, L., Guo, F., Rauf, M., Yuan, X. C., & Cai, B. (2020). A critical review on crystal growth techniques for scalable deposition of photovoltaic perovskite thin films. In *Materials* (Vol. 13, Issue 21, pp. 1–42). MDPI AG. https://doi.org/10.3390/ma13214851

Acuña, D., Krishnan, B., Shaji, S., Sepúlveda, S., & Menchaca, J. L. (2016). Growth and properties of lead iodide thin films by spin coating. *Bulletin of Materials Science*, *39*(6), 1453–1460. https://doi.org/10.1007/s12034-016-1282-z

Asghar, M. I., Zhang, J., Wang, H., & Lund, P. D. (2017). Device stability of perovskite solar cells – A review. In *Renewable and Sustainable Energy Reviews*. https://doi.org/10.1016/j.rser.2017.04.003

Assadi, M. K., Bakhoda, S., Saidur, R., & Hanaei, H. (2018). Recent progress in perovskite solar cells. In *Renewable and Sustainable Energy Reviews*. https://doi.org/10.1016/j.rser.2017.06.088

Bella, F., Renzi, P., Cavallo, C., & Gerbaldi, C. (2018). Caesium for Perovskite Solar Cells: An Overview. *Chemistry - A European Journal*, *24*(47), 12183–12205. https://doi.org/10.1002/chem.201801096

Bush, K. A., Frohna, K., Prasanna, R., Beal, R. E., Leijtens, T., Swifter, S. A., & McGehee, M. D. (2018). Compositional Engineering for Efficient Wide Band Gap Perovskites with Improved Stability to Photoinduced Phase Segregation. *ACS Energy Letters*. https://doi.org/10.1021/acsenergylett.7b01255

Carl, A. D., Kalan, R. E., Obayemi, J. D., Kana, M. G. Z., Soboyejo, W. O., & Grimm, R. L. (2017). Synthesis and characterization of alkylamine-functionalized Si(111) for perovskite adhesion with minimal interfacial oxidation or electronic defects. *ACS Applied Materials and Interfaces*, *9*(39), 34377–34388. https://doi.org/10.1021/acsami.7b07117

Caselli, V. M., Wei, Z., Ackermans, M. M., Hutter, E. M., Ehrler, B., & Savenije, T. J. (2020). Charge Carrier Dynamics upon Sub-bandgap Excitation in Methylammonium Lead Iodide Thin Films: *Effects of Urbach Tail, Deep Defects, and Two-Photon Absorption*. https://doi.org/10.1021/acsenergylett.0c02067

Chantana, J., Kawano, Y., Nishimura, T., Mavlonov, A., & Minemoto, T. (2020). Impact of Urbach energy on open-circuit voltage deficit of thin-film solar cells. *Solar Energy Materials and Solar Cells*, *210*, 110502. https://doi.org/10.1016/j.solmat.2020.110502

Chavan, R. D., Prochowicz, D., Yadav, P., Tavakoli, M. M., Nimbalkar, A., Bhoite, S. P., & Hong, C. K. (2019). Effect of CsCl Additive on the Morphological and Optoelectronic Properties of Formamidinium Lead Iodide Perovskite. *Solar RRL*, *3*(11), 1900294. https://doi.org/10.1002/solr.201900294

Chen, B., Yang, M., Priya, S., & Zhu, K. (2016). Origin of J-V Hysteresis in Perovskite Solar Cells. In *Journal of Physical Chemistry Letters*. https://doi.org/10.1021/acs.jpclett.6b00215

Chen, S., Dong, J., Wu, J., Hou, S., Xing, J., Liu, H., & Hao, H. (2019). CsBr interface modification to improve the performance of perovskite solar cells prepared in ambient air. *Solar Energy Materials and Solar Cells*, *201*, 110110. https://doi.org/10.1016/j.solmat.2019.110110

Chouhan, L., Ghimire, S., Subrahmanyam, C., Miyasaka, T., & Biju, V. (2020). Synthesis, optoelectronic properties and applications of halide perovskites. In *Chemical Society Reviews*. https://doi.org/10.1039/c9cs00848a

Dong, X., Chen, D., Zhou, J., Zheng, Y. Z., & Tao, X. (2018). High crystallization of a multiple cation perovskite absorber for low-temperature stable ZnO solar cells with high-efficiency of over 20%. *Nanoscale*, *10*(15), 7218–7227. https://doi.org/10.1039/c8nr00152a

Ezealigo, B. N., Nwanya, A. C., Ezugwu, S., Offiah, S., Obi, D., Osuji, R. U., Bucher, R., Maaza, M., Ejikeme, P., & Ezema, F. I. (2020). Method to control the optical properties: Band gap energy of mixed halide Organolead perovskites. *Arabian Journal of Chemistry*, *13*(1), 988–997. https://doi.org/10.1016/j.arabjc.2017.09.002

Frolova, L. A., Dremova, N. N., & Troshin, P. A. (2015). The chemical origin of the p-type and n-type doping effects in the hybrid methylammonium-lead iodide (MAPbI3) perovskite solar cells. *Chemical Communications*, *51*(80), 14917–14920. https://doi.org/10.1039/c5cc05205j

Fu, L., Li, H., Wang, L., Yin, R., Li, B., & Yin, L. (2020). Defect passivation strategies in perovskites for an enhanced photovoltaic performance. In *Energy and Environmental Science* (Vol. 13, Issue 11, pp. 4017–4056). Royal Society of Chemistry. https://doi.org/10.1039/d0ee01767a

Green, M. A., Hishikawa, Y., Dunlop, E. D., Levi, D. H., Hohl-Ebinger, J., & Ho-Baillie, A. W. Y. (2018). Solar cell efficiency tables (version 51). *Prog. Photovolt: Res. Appl.* https://doi.org/10.1002/pip.2978

Guo, F., Qiu, S., Hu, J., Wang, H., Cai, B., Li, J., Yuan, X., Liu, X., Forberich, K., Brabec, C. J., & Mai, Y. (2019). A Generalized Crystallization Protocol for Scalable Deposition of High-Quality Perovskite Thin Films for Photovoltaic Applications. *Advanced Science*. https://doi.org/10.1002/advs.201901067

Hierrezuelo-Cardet, P., Palechor-Ocampo, A. F., Caram, J., Ventosinos, F., Pérez-Del-Rey, D., Bolink, H. J., & Schmidt, J. A. (2020). External quantum efficiency measurements used to study the stability of differently deposited perovskite solar cells. *Journal of Applied Physics*, *127*(23), 235501. https://doi.org/10.1063/5.0011503

Hussain, I., Tran, H. P., Jaksik, J., Moore, J., Islam, N., & Uddin, M. J. (2018). Functional materials, device architecture, and flexibility of perovskite solar cell. *Emergent*

Materials. https://doi.org/10.1007/s42247-018-0013-1

Juarez-Perez, E. J., Wußler, M., Fabregat-Santiago, F., Lakus-Wollny, K., Mankel, E., Mayer, T., Jaegermann, W., & Mora-Sero, I. (2014). Role of the selective contacts in the performance of lead halide perovskite solar cells. *Journal of Physical Chemistry Letters*, *5*(4), 680–685. https://doi.org/10.1021/jz500059v

Kim, H. S., Hagfeldt, A., & Park, N. G. (2019). Morphological and compositional progress in halide perovskite solar cells. *Chemical Communications*. https://doi.org/10.1039/c8cc08653b

Kundu, S., & Kelly, T. L. (2020). In situ studies of the degradation mechanisms of perovskite solar cells. *EcoMat*. https://doi.org/10.1002/eom2.12025

Landi, G., Neitzert, H. C., Barone, C., Mauro, C., Lang, F., Albrecht, S., Rech, B., & Pagano, S. (2017). Correlation between Electronic Defect States Distribution and Device Performance of Perovskite Solar Cells. *Advanced Science*. https://doi.org/10.1002/advs.201700183

Li, C., Lu, X., Ding, W., Feng, L., Gao, Y., & Guo, Z. (2008). Formability of ABX 3 (X = F, Cl, Br, I) halide perovskites. *Acta Crystallographica Section B: Structural Science*. https://doi.org/10.1107/S0108768108032734

Li, W., Zhang, W., Van Reenen, S., Sutton, R. J., Fan, J., Haghighirad, A. A., Johnston, M. B., Wang, L., & Snaith, H. J. (2016). Enhanced UV-light stability of planar heterojunction perovskite solar cells with caesium bromide interface modification. *Energy and Environmental Science*, *9*(2), 490–498. https://doi.org/10.1039/c5ee03522h

Li, Zhen, Yang, M., Park, J. S., Wei, S. H., Berry, J. J., & Zhu, K. (2016). Stabilizing Perovskite Structures by Tuning Tolerance Factor: Formation of Formamidinium and Cesium Lead Iodide Solid-State Alloys. *Chemistry of Materials*, *28*(1), 284–292. https://doi.org/10.1021/acs.chemmater.5b04107

Li, Zhenzhen, Xu, J., Zhou, S., Zhang, B., Liu, X., Dai, S., & Yao, J. (2018). CsBr-Induced Stable CsPbI 3- x Br x (x < 1) Perovskite Films at Low Temperature for Highly Efficient Planar Heterojunction Solar Cells. *ACS Applied Materials and Interfaces*, *10*(44), 38183–38192. https://doi.org/10.1021/acsami.8b11474

Liu, R., & Xu, K. (2020). Solvent engineering for perovskite solar cells: A review. In *Micro and Nano Letters* (Vol. 15, Issue 6, pp. 349–353). Institution of Engineering and Technology. https://doi.org/10.1049/mnl.2019.0735

Liu, T., Lai, H., Wan, X., Zhang, X., Liu, Y., & Chen, Y. (2018). Cesium Halides-Assisted Crystal Growth of Perovskite Films for Efficient Planar Heterojunction Solar Cells. *Chemistry of Materials*. https://doi.org/10.1021/acs.chemmater.8b02002

Myung, C. W., Yun, J., Lee, G., & Kim, K. S. (2018). A New Perspective on the Role of A-Site Cations in Perovskite Solar Cells. *Advanced Energy Materials*. https://doi.org/10.1002/aenm.201702898

Ono, L. K., & Qi, Y. (2016). Surface and Interface Aspects of Organometal Halide Perovskite Materials and Solar Cells. *J. Phys. Chem. Lett*. https://doi.org/10.1021/acs.jpclett.6b01951

Oyewole, D. O., Koech, R. K., Ichwani, R., Ahmed, R., Tamayo, J. H., Adeniji, S. A., Cromwell, J., Ulloa, E. C., Oyewole, O. K., Agyei-Tuffour, B., Titova, L. V, Burnham, N. A., & Soboyejo, W. O. (2021). Annealing effects on interdiffusion in layered FA-rich perovskite solar cells Annealing effects on interdiffusion in layered FA-rich perovskite solar cells AIP Advances. *AIP Advances*, *11*, 65327. https://doi.org/10.1063/5.0046205

Pang, S., Zhang, C., Dong, H., Zhang, Z., Chen, D., Zhu, W., Chang, J., Lin, Z., Zhang, J., & Hao, Y. (2021). Synchronous Interface Modification and Bulk Passivation via a One-Step Cesium Bromide Diffusion Process for Highly Efficient Perovskite Solar Cells. *ACS Applied Materials and Interfaces*. https://doi.org/10.1021/acsami.1c00066

Prasanna, R., Gold-Parker, A., Leijtens, T., Conings, B., Babayigit, A., Boyen, H. G., Toney, M. F., & McGehee, M. D. (2017). Band Gap Tuning via Lattice Contraction and Octahedral Tilting in Perovskite Materials for Photovoltaics. *Journal of the American Chemical Society*. https://doi.org/10.1021/jacs.7b04981

Roy, P., Kumar Sinha, N., Tiwari, S., & Khare, A. (2020). A review on perovskite solar cells: Evolution of architecture, fabrication techniques, commercialization issues and status. In *Solar Energy* (Vol. 198, pp. 665–688). Elsevier Ltd. https://doi.org/10.1016/j.solener.2020.01.080

Saliba, M., Matsui, T., Seo, J. Y., Domanski, K., Correa-Baena, J. P., Nazeeruddin, M. K., Zakeeruddin, S. M., Tress, W., Abate, A., Hagfeldt, A., & Grätzel, M. (2016). Cesium-containing triple cation perovskite solar cells: Improved stability, reproducibility and high efficiency. *Energy and Environmental Science*, *9*(6), 1989–1997. https://doi.org/10.1039/c5ee03874j

Shao, S., & Loi, M. A. (2020). The Role of the Interfaces in Perovskite Solar Cells. In *Advanced Materials Interfaces* (Vol. 7, Issue 1, p. 1901469). Wiley-VCH Verlag. https://doi.org/10.1002/admi.201901469

Sherkar, T. S., Momblona, C., Gil-Escrig, L., Ávila, J., Sessolo, M., Bolink, H. J., & Koster, L. J. A. (2017). Recombination in Perovskite Solar Cells: Significance of Grain Boundaries, Interface Traps, and Defect Ions. *ACS Energy Letters*. https://doi.org/10.1021/acsenergylett.7b00236

Shi, Z., & Jayatissa, A. H. (2018). Perovskites-based solar cells: A review of recent progress, materials and processing methods. In *Materials*. https://doi.org/10.3390/ma11050729

Stolterfoht, M., Caprioglio, P., Wolff, C. M., Márquez, J. A., Nordmann, J., Zhang, S., Rothhardt, D., Hörmann, U., Amir, Y., Redinger, A., Kegelmann, L., Zu, F., Albrecht, S., Koch, N., Kirchartz, T., Saliba, M., Unold, T., & Neher, D. (2019). The impact of energy alignment and interfacial recombination on the internal and external open-circuit voltage of perovskite solar cells. *Energy and Environmental Science*, *12*(9), 2778–2788. https://doi.org/10.1039/c9ee02020a

Tai, Q., Tang, K. C., & Yan, F. (2019). Recent progress of inorganic perovskite solar cells. In *Energy and Environmental Science*. https://doi.org/10.1039/c9ee01479a

Tailor, N. K., Abdi-Jalebi, M., Gupta, V., Lu, H., Dar, M. I., Li, G., & Satapathi, S. (2020). Recent progress in morphology optimization in perovskite solar cells. *Journal of Materials Chemistry A*. https://doi.org/10.1039/d0ta00143k

Tang, S., Huang, S., Wilson, G. J., & Ho-Baillie, A. (2020). Progress and Opportunities for Cs Incorporated Perovskite Photovoltaics. In *Trends in Chemistry* (Vol. 2, Issue 7, pp. 638–653). Cell Press. https://doi.org/10.1016/j.trechm.2020.04.002

Ueoka, N., Oku, T., Ohishi, Y., Tanaka, H., Suzuki, A., Sakamoto, H., Yamada, M., Minami, S., & Tsukada, S. (2018). Effects of CsBr addition on the performance of $CH_3NH_3PbI_3$-xClx-based solar cells. *AIP Conference Proceedings*, *1929*(1), 020026. https://doi.org/10.1063/1.5021939

Wali, Q., Iftikhar, F. J., Khan, M. E., Ullah, A., Iqbal, Y., & Jose, R. (2020). Advances in stability of perovskite solar cells. In *Organic Electronics*. https://doi.org/10.1016/j.orgel.2019.105590

Wang, B., Wong, K. Y., Yang, S., & Chen, T. (2016). Crystallinity and defect state engineering in organo-lead halide perovskite for high-efficiency solar cells. *Journal of Materials Chemistry A*, *4*(10), 3806–3812. https://doi.org/10.1039/c5ta09249c

Wang, T., Cheng, Z., Zhou, Y., Liu, H., & Shen, W. (2019). Highly efficient and stable perovskite solar cells via bilateral passivation layers . *Journal of Materials Chemistry A*. https://doi.org/10.1039/c9ta08084h

Wolff, C. M., Zu, F., Paulke, A., Toro, L. P., Koch, N., & Neher, D. (2017). Reduced Interface-Mediated Recombination for High Open-Circuit Voltages in $CH_3NH_3PbI_3$ Solar Cells. *Advanced Materials*, *29*(28). https://doi.org/10.1002/adma.201700159

Xiao, S., Li, Y., Zheng, S., & Yang, S. (2020). Post-treatment techniques for high-performance perovskite solar cells. *MRS Bulletin*, *45*(6), 431–438. https://doi.org/10.1557/mrs.2020.141

Xu, J., Boyd, C. C., Yu, Z. J., Palmstrom, A. F., Witter, D. J., Larson, B. W., France, R. M., Werner, J., Harvey, S. P., Wolf, E. J., Weigand, W., Manzoor, S., A M van Hest, M. F., Berry, J. J., Luther, J. M., Holman, Z. C., & McGehee, M. D. (2020). Triple-halide wide-band gap perovskites with suppressed phase segregation for efficient tandems Downloaded from. In *Science*.

Xu, L., Deng, L. L., Cao, J., Wang, X., Chen, W. Y., & Jiang, Z. (2017). Solution-Processed Cu(In, Ga)(S, $Se)_2$ Nanocrystal as Inorganic Hole-Transporting Material for Efficient and Stable Perovskite Solar Cells. *Nanoscale Research Letters*, *12*(1), 1–8. https://doi.org/10.1186/s11671-017-1933-z

Xue, Y., Tian, J., Wang, H., Xie, H., Zhu, S., Zheng, B., Gao, C., & Liu, X. (2018). Localized incorporation of cesium ions to improve formamidinium lead iodide layers in perovskite

solar cells. *RSC Advances*. https://doi.org/10.1039/c8ra04742a

Yakiangngam, J., Monnoi, S., Ruankham, P., Intaniwet, A., & Choopun, S. (2019). Optimization of a precursor-PbI_2 layer by re-crystallization for efficiency improvement in perovskite solar cells. *Materials Today: Proceedings*, *17*, 1210–1216. https://doi.org/10.1016/j.matpr.2019.05.346

Zeng, W., Liu, X., Guo, X., Niu, Q., Yi, J., Xia, R., Min, Y., Kim, Y., & Kim, H. (2017). Morphology analysis and optimization: Crucial factor determining the performance of perovskite solar cells. In *Molecules* (Vol. 22, Issue 4). MDPI AG. https://doi.org/10.3390/molecules22040520

Zhang, F., & Zhu, K. (2019). Additive Engineering for Efficient and Stable Perovskite Solar Cells. In *Advanced Energy Materials*. https://doi.org/10.1002/aenm.201902579

Zu, F., Amsalem, P., Ralaiarisoa, M., Schultz, T., Schlesinger, R., & Koch, N. (2017). Surface State Density Determines the Energy Level Alignment at Hybrid Perovskite/Electron Acceptors Interfaces. *ACS Applied Materials and Interfaces*, *9*(47), 41546–41552. https://doi.org/10.1021/acsami.7b12586

CHAPTER SIX

EFFECTS OF POLYETHYLENE OXIDE POLYMER ON THE PHOTOPHYSICAL PROPERTIES AND OPERATIONAL STABILITY OF FA-RICH PEROVSKITE SOLAR CELLS

6.1 Introduction

This chapter presents the results on the use of polyethylene oxide (PEO) polymer as an additive in perovskite film to achieve synergetic improvement in the PCE and stability of PSC. The chapter also highlights the important role of PEO in tuning the optoelectronic properties of perovskite films and the overall photo-physical properties of PSC while boosting its resistance to light- and moisture-induced degradation.

Perovskite solar cell (PSC) is a nascent low-cost solar cell technology that has caused a paradigm shift in the field of photovoltaics because of its potential for solar harnessing systems with low energy payback times (Bhat et al., 2018; Ibn-Mohammed et al., 2017; Kamat, 2013). The superior photovoltaic (PV) characteristics of PSCs originate from the excellent optoelectronic properties of their organo-metallic halide perovskite-based photoactive layers (Chen et al., 2015; Manser et al., 2016). Motivated by these properties, multi-faceted research efforts have been expended towards improving their processing conditions, device architecture, and material properties (Roy et al., 2020; Wu et al., 2021). This has led to a rapid evolution in their power conversion efficiencies (PCEs) to the current recorded value that rivals the highest recorded value for the mature crystalline silicon-based PV technology (Gai et al., 2019).

Unlike the conventional crystalline silicon-based PV technologies, PSC is still faced with the problem of degradation when exposed to the conditions in the environment. The ongoing research efforts are directed towards addressing this challenge while trying to push the PCE higher (Xiang et al., 2021). Among the several approaches that have been explored, those that aim at engineering both the AL and the interface with the CTLs have been shown to be instrumental in achieving synergetic improvement in the PCE and the long-term stability in PSCs (Azmi et al., 2018; Koech et al., 2021; Lyu et al., 2021; Yang & Park, 2021). The improvement arises from the suppression of defects in the bulk of the perovskite film and the interface with the CTLs that are usually difficult to avoid due to the solution-based processing of perovskite films (Lee et al., 2018; Wang et al., 2018). These defects not only act as recombination centers but they also provide degradation pathways in perovskite films thus contributing to the loss of charge carriers and performance degradation (Lanzetta et al., 2020; Leijtens et al., 2016). Therefore, in order to suppress the power loss and degradation mechanisms in PSCs, in-situ morphological control in the AL is a quintessential step (Brakkee & Williams, 2020; Wang et al., 2018; Zhao et al., 2018).

Additive engineering can achieve this goal as well as modulate the interfacial properties of the entire PSCs (Wang et al., 2021; Zhang et al., 2021). Polymeric additives incorporated into perovskite precursors have been shown to aid the homogeneous nucleation and crystallization of perovskite films leading to the formation of large perovskite grains with reduced grain boundaries (Bi et al., 2016; Mei et al., 2021). Furthermore, the functional groups present in polymeric compounds enable them to coordinate and cross-link well with the uncoordinated metal ions and other atomic species in perovskite film thus reducing surface defects, increasing the charge carrier lifetime, reducing ion migration, and suppressing

moisture ingress in perovskite films (Bi et al., 2016; Han et al., 2019; Qi et al., 2014). Polymers can also modulate the interfacial barriers at the interfaces between the AL and CTLs. In particular, ethylene-based polymeric additives such as polyethylene oxide (PEO) not only act as cross-linking and crystallization inhibition agents but they also tune the interface energetics, suppress the ion migration, and improve the tolerance of perovskite films to degradation agents (Arya & Sharma, 2017; Bi et al., 2016; Silva et al., 2020; Wang et al., 2020). These properties of PEO have recently been used to modify both the perovskite bulk and the interface properties in PSC leading to improvement in PCE and stability (Kim et al., 2018; Lee et al., 2019; Qin et al., 2019). Although these studies have revealed the important role of PEO in the performance of PSCs, very few studies have focussed on the impact of PEO on the microstructure, electronic band structure as well as the charge carrier, and the excited state dynamics in FA-rich mixed halide perovskite films.

In this chapter, we used a long-chain PEO polymer to passivate defects in the perovskite film, modulate the interfacial energetics and improve the PV performance parameters of a regular planar PSC. Unlike previous studies, the PEO additive in this work was incorporated on the organic components of perovskite precursors before spin coating on lead iodide to form perovskite thin films. With this, large-grained perovskite films with improved optoelectronic properties were formed, enabling the fabricated PEO-modified PSC to achieve a better PCE and stability when compared to the control device. The champion device containing 5 wt% of PEO showed the highest PCE of 18.03% with improved resistance to light- and moisture-induced degradation in performance. This study provides important information on the role of PEO additives in the fabrication of efficient and stable PSCs.

6.2 Materials and methods

6.2.1 Materials

Unless otherwise stated, most of the materials used in this work were purchased from Sigma Aldrich and used as received. Apart from Polyethylene Oxide (PEO) polymer, all the other materials have been listed in chapter four.

6.2.2 Materials processing

After sequential cleaning of pre-patterned FTO-coated glass substrate in a detergent, acetone, and IPA, an ETL was formed from mixed TiO_2 and SnO_2 precursor solutions as per the procedure described in the preceding chapters. The perovskite AL was formed on the ETL via a two-step spin-coating process where the lead (II) Iodide (PbI_2) was first spin-coated followed by the organic components that were mixed with PEO in different weight proportions. The weight proportion of PEO in the organic mixed precursor solution was varied from 0 wt% (control), 2 wt%, 5 wt%, and 10 wt% so as to study the variation of the properties of the perovskite film with PEO proportion. After forming the perovskite film, a Spiro-OMeTAD-based HTL was deposited on it via spin-coating technique. The gold electrode was then thermally evaporated on the HTL to get a complete planar PSC.

6.2.3 Materials characterization

The morphological and structural features of the prepared perovskite films were respectively studied using a field emission scanning electron microscope (JEOL JSM-700F, Hollingsworth & Vose, MA, USA) and X-ray diffractometer (Malvern PANalytical, Westborough, MA, USA). The optical properties and the charge carrier dynamics of the films were probed using techniques such as ultraviolet-visible spectroscopy, photoluminescence, ultrafast transient absorption spectroscopy, x-ray photoelectron spectroscopy, and ultraviolet

photoelectron spectroscopy. The transient absorption spectroscopy (TAS) measurements of perovskite films were done using a HARPIA-TA ultrafast transient absorption spectrometer. In the measurement, 1030nm femtosecond pulses from a 40W Ytterbium laser (Carbide, Light Conversion) generated probe white light through a sapphire crystal. A 10W of the laser was coupled to an OPA (Orpheus, Light Conversion) to generate 400nm pump pulses with a fluence of 0.51 J/m^2. Pump and probe signals, with 1mm spot size were focused on the sample whereupon the difference in absorption was detected by an Andor spectrograph and the difference in absorption; for a single wavelength for every delay time; was detected by a Si photodiode. The J-V, EIS, and EQE characteristics of the fabricated PSC device were studied on a device area of 0.05 cm^2 using a Keithley source meter, a potentiostat (SP-300, BioLogic Instrument), and a QuantX-300 quantum efficiency measurement system respectively.

6.3 Results and discussion

6.3.1 Effect of PEO on microstructural properties of perovskite film

Controlling the morphology of perovskite film is an important route to obtain large and densely packed grains with reduced defect densities that will enable the fabrication of PSCs with improved performance characteristics (Tailor et al., 2020). The PEO additive incorporated into the perovskite organic precursor solution was able to tune the morphology of the film as can be seen in the SEM micrographs of Figure 6.1 (a)-(d). It is evident that the morphology of the perovskite films improves as the proportion of PEO increases up to 5 wt%. Thereafter, a slight change in the film morphology is observed. The perovskite film containing 10 wt% of PEO appears less compact and the PEO is seen to occupy the grain boundaries.

An analysis of the grain sizes of the different films reveals that the average grain size increased with PEO content up to 5 wt% and a slight decrease is observed when the

percentage weight of PEO increased to 10 wt%. Specifically, the grain size increased from an average value of 0.8 ± 0.4 μm for the pure perovskite film to 1.3 ± 0.5 μm for the perovskite film containing 5 wt% of PEO and later decreased to about 1.2 ± 0.5 μm for the film with 10% PEO. Similarly, the cross-sectional SEM images of Figure 6.2 (a)-(d) indicate that the grain size increased longitudinally as the proportion of PEO in perovskite film increased up to 5 wt%. The available grain boundary areas are therefore greatly reduced when 5 wt.% of PEO is introduced into the perovskite film. This reduces the non-radiative recombination and charge carrier trapping centers in the AL which is important in PCE improvement in PSCs.

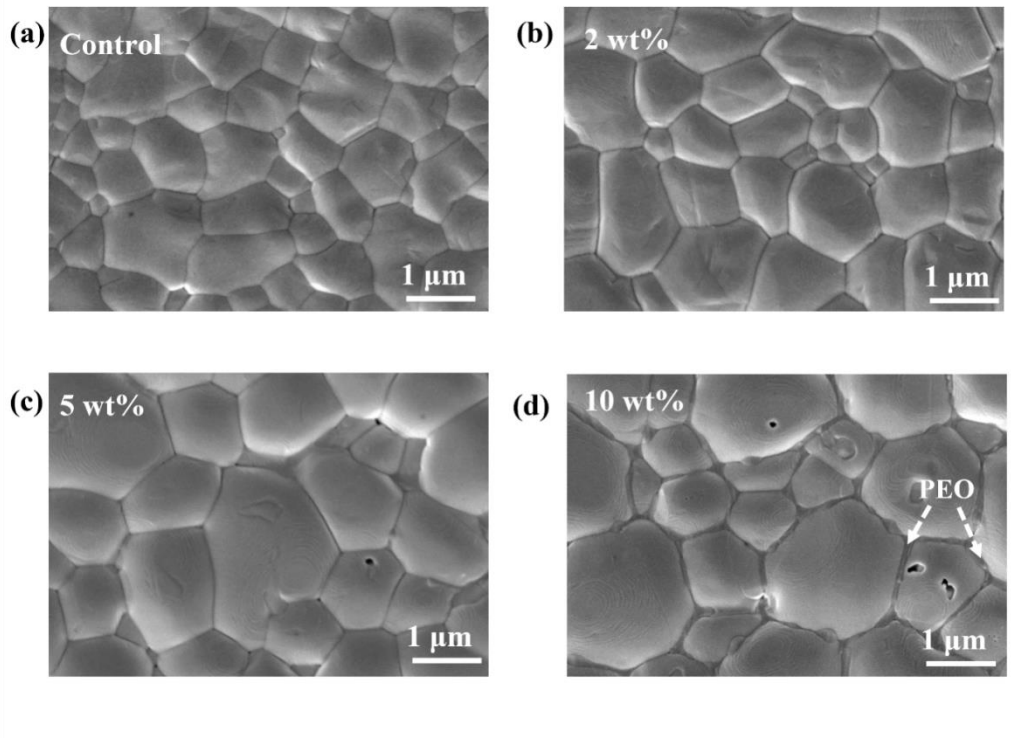

Figure 6.1: SEM top surface images of perovskite films with (a) 0 (b) 2 (c) 5 and (d) 10 wt% of PEO

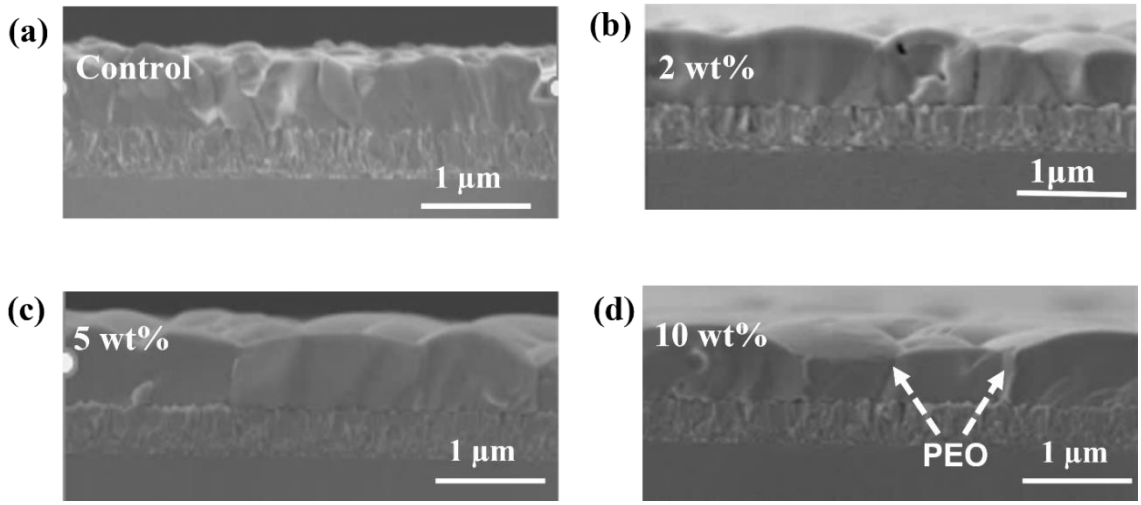

Figure 6.2: SEM cross-sectional images of perovskite films with (a) 0 (b) 2 (c) 5 and (d) 10 wt% of PEO

Additives incorporated into perovskite films can influence the nucleation and growth kinetics of the crystals thus affecting their microstructural properties. Some additives can cause metal-halogen-metal bond alteration and phase transformation in perovskite films through the filling of lattice vacancies and changes in the unit cell dimension (Soe et al., 2016). In the case of the PEO additive, the XRD analysis of the perovskite films with and without PEO reveals that all the films crystallized in the cubic perovskite phase as indicated by their preferred orientation along the planes (110) and (220) in the XRD spectra of Figure 6.3 (a). This means that PEO did not alter the phase of the perovskite film despite the morphological differences observed from the SEM images in Figure 6.1. However, the PEO additive led to a reduction in the crystallinity of the perovskite film as confirmed by the gradual decrease in the intensity of the major peak at (110) as the weight proportion of PEO in the film increased. We also noted that PEO did not alter the crystal lattice parameter of the perovskite films since the position of the major peak did not show any observable shift.

Therefore, the PEO additive may have interacted with the perovskite to form new chemical bonds with uncoordinated ionic species without necessarily changing its crystal structure.

6.3.2 Interaction of PEO with perovskite film

To obtain more information on the interaction of PEO with the perovskite films, we carried out FTIR studies as a function of the weight proportion of PEO in the film. The FTIR spectra; as seen in Figure 6.3 (b); show the emergence of new peaks in the PEO-modified perovskite films at wave number (k) values in the range 1517-1528 cm^{-1}, ascribable to the C–N stretch vibrational mode. The peak appears at k value of 1528 cm^{-1} for the film containing 2 wt% of PEO and red-shifts to 1517 cm^{-1} for the film with 10 wt% of PEO. Similarly, the peak signature for C=O stretch; appearing at 1711 cm^{-1}; in the control film redshifts to 1700 cm^{-1} for perovskite with 10 wt% of PEO. This redshift in the position of the peaks is an indication of the coordination effects between functional groups in PEO with the perovskite crystals which may affect the intermolecular bond strengths. The observation has been attributed; in prior work; to the weakening of the C=O double bond due to the coordination effect from the oxygen atom in the PEO (Shi et al., 2020; Wang et al., 2020). Moreover, the same effect can arise from electron delocalization from the carbonyl (C=O) group due to the formation of Lewis base-acid adduct between the oxygen in the PEO and PbI_2 in the perovskite (Zhao et al., 2020).

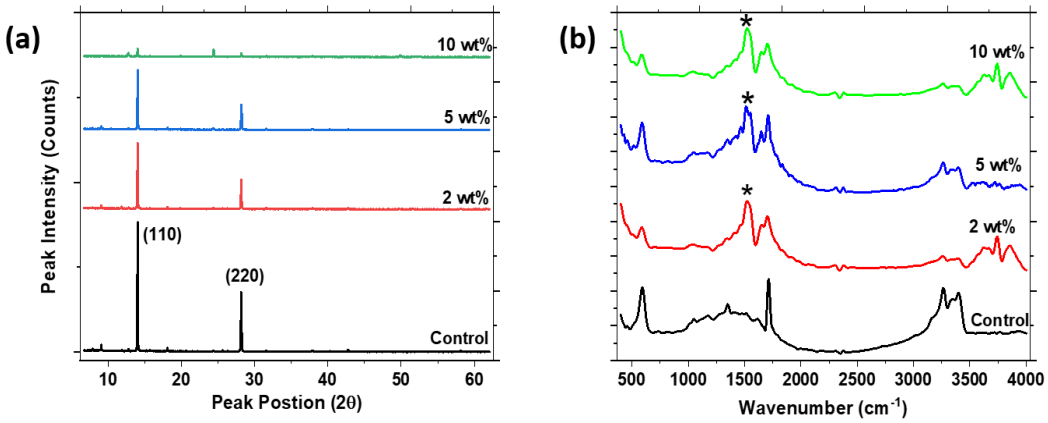

Figure 6.3: (a) XRD patterns, and (b) FTIR spectra of the perovskite films at different weight proportions of PEO

6.3.3 Effect of PEO on the surface chemistry of perovskite films

Due to the possible interaction of PEO with uncoordinated atomic species in perovskite film, the surface chemical state of the film may change when PEO is introduced into it. To find out whether the PEO loading influenced the surface chemistry of the perovskite films, we probed the variation in the surface characteristics of the films using XPS. The high-resolution XP spectra of the perovskite film; as a function of the percentage weight of PEO; are presented in Figure 6.4. It is seen that the XP spectra of all the films are nearly identical except for the additional features at binding energies of ~286 eV and ~532 eV (shaded blue) that are visible in the XP spectra of perovskite films modified with PEO. These features are those of the O 1s and C 1s core-level peaks which can be ascribed to the PEO additive. The presence of these features in the PEO-modified perovskite films strongly reaffirms the interaction of PEO with the perovskite as earlier revealed by FTIR results of Figure 6.3 (b). The features shaded in red are those of the adventitious and formamidinium

carbon originating from the perovskite itself while the ones shaded in orange are those of reduced lead which are indicative of beam damage in the films.

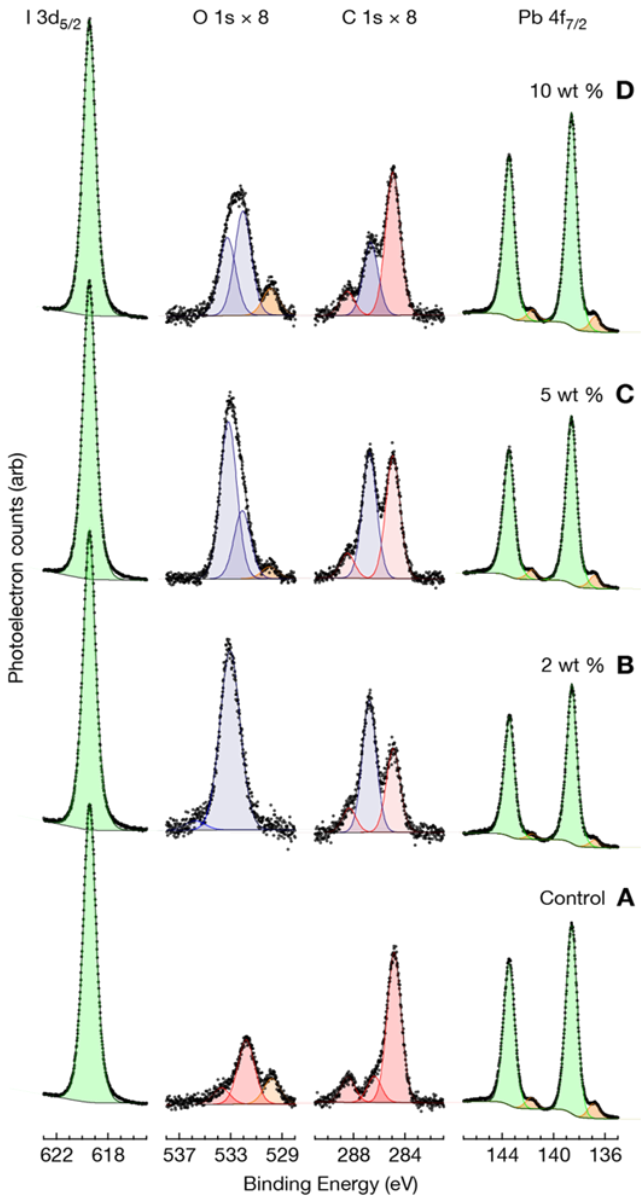

Figure 6.4: High-resolution XP spectra of perovskite films at different wt% of PEO

6.3.4 Effect of PEO on the optical properties of FA-rich perovskite film

The optical response of perovskite photoactive material is an important aspect in its PV application as it determines the photon absorption and photo-generation processes which

are the backbone of solar to electricity conversion (Ball et al., 2015). Most lead-based perovskite films have their light absorption edge around 800 nm which can either be extended or reduced with the incorporation of additives. We studied the optical response of the FA-rich perovskite film as a function of PEO wt% and the results are displayed in Figure 6.5 (a)-(d). The optical absorption properties of the perovskite films (Figure 6.5 (a)) indicate that the absorbance of the films in the visible region improved with the wt% of PEO up to 5 % and decreased thereafter. The decrease is attributed to the microstructural changes that were observed in the films when PEO proportion is increased beyond 5 wt% as shown in the SEM images in Figure 6.1.

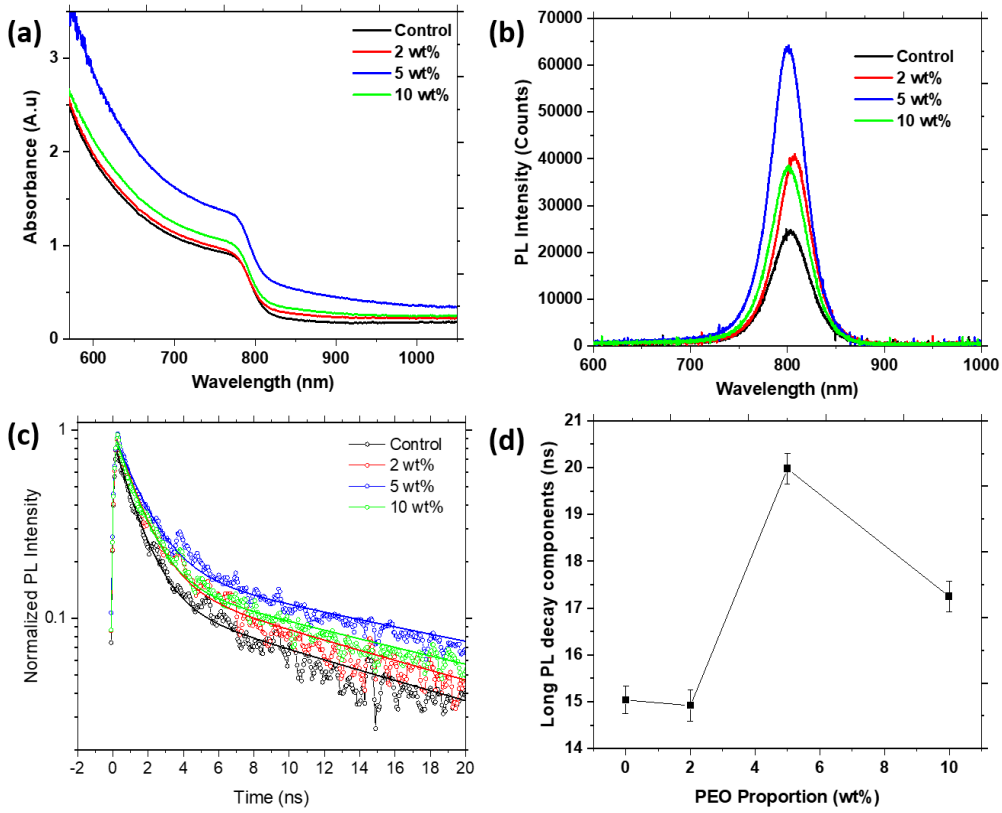

Figure 6.5: (a) UV-Vis spectra (b) steady stead PL (c) TRPL and, (d) long decay lifetime as a function of wt % of PEO (Fluence 28.3 J/m^2)

Photoluminescence (PL) properties and charge carrier lifetimes of the FA-rich perovskite films with and without PEO were studied using steady-state PL and time-resolved PL (TRPL) (Figure 6.5(b)-(c)). Detailed interpretation of PL and TRPL of perovskite films and devices is non-trivial and requires consideration of multiple interdependent processes such as Auger recombination, bimolecular recombination, trap-assisted Shockley-Read-Hall recombination, photon recycling, and carrier diffusion within the films and across the interfaces (Baloch et al., 2018; Kirchartz et al., 2020; Peán et al., 2020). Here, our goal is limited to elucidating the impact of PEO on carrier lifetime in FA-rich perovskite films. The results of the PL studies (Figure 6.5 (b)) indicate that all the perovskite films exhibit a strong band edge emission peak at ~ 1.55 eV (800 nm) with a negligible shift as PEO content increases. We also observe that at the same excitation conditions (485 nm, 28.3 J/m^2 & 50 ps laser pulses with repletion rate of 10 kHz), PL intensity increases with increasing PEO content up to 5 wt% and decreases at 10 wt%. The highest PL intensity (~ 3 times stronger compared to control) observed in the film with 5wt% of PEO likely results from increased optical absorption of the excitation (Figure 6.5(a)) as well as from a reduction in non-radiative defect-mediated recombination. This agrees well with its optimized morphological properties such as larger, more uniform grains, seen in the SEM micrographs in Figure 6.1(c). The TRPL measurements show kinetics with sub-30 ns decay times (Figure 6.5(c)). We find that we can describe them with a bi-exponential decay model to elucidate the influence of PEO. Internal radiative recombination lifetime in perovskites is typically significantly longer than the observed kinetics, often reaching tens of microseconds (Brenes et al., 2017), allowing us to tentatively ascribe the fast and slow (long) decay components to competing non-radiative recombination at bulk and surface trap states, respectively (Xing et al., 2014). We find that the fast decay component,

with a time of constant ~ 1.1 ns, is unchanged by the PEO addition. On the other hand, the long PL decay component becomes slower with an increase in PEO content up until the 5 wt% (Figure 6.5(d)). This is possibly driven by the increase in grain size and the corresponding reduction of the surface to volume ratio which reduces the surface trap recombination rate. At 10 wt%, the surface trap recombination rate increases again as PEO begins to accumulate at the grain boundaries as can be seen in Figure 6.1(d). The time constant for the long PL decay component in perovskite films was plotted as a function of the weight proportion of PEO (Figure 6.5(d)) where it becomes clear that the film with 5 wt% of PEO exhibited the least surface trap recombination rate. This means that, at this proportion, PEO was able to passivate defects on the surface of perovskite film.

To obtain more insights into the optical properties of perovskite films, we studied the excited state dynamics of the FA-rich perovskite films over sub-picosecond to nanoseconds time scales by carrying out ultrafast TAS (Figure 6.6). Figure 6.6 (a) shows TA spectra of the different perovskite films in the delay time range of 0.4 ps – 10 μs following excitation with 50 fs, 485 nm pulse with 0.51 J/m^2 fluence. Transient absorption spectra exhibit a negative band in the 1.61-1.63 eV range attributed to the bleaching of the absorption band edge due to the valence band depopulation (Dar et al., 2017; Serpetzoglou et al., 2017; Ugur et al., 2019; Wang et al., 2014). It is also seen that the PB peak shows a small redshift with increasing pump delay times (Figure 6.6 (b)). It also shifts from 1.617 eV to 1.633 eV when the proportion of PEO is increased from 0 to 5 wt% and thereafter, it shifts to a lower value of 1.631 eV for a weight proportion of 10 %. The shifts may be caused by the morphological changes in the film or intra-band excitonic states within the bandgap of the film (Yang et al.,

2015). Positive transient absorption bands on both sides of the bleach arise due to the excitation-induced changes in the refractive index.

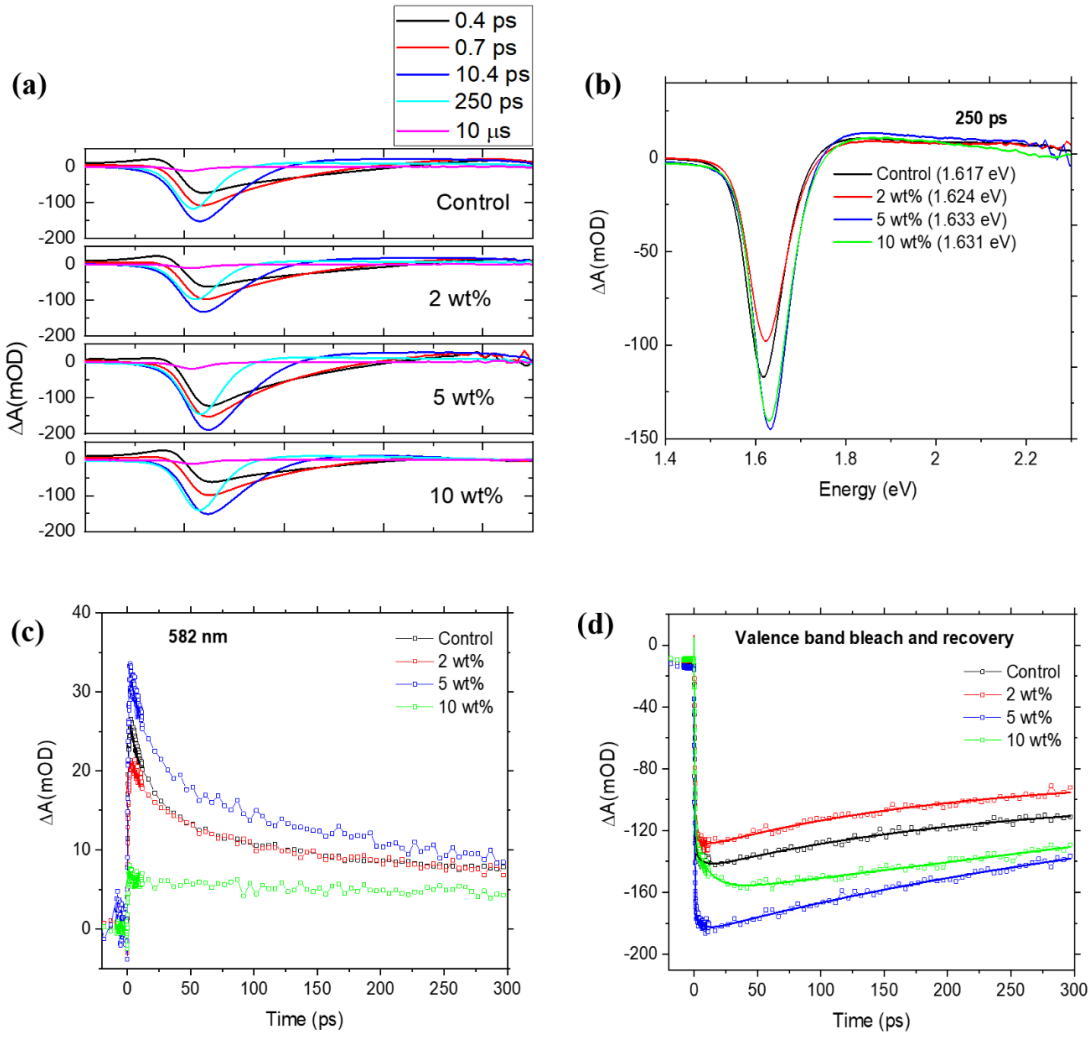

Figure 6.6: (a) Transient absorption dynamics of the perovskite films at (a) different delay times and (b) fixed delay time (c) Decay kinetics of absorption edge bleach (d) Bleach recovery kinetics

As Figure 6.6 (b) shows, transient absorption spectra at a fixed pump-probe delay time (here shown at 250 ps) are qualitatively similar in all the films. However, decay kinetics of the

absorption edge bleach show important differences (Figure 6.6 (c)). For all the films, the initial onset of the absorption edge bleach occurs on ~ 0.5 ps time scale as the hot photo-injected carriers thermalize to the band edges. However, in the film with 10 wt% PEO content, absorption bleach continues to increase in magnitude beyond the sub-picosecond time scale, with the time constant of 12 ± 2 ps. We recall here that SEM images clearly show that at this high loading, a considerable fraction of PEO accumulates at the perovskite grain boundaries (Figure 6.1 (d)). As PEO itself has considerable optical absorption at 485 nm (Elimat et al., 2010), we tentatively attribute this slow build-up of perovskite valence band depopulation by injection of photoexcited holes from PEO to perovskite.

Bleach recovery kinetics provides additional information on the optical behavior of the perovskite films (Figure 6.6(d)). In films with PEO content up to 5 wt%, recovery is biexponential over the 300 ps experimental time window, with a slower component that cannot be resolved by TA but likely lasts for microseconds. In fact, the bleach is not fully recovered on the time scale given by the excitation and probe repetition rate of 100 kHz (10 μs), as shown in transient absorption spectra in Figure 6.6 (a). The fast recovery component is similar in all three films at 5-7 ps. The slower component is ~ 200 ps for the control (0 wt%) and 2 wt% films, but it slows down to ~ 450 ps in the optimal performance film with 5 wt% PEO and recovers even slower in phase-segregated film (10 wt%).

Through its interaction with the uncoordinated ionic species in the perovskite film, PEO can induce surface dipole formation or cause band bending between the bulk and surface of the perovskite films which will influence their electronic structure and the dynamics of charge carriers (Daboczi et al., 2021; Wong et al., 2021). To develop a deeper understanding of the influence of PEO on the electronic band structure of the different FA-rich perovskite

films, we carried out UPS studies on the films containing varied weight proportions of PEO. Figure 6.7 (a) shows the variation of the surface work function (Φ_{WF}) of the perovskite films with the wt% of PEO. We can see clearly that the value of Φ_{WF} decreases as the PEO proportion increases up to 5 wt% where it begins to show a slight increase. The decrease in Φ_{WF} is an indication of an upward shift in the position of the Fermi level (E_f) which may arise due to an increase in the donor density (n-type conductivity) resulting from the additional electrons from the electron-rich oxygen in PEO. The variation in Φ_{WF} with the weight proportion of PEO can have some influence on the interfacial charge transport between the AL and ETL/HTL in the fabricated planar PSC (Figure 6.7 (b)) which will affect its PCE.

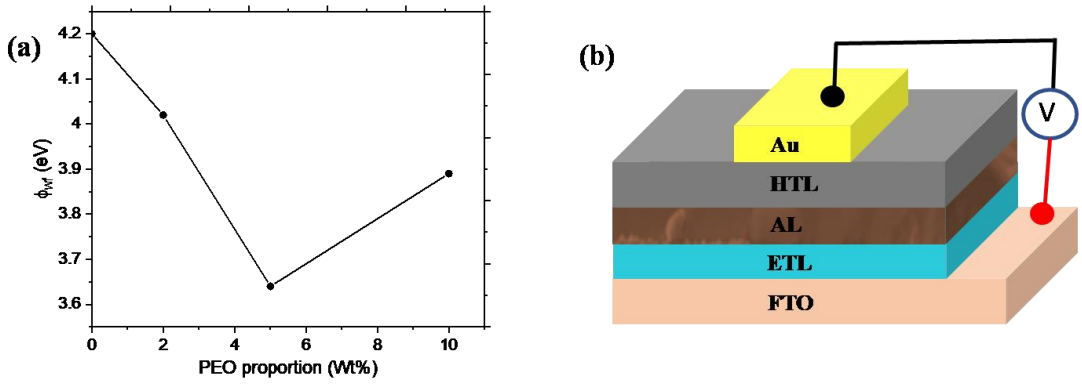

Figure 6.7: (a) Work function of perovskite films as a function of the weight proportions of PEO (b) Architecture of the fabricated PSC device

6.3.5 Performance characteristics of the PSC

Photovoltaic performance characteristics of PSCs are influenced by several factors which include the light absorption and charge transport properties of the photoactive layer. These factors influence the efficiency of charge carrier generation and collection which consequently affect the current density and photovoltage of the resulting PSC device. To

investigate the effect of PEO on the photovoltaic performance characteristics of PSC, we fabricated a series of planar PSC devices with varying weight proportions of PEO in the AL. We then studied the variation of the PV, electrochemical impedance, and charge carrier collection properties of the different PSCs with the proportion of PEO in the AL. Figure 6.8 (a-d) shows the J-V curves, EQE curves, and EIS of the champion devices for both the PEO-modified and the control PSCs. As depicted from Figure 6.8 (a), the V_{oc} and J_{sc} values for the champion devices were slightly higher for the PEO-modified device when compared to those of the control device. The PCE for the champion device modified with 5 wt% of PEO in the AL was 18.03% while that for the control device was 17.34 %. To assess the overall effect of the PEO additive on the PV performance parameters of the fabricated FA-Rich PSC, several devices with and without PEO were fabricated under the same conditions. Figure 6.8(b) shows the statistical analysis of the PCEs for a set of 29 devices with and without PEO. As can be seen from the figure, the peak of the normal distribution curve for the PEO-modified PSC devices is at a higher PCE value than that of the control device, an indication that the PEO-modified device exhibited better average PCE than the control device. The mean value of the PCE was 9.07% higher for the device in which 5 wt% of PEO was incorporated into its AL. A clear picture of the variation in the mean values of the PV parameters with the weight proportion of PEO is shown in Table 6.1. The variation in these parameters with the proportion of PEO in the AL can partly be attributed to the defect passivation and electronic band structure modification effects of PEO as revealed by the SEM and UPS studies. The charge carrier collection efficiencies of the PSC devices at each wavelength are shown by the EQE curves of Figure 6.8 (c). The EQE values of PSC with 5 wt% of PEO are generally higher than those of the control device at all the wavelengths under consideration. This means

that the PEO-modified device has better charge carrier collection efficiency than the control device.

Table 6.1: PV performance parameters for PSCs with different PEO content in the AL

Wt% of PEO	**PCE**	**J_{sc}**	**V_{oc}**	**FF**
0	17.34 (14.98 ± 1.29)	24.54 (23.15 ± 0.77)	0.992 (0.929 ± 0.04)	76.60 (69.76 ± 5.75)
2	16.57 (15.56 ± 0.84)	23.71 (23.0 ± 0.84)	0.992 (0.966 ± 0.03)	73.10 (70.05 ± 3.12)
5	18.03 (16.34 ± 0.86)	24.52 (23.64 ± 0.56)	1.01 (0.970 ± 0.02)	76.15 (71.25 ± 2.87)
10	14.5 (13.12 ± 2.07)	22.61 (21.45 ± 1.48)	0.992 (0.963 ± 0.05)	66.68 (63.12 ± 4.65)

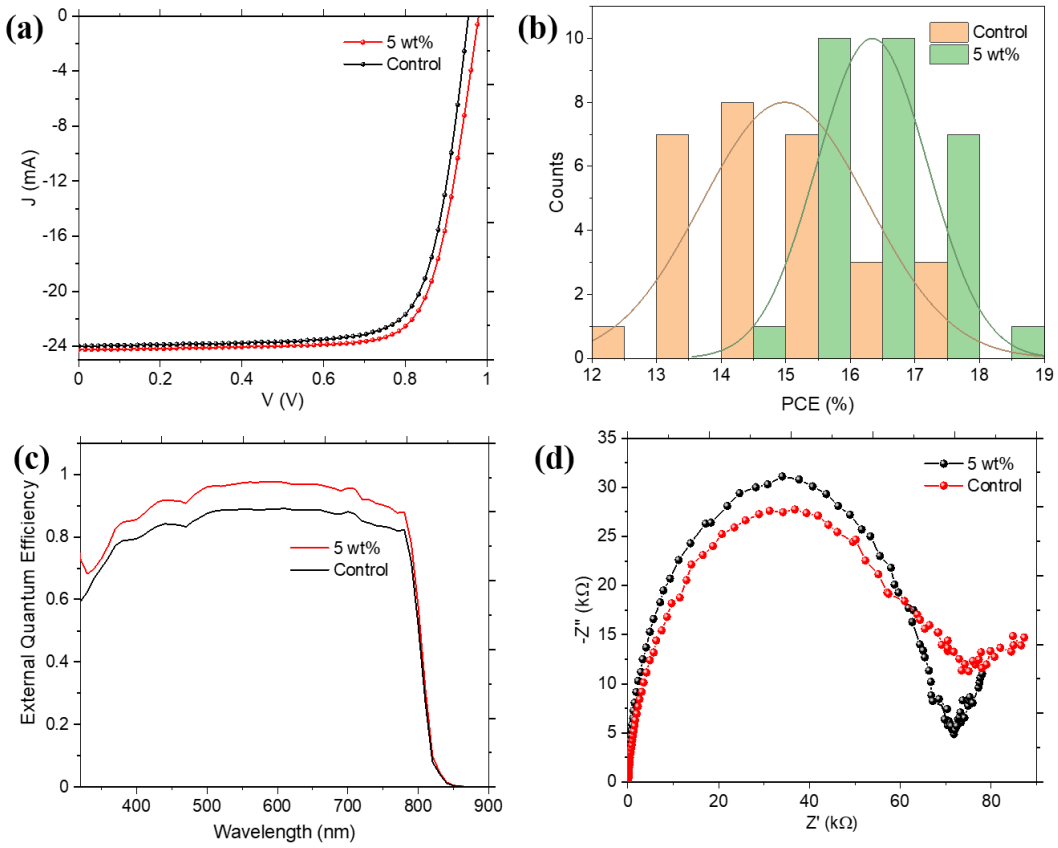

Figure 6.8: Comparison of (a) J-V curves, (b) Statistical distribution of the PCE, (c) EQE, and (d) Nyquist plot for the control and PEO-modified PSC devices

To find out the reason behind the observed differences in the charge carrier collection efficiencies of the PSC devices, we analyzed their electrochemical impedance characteristics in the dark. The results; expressed in the form of a Nyquist plot (Figure 6.8(d)); indicate that the device with the PEO-modified AL had slightly higher recombination resistance and lower series resistance when compared to the control device. This means that the loss of charge carriers via recombination is smaller in the PEO-modified device in comparison with the control device, justifying the observed higher EQE in the device.

To understand the effect of PEO additive on the operational stability of PSCs, we analyzed the variation of the PCE of the control and PEO-containing devices under continuous illumination and when stored under ambient conditions without any form of encapsulation. Figure 6.9 (a-b) shows the temporal variation in the normalized PCE of the devices under continuous illumination and storage in humid conditions. It is obvious from Figure 6.9(a) that the PEO-modified device had its normalized PCE remaining almost constant during the 2500 seconds of continuous illumination while the normalized PCE for the control device showed a continuous decrease after about 500 seconds. Furthermore, it is seen in Figure 6.9 (b) that the PEO-modified device was able to retain about 80 % of its initial PCE for up to 140 hrs of storage in an un-encapsulated state while that of the control device dropped below 80 % after just about 85 hrs. These results indicate that the PEO additive improves the light- and moisture-induced degradation resistance in FA-rich PSCs.

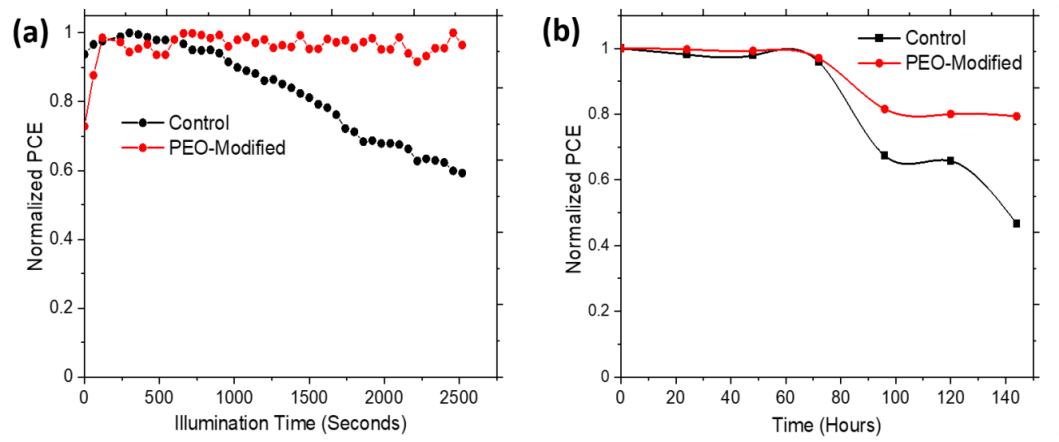

Figure 6.9: Stability of PSCs under (a) Continuous illumination (b) Storage in ambient conditions

6.4 **Summary and concluding remarks**

The incorporation of the right proportion of PEO into the perovskite layer improves the optoelectronic properties of the film and modulates the interfacial energetics in PSCs. Consequently, the light absorption and charge carrier dynamics in PSC are enhanced leading to an improvement in the photocurrent and the PCE. A planar PSC whose AL was modified with 5wt% of PEO demonstrated better PCE and operational stability relative to the control device fabricated under the same conditions. The PCE of the champion device with 5 wt% in its AL was 18.03% while that of the control device was 17.34%. The higher PCE in the PEO-modified device originated from its reduced recombination that led to better charge carrier collection efficiency as revealed by the EIS and EQE studies. The PEO-modified device was able to retain over 80 % of its initial PCE after being stored for about 140 hrs under humid conditions (average relative humidity of 62.5±3.25 %) without encapsulation.

6.5 References

Arya, A., & Sharma, A. L. (2017). Insights into the use of polyethylene oxide in energy storage/conversion devices: a critical review. *Journal of Physics D: Applied Physics*, *50*(44), 443002. https://doi.org/10.1088/1361-6463/AA8675

Azmi, R., Lee, C. L., Jung, I. H., & Jang, S.-Y. (2018). Simultaneous Improvement in Efficiency and Stability of Low-Temperature-Processed Perovskite Solar Cells by Interfacial Control. *Advanced Energy Materials*, *8*(14), 1702934. https://doi.org/10.1002/AENM.201702934

Ball, J. M., Stranks, S. D., Hörantner, M. T., Hüttner, S., Zhang, W., Crossland, E. J. W., Ramirez, I., Riede, M., Johnston, M. B., Friend, R. H., & Snaith, H. J. (2015). Optical properties and limiting photocurrent of thin-film perovskite solar cells. *Energy and Environmental Science*. https://doi.org/10.1039/c4ee03224a

Bhat, A., Dhamaniya, B. P., Chhillar, P., Korukonda, T. B., Rawat, G., & Pathak, S. K. (2018). Analysing the Prospects of Perovskite Solar Cells within the Purview of Recent Scientific Advancements. *Crystals 2018, Vol. 8, Page 242*, *8*(6), 242. https://doi.org/10.3390/CRYST8060242

Bi, D., Yi, C., Luo, J., Décoppet, J. D., Zhang, F., Zakeeruddin, S. M., Li, X., Hagfeldt, A., & Grätzel, M. (2016). Polymer-templated nucleation and crystal growth of perovskite films for solar cells with efficiency greater than 21%. *Nature Energy 2016 1:10*, *1*(10), 1–5. https://doi.org/10.1038/nenergy.2016.142

Brakkee, R., & Williams, R. M. (2020). Minimizing Defect States in Lead Halide Perovskite Solar Cell Materials. *Applied Sciences 2020, Vol. 10, Page 3061*, *10*(9), 3061. https://doi.org/10.3390/APP10093061

Chen, J., Zhou, S., Jin, S., Li, H., & Zhai, T. (2015). Crystal organometal halide perovskites with promising optoelectronic applications. *Journal of Materials Chemistry C*, *4*(1), 11–27. https://doi.org/10.1039/C5TC03417E

Daboczi, M., Ratnasingham, S. R., Mohan, L., Pu, C., Hamilton, I., Chin, Y. C., McLachlan, M. A., & Kim, J. S. (2021). Optimal Interfacial Band Bending Achieved by Fine Energy Level Tuning in Mixed-Halide Perovskite Solar Cells. *ACS Energy Letters*, *6*(11), 3970–3981. https://doi.org/10.1021/ACSENERGYLETT.1C02044/SUPPL_FILE/NZ1C02044_SI_001.PDF

Gai, C., Wang, J., Wang, Y., & Li, J. (2019). The Low-Dimensional Three-Dimensional Tin Halide Perovskite: Film Characterization and Device Performance. *Energies 2020, Vol. 13, Page 2*, *13*(1), 2. https://doi.org/10.3390/EN13010002

Han, T. H., Lee, J. W., Choi, C., Tan, S., Lee, C., Zhao, Y., Dai, Z., De Marco, N., Lee, S. J.,

Bae, S. H., Yuan, Y., Lee, H. M., Huang, Y., & Yang, Y. (2019). Perovskite-polymer composite cross-linker approach for highly-stable and efficient perovskite solar cells. *Nature Communications 2019 10:1*, *10*(1), 1–10. https://doi.org/10.1038/s41467-019-08455-z

Ibn-Mohammed, T., Koh, S. C. L., Reaney, I. M., Acquaye, A., Schileo, G., Mustapha, K. B., & Greenough, R. (2017). Perovskite solar cells: An integrated hybrid lifecycle assessment and review in comparison with other photovoltaic technologies. *Renewable and Sustainable Energy Reviews*, *80*, 1321–1344. https://doi.org/10.1016/J.RSER.2017.05.095

Kamat, P. V. (2013). Evolution of perovskite photovoltaics and decrease in energy payback time. *Journal of Physical Chemistry Letters*, *4*(21), 3733–3734. https://doi.org/10.1021/JZ402141S

Kim, M., Motti, S. G., Sorrentino, R., & Petrozza, A. (2018). Enhanced solar cell stability by hygroscopic polymer passivation of metal halide perovskite thin film. *Energy & Environmental Science*, *11*(9), 2609–2619. https://doi.org/10.1039/C8EE01101J

Koech, R. K., Ichwani, R., Martin, J. L., Oyewole, D. O., Oyelade, O. V., Olanrewaju, Y. A., Sanni, D. M., Adeniji, S. A., Grimm, R. L., Bello, A., Oyewole, O. K., Ntsoenzok, E., & Soboyejo, W. O. (2021). A study of the effects of a thermally evaporated nanoscale CsBr layer on the optoelectronic properties and stability of formamidinium-rich perovskite solar cells. *AIP Advances*, *11*(9), 095112. https://doi.org/10.1063/5.0064398

Lanzetta, L., Aristidou, N., & Haque, S. A. (2020). Stability of Lead and Tin Halide Perovskites: The Link between Defects and Degradation. *The Journal of Physical Chemistry Letters*, *11*(2), 574–585. https://doi.org/10.1021/ACS.JPCLETT.9B02191

Lee, J. W., Bae, S. H., De Marco, N., Hsieh, Y. T., Dai, Z., & Yang, Y. (2018). The role of grain boundaries in perovskite solar cells. *Materials Today Energy*, *7*, 149–160. https://doi.org/10.1016/J.MTENER.2017.07.014

Lee, S., Cho, J. S., & Kang, D. W. (2019). Perovskite/polyethylene oxide composites: Toward perovskite solar cells without anti-solvent treatment. *Ceramics International*, *45*(17), 23399–23405. https://doi.org/10.1016/J.CERAMINT.2019.08.042

Lyu, M., Park, S., Lee, H., Ma, B. S., Park, S. H., Hong, K. H., Kim, H., Kim, T. S., Noh, J. H., Son, H. J., & Park, N. G. (2021). Simultaneous Enhanced Efficiency and Stability of Perovskite Solar Cells Using Adhesive Fluorinated Polymer Interfacial Material. *ACS Applied Materials & Interfaces*, *13*(30), 35595–35605. https://doi.org/10.1021/ACSAMI.1C05822

Manser, J. S., Christians, J. A., & Kamat, P. V. (2016). Intriguing Optoelectronic Properties of Metal Halide Perovskites. In *Chemical Reviews*. https://doi.org/10.1021/acs.chemrev.6b00136

Mei, Y., Sun, M., Liu, H., Li, X., & Wang, S. (2021). Polymer additive assisted crystallization of perovskite films for high-performance solar cells. *Organic Electronics*, *96*, 106258.

https://doi.org/10.1016/J.ORGEL.2021.106258

Qi, Y., Hector, L. G., James, C., & Kim, K. J. (2014). Lithium Concentration Dependent Elastic Properties of Battery Electrode Materials from First Principles Calculations. *Journal of The Electrochemical Society*, *161*(11), F3010. https://doi.org/10.1149/2.0031411JES

Qin, P., Wu, T., Wang, Z., Zheng, X., Yu, X., Fang, G., & Li, G. (2019). Vitrification Transformation of Poly(Ethylene Oxide) Activating Interface Passivation for High-Efficiency Perovskite Solar Cells. *Solar RRL*, *3*(10), 1900134. https://doi.org/10.1002/SOLR.201900134

Roy, P., Kumar Sinha, N., Tiwari, S., & Khare, A. (2020). A review on perovskite solar cells: Evolution of architecture, fabrication techniques, commercialization issues and status. In *Solar Energy* (Vol. 198, pp. 665–688). Elsevier Ltd. https://doi.org/10.1016/j.solener.2020.01.080

Shi, X., Wu, Y., Chen, J., Cai, M., Yang, Y., Liu, X., Tao, Y., Guli, M., Ding, Y., & Dai, S. (2020). Thermally stable perovskite solar cells with efficiency over 21% via a bifunctional additive. *Journal of Materials Chemistry A*, *8*(15), 7205–7213. https://doi.org/10.1039/D0TA01255F

Silva, J. C. da, Araújo, F. L. de, Szostak, R., Marchezi, P. E., Moral, R. F., Freitas, J. N. de, & Nogueira, A. F. (2020). Effect of the incorporation of poly(ethylene oxide) copolymer on the stability of perovskite solar cells. *Journal of Materials Chemistry C*, *8*(28), 9697–9706. https://doi.org/10.1039/D0TC02078H

Soe, C. M. M., Stoumpos, C. C., Harutyunyan, B., Manley, E. F., Chen, L. X., Bedzyk, M. J., Marks, T. J., & Kanatzidis, M. G. (2016). Room Temperature Phase Transition in Methylammonium Lead Iodide Perovskite Thin Films Induced by Hydrohalic Acid Additives. *ChemSusChem*, *9*(18), 2656–2665. https://doi.org/10.1002/CSSC.201600879

Stamplecoskie, K. G., Manser Ab, J. S., & Kamat, P. V. (2014). Dual nature of the excited state in organic-inorganic lead halide perovskites: Broader context. https://doi.org/10.1039/c4ee02988g

Tailor, N. K., Abdi-Jalebi, M., Gupta, V., Hu, H., Dar, M. I., Li, G., & Satapathi, S. (2020). Recent progress in morphology optimization in perovskite solar cell. *Journal of Materials Chemistry A*, *8*(41), 21356–21386. https://doi.org/10.1039/D0TA00143K

Tomas Leijtens, E. Eperon, G., J. Barker, A., Giulia Grancini, Wei Zhang, M. Ball, J., Srimath Kandada, A. R., J. Snaith, H., & Annamaria Petrozza. (2016). Carrier trapping and recombination: the role of defect physics in enhancing the open circuit voltage of metal halide perovskite solar cells. *Energy & Environmental Science*, *9*(11), 3472–3481. https://doi.org/10.1039/C6EE01729K

Wanchun Xiang, (Frank) Liu, S., & Wolfgang Tress. (2021). A review on the stability of inorganic metal halide perovskites: challenges and opportunities for stable solar cells. *Energy & Environmental Science*, *14*(4), 2090–2113.

https://doi.org/10.1039/D1EE00157D

Wang, F., Bai, S., Tress, W., Hagfeldt, A., & Gao, F. (2018). Defects engineering for high-performance perovskite solar cells. In *npj Flexible Electronics*. https://doi.org/10.1038/s41528-018-0035-z

Wang, J., Jin, G., Zhen, Q., He, C., & Duan, Y. (2021). Bulk Passivation and Interfacial Passivation for Perovskite Solar Cells: Which One is More Effective? *Advanced Materials Interfaces*, *8*(9), 2002078. https://doi.org/10.1002/ADMI.202002078

Wang, K., Zheng, L., Zhu, T., Liu, L., Becker, M. L., & Gong, X. (2020). High performance perovskites solar cells by hybrid perovskites co-crystallized with poly(ethylene oxide). *Nano Energy*, *67*. https://doi.org/10.1016/J.NANOEN.2019.104229

Wong, M. H., An, Q., Kress, J., Mörsdorf, J.-M., Ballmann, J., & Vaynzof, Y. (2021). Surface dipole assisted charge carrier extraction in inverted architecture perovskite solar cells. *Applied Physics Letters*, *119*(23), 233903. https://doi.org/10.1063/5.0068670

Wu, T., Qin, Z., Wang, Y., Wu, Y., Chen, W., Zhang, S., Cai, M., Dai, S., Zhang, J., Liu, J., Zhou, Z., Liu, X., Segawa, H., Tan, H., Tang, Q., Fang, J., Li, Y., Ding, L., Ning, Z., … Han, L. (2021). The Main Progress of Perovskite Solar Cells in 2020–2021. *Nano-Micro Letters 2021 13:1*, *13*(1), 1–18. https://doi.org/10.1007/S40820-021-00672-W

Yang, I. S., & Park, N. G. (2021). Dual Additive for Simultaneous Improvement of Photovoltaic Performance and Stability of Perovskite Solar Cell. *Advanced Functional Materials*, *31*(20), 2100396. https://doi.org/10.1002/ADFM.202100396

Yang, Y., Ostrowski, D. P., France, R. M., Zhu, K., van de Lagemaat, J., Luther, J. M., & Beard, M. C. (2015). Observation of a hot-phonon bottleneck in lead-iodide perovskites. *Nature Photonics 2015 10:1*, *10*(1), 53–59. https://doi.org/10.1038/nphoton.2015.213

Zhang, F., Hou, Y., Wang, S., Zhang, H., Zhou, F., Hao, Y., Ye, S., Cai, H., Song, J., & Qu, J. (2021). Solvent-Additive Engineering-Assisted Improvement of Interface Contact for Producing Highly Efficient Inverted Perovskite Solar Cells. *Solar RRL*, *5*(7), 2100190. https://doi.org/10.1002/SOLR.202100190

Zhao, P., Kim, B. J., & Jung, H. S. (2018). Passivation in perovskite solar cells: A review. In *Materials Today Energy*. https://doi.org/10.1016/j.mtener.2018.01.004

Zhao, Y., Zhu, P., Huang, S., Tan, S., Wang, M., Wang, R., Xue, J., Han, T. H., Lee, S. J., Zhang, A., Huang, T., Cheng, P., Meng, D., Lee, J. W., Marian, J., Zhu, J., & Yang, Y. (2020). Molecular Interaction Regulates the Performance and Longevity of Defect Passivation for Metal Halide Perovskite Solar Cells. *Journal of the American Chemical Society*, *142*(47), 20071–20079. https://doi.org/10.1021/JACS.0C09560/SUPPL_FILE/JA0C09560_SI_001.PDF

CHAPTER SEVEN

CONCLUSIONS AND RECOMMENDATIONS FOR FUTURE WORK

7.1 Introduction

This chapter summarizes the important conclusions based on the results of the experimental studies that were carried out in this research work. The chapter also highlights some important aspects of research in PSCs that need to be carried out in the future as a follow-up to this work.

7.2 Conclusions

Since PSC is a multi-layered device consisting of different components, the properties of the individual components need to be optimized for optimum performance. However, this process is not as straightforward as one would expect because of the molecular interactions that occur among the components during processing. These interactions may occur via interdiffusion mechanism during thermal annealing or during device operation thus altering the properties of the adjacent components in a way that can be beneficial or detrimental to the performance of the resulting PSC device. From the individual studies that were carried out in this work, the following conclusions can be drawn:

(1) The incorporation of additives in the ETL is a good strategy to improve the charge carrier extraction, transportion, and collection efficiencies in PSCs. For example, the incorporation of the right proportion of SnO_2 into the TiO_2-based ETL in planar FA-rich PSC led to an improvement in its electrical conductivity and optical transmission ability with a consequent improvement in the PCE of the device. As a result of the improvement in electrical conductivity of the ETL, the series resistance R_s of the ensuing PSC device decreased thus improving its *FF* and PCE.

(2) The charge carrier generation, dissociation, and separation processes are the fundamental processes that control the behavior of any PV device and are majorly dependent on the properties of the AL. The stoichiometry of the AL layer therefore greatly influences these ultrafast dynamic processes. The incorporation of additives in the AL that can increase the efficiency of these processes is thus an important step in performance optimization in PSCs. However, this should go hand in hand with mechanisms to enhance interfacial charge extraction and transportation efficiency so as to ensure efficient collection at the electrodes. In our study, we found that a thermally evaporated CsBr layer of appropriate thickness can achieve this goal. In chapter five of this dissertation, a 50 nm thick CsBr layer was found to be important in enhancing the morphology of the AL and tuning the interfacial properties in PSC. This was very useful in improving the charge transport kinetics and resistance to degradation in the fabricated FA-rich PSC leading to a synergetic improvement in the PCE and operational stability. The PCE of CsBr-modified PSC increased by 15 % relative to that of the control device without the CsBr layer. The 50 nm thick CsBr layer also enabled the PSC to retain 70 % of its initial PCE for over 120 days of storage under ambient conditions.

(3) The incorporation of the right proportion of PEO into the perovskite AL not only improves the optoelectronic properties of the film but it also modulates the interfacial energetics in PSCs. Consequently, the light absorption and charge carrier dynamics in PSC are enhanced leading to improvement in the photocurrent and the PCE. A planar PSC whose AL was modified with 5 wt% of PEO demonstrated better PCE and operational stability relative to the control device fabricated under the same conditions. The PCE of the champion device with 5 wt% of PEO in its AL was 18.03% while that of

the control device was 17.34%. Thus about 9 % increase in PCE was achieved upon the incorporation of the PEO additive in the AL. The higher PCE in the PEO-modified device originated from its reduced recombination rate that led to better charge carrier collection efficiency as revealed by the EIS and EQE studies. The PEO-modified device was able to retain over 80 % of its initial PCE after being stored for about 140 hrs under humid conditions (average relative humidity of 62.5±3.25 %) without encapsulation.

7.3 Recommendations for future work

From the research conducted in this work, the following aspects need further investigation in order to come up with more cost-effective strategies to improve the performance of FA-rich PSCs. First and foremost, a cost-benefit analysis based on the achieved gains in the performance versus the additional costs incurred in the processing of the solar cell needs to be carried out along with any performance optimization method. In this regard, there is a need to establish the optimum annealing conditions for the SnO_2-TiO_2 composite ETL. Though the optimum annealing temperature for TiO_2 is known to be 500 °C for 30 minutes, this temperature is very high for SnO_2. Therefore, it is expected that a lower annealing temperature may work well for the SnO_2-TiO_2 composite ETL. We, therefore, recommend that a follow-up study focusing on the variation of the optoelectronic properties of SnO_2-TiO_2 as a function of annealing temperature needs to be done.

Secondly, in our study on the use of CsBr additive in the AL, we used the thermal evaporation technique to incorporate CsBr in the AL given the difficulty of dissolving it in most solvents. Though the thermally evaporated CsBr layer was instrumental in enhancing the device PCE and stability, the time lapse between the deposition of PbI_2 and CsBr was long due to the waiting time for a good vacuum to build up in the thermal evaporator. This not only

compromises the achievable PCE, but it also prolongs the fabrication process of PSC devices. This calls for the need to device another CsBr deposition procedure that is faster and scalable. Future research work should therefore focus on this aspect. On the same note, there is a need to understand how the optoelectronic properties of perovskite films and the PV performance characteristics of the resulting PSC devices evolve with the time lapse between the deposition of PbI_2 and the organic components during the fabrication process. This will not only offer some useful insights on proper control of the two-step fabrication process of PSC but will also help in the choice of an appropriate CsBr deposition method for the CsBr-modified PSC devices. Furthermore, in order to achieve an optimized performance in the CsBr-modified PSCs, future studies should focus on establishing the best annealing conditions for the CsBr-modified perovskite films that form the ALs in these systems.

Thirdly, PEO is a polymeric additive that has the ability to boost the PCE and stability of PSCs as per our study in chapter six. As a polymer, it can influence the mechanical behavior of the rigid perovskite films. Research should therefore be carried out to understand how the mechanical properties of perovskite films scale with the PEO loading. This will open new frontiers of using PEO as an additive to enable the fabrication of PSCs that are mechanically compliant and can thus be mounted on non-planar surfaces. Future research work should investigate the possibility of fabricating flexible PSC devices using PEO as a mechanical property modulating agent.

Fourthly, from the experimental works carried out in chapter five and chapter six of this dissertation, the incorporation of both the CsBr and PEO additives in the AL resulted in PCE and stability improvement in PSCs. The percentage improvement in the PCE of the CsBr-modified PSCs; relative to the control device; was found to be higher than that of the

PEO-modified PSCs. However, this observation is not conclusive as the CsBr-modified and the PEO-modified PSC devices were fabricated at different times. A follow-up study that seeks to directly compare the performace of the devices with CsBr and PEO additives in the AL under the same processing conditions is important. This will help one to understand the best modification strategy for improving the PCE and the stability of FA-rich PSCs.

Lastly, a suitable HTL that is less expensive and resistant to degradation is needed for FA-Rich PSC. The widely used Spiro-OMeTAD HTL is not only expensive but it has also been shown; by our study; to be the beginning point in device degradation. Therefore, it is important to carry out some studies that are aimed at finding a low-cost HTL material that can help to improve the operational stability of PSC without compromising on its PCE.